

MHD FREE CONVECTION IN A SQUARE CAVITY WITH HEATED OBSTACLE OF DIFFERENT ASPECT RATIO

Abdul Halim Bhuiyan* and M. A. Alim

Department of Mathematics, Bangladesh University of Engineering and Technology,
Dhaka-1000, Bangladesh.*Email: ahalim@math.buet.ac.bd

ABSTRACT: Laminar free convection flow in the presence of magnetic field in a square cavity with heated obstacle was studied in this paper. The lower wall of the cavity was heated and upper wall of the cavity was cold whereas side walls of the cavity were considered to be adiabatic. Finite element method based on Galerkin weighted residual approach was used to solve governing equations. Results are presented in terms of streamlines, isotherms and heat transfer rate for different values of Hartmann number (Ha) and different aspect ratio of the heated obstacle. The obtained results showed some very interesting results.

Keywords: Free convection, MHD, aspect ratio, enclosure, solid block, finite element method.

1. INTRODUCTION

Free convection in cavity has received considerable attention from researchers. Shapes of the most of the cavities commonly used in industries are cylindrical, square, rectangular, trapezoidal and triangular etc. Square cavities have manifold application in various fields. Taghikhani and Chavoshi [1] numerically investigated two dimensional magneto-hydrodynamics (MHD) free convection with internal heating in a square cavity. They observed that the effect of the magnetic field is to reduce the convective heat transfer inside the cavity. Bakhshan and Ashoori [2] numerically analyzed fluid behavior in a rectangular enclosure under the effect of magnetic field. They observed that Nusselt number rises with increasing Grashof and Prandtl numbers. Öztop and Al-Salem [3] numerically investigated effects of joule heating on MHD natural convection in non-isothermally heated enclosure. They observed that positive stream functions are decreased and thermal boundary layer becomes larger for increasing Hartmann number. Parvin and Nasrin [4] numerically analyzed the flow and heat transfer characteristics for MHD free convection in an enclosure with a heated obstacle. They found that buoyancy-induced vortex in the streamlines increase and thermal layer near the heated surface becomes thick with increasing Rayleigh number. Mousa [5] numerically investigated modeling of laminar buoyancy convection in a square cavity containing an obstacle. He observed that in case of relatively high Rayleigh numbers (10^5 – 10^6), the heat transfer rate increases when the aspect ratio of the adiabatic square obstacle increases, for high Rayleigh number (10^7), the increase in the size of the inside square obstacle does not affect the heat transfer rate significantly. Natural convection in a square cavity localized heating from below was investigated by Santosh et al. [6]. They observed that heat transfer increases when the heater source is placed towards the cold wall. Ece and Büyük [7] numerically analyzed natural convection flow under a magnetic field in an inclined rectangular enclosure heated and cooled on adjacent walls. Roy and Tanmay [8] numerically investigated finite element analysis of natural convection flows in a square cavity with non-uniformly heated wall(s). Rahman and Sharif [9] numerical study on laminar natural convection in inclined rectangular enclosures of various aspect ratios. Aydin and Yang [10] numerically investigated natural convection in enclosures with localized heating from below and symmetrically cooled from side walls. Kimura and Bejan [11] numerically analyzed natural convection in a differentially heated corner region. Ganzarolli and Milanez [12] numerically investigated natural convection in rectangular enclosure heated from below and symmetrically cooled from the sides. In the light of the above literatures, the present study addresses the effects of MHD free convection on heat flow within a square cavity.

NUMENCLATURE

AR	Aspect ratio of the solid block	h	Local heat transfer coefficient ($W m^{-2} K^{-1}$)
B_0	Applied magnetic field	Ha	Hartmann number
C_p	Specific heat at constant pressure ($J kg^{-1} K^{-1}$)	k	Thermal conductivity ($W m^{-1} K^{-1}$)
g	Acceleration due to gravity ($m s^{-1}$)	L	Width of the enclosure (m)

Mechanical Engineering Division
Bangladesh

The Institution of Engineers,

Nu	Nusselt number	x, y	Dimensional coordinates (m)
p	Pressure of the fluid	X, Y	Dimensionless coordinates
P	Dimensionless pressure of the fluid	Greek Symbols	
Pr	Prandtl number	α	Fluid thermal diffusivity ($m^2 s^{-1}$)
Ra	Reyleigh number	β	Thermal expansion coefficient (K^{-1})
T	Dimensional temperature (K)	ν	Kinematic viscosity ($m^2 s^{-1}$)
T_c	Cold temperature of fluid (K)	θ	Dimensionless temperature
T_h	Heat temperature of fluid (K)	ρ	Density ($kg m^{-3}$)
u, v	Dimensional velocity components (m s^{-1})	μ	Dynamic viscosity ($N s m^{-2}$)
U, V	Dimensionless velocities	σ	electrically conductivity of the fluid

2. PHYSICAL MODEL

A schematic of a two-dimensional square cavity of width L and a solid block is shown in Fig. 1. The left and right walls are considered to be adiabatic. The top wall is kept at a constant temperature T_c . The bottom wall and solid block are assumed to be uniform temperature be T_h . Here $T_c < T_h$. The uniform magnetic field B_0 is also applied to the fluid in the direction parallel to y . Based on the model, laminar, incompressible steady equations are written by considering a uniform applied magnetic field. The gravitational force (g) acts in the vertically downward direction. We assumed that Boussinesq approximation is valid and radiation mode of the heat transfer and Joule heating are neglected. Thus, using the coordinate system shown in Fig. 1, the governing equations can be written in dimensional form

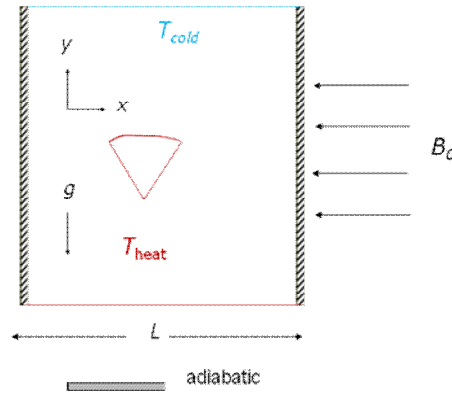


Fig. 1. The flow configuration and coordinate system

$$\frac{\partial u}{\partial x} + \frac{\partial v}{\partial y} = 0 \quad (1)$$

$$\rho \left(u \frac{\partial u}{\partial x} + v \frac{\partial u}{\partial y} \right) = -\frac{\partial p}{\partial x} + \mu \left(\frac{\partial^2 u}{\partial x^2} + \frac{\partial^2 u}{\partial y^2} \right) \quad (2)$$

$$\rho \left(u \frac{\partial v}{\partial x} + v \frac{\partial v}{\partial y} \right) = -\frac{\partial p}{\partial y} + \mu \left(\frac{\partial^2 v}{\partial x^2} + \frac{\partial^2 v}{\partial y^2} \right) + \rho g \beta (T - T_c) - \sigma B_0^2 v \quad (3)$$

$$u \frac{\partial T}{\partial x} + v \frac{\partial T}{\partial y} = \alpha \left(\frac{\partial^2 T}{\partial x^2} + \frac{\partial^2 T}{\partial y^2} \right) \quad (4)$$

We introduce the following dimensionless variables

$$X = \frac{x}{L}, \quad Y = \frac{y}{L}, \quad U = \frac{uL}{\alpha}, \quad V = \frac{vL}{\alpha}, \quad P = \frac{pL^2}{\rho\alpha^2}, \quad \theta = \frac{T - T_c}{T_h - T_c}, \quad Pr = \frac{\nu}{\alpha},$$

$$Gr = \frac{g\beta L^3 (T_h - T_c)}{\nu^2}, \quad Ha^2 = \frac{\sigma B_0^2 L^3}{\mu}, \quad Ra = \frac{g\beta L^3 (T_h - T_c) Pr}{\nu^2}, \quad \sigma = \frac{\rho^2 \alpha}{L^2}, \quad \alpha = \frac{k}{\rho C_p}$$

Thus, Eqs. (1)-(4) become

$$\frac{\partial U}{\partial X} + \frac{\partial V}{\partial Y} = 0 \tag{5}$$

$$U \frac{\partial U}{\partial X} + V \frac{\partial U}{\partial Y} = -\frac{\partial P}{\partial X} + \text{Pr} \left(\frac{\partial^2 U}{\partial X^2} + \frac{\partial^2 U}{\partial Y^2} \right) \tag{6}$$

$$U \frac{\partial V}{\partial X} + V \frac{\partial V}{\partial Y} = -\frac{\partial P}{\partial Y} + \text{Pr} \left(\frac{\partial^2 V}{\partial X^2} + \frac{\partial^2 V}{\partial Y^2} \right) + \frac{Ra}{\text{Pr}} \theta - Ha^2 \text{Pr} V \tag{7}$$

$$(8) \quad U \frac{\partial \theta}{\partial X} + V \frac{\partial \theta}{\partial Y} = \frac{\partial^2 \theta}{\partial X^2} + \frac{\partial^2 \theta}{\partial Y^2}$$

The boundary conditions are: at top wall and solid block surface $U = V = 0, \theta = 1$

At bottom wall $U = V = 0, \theta = 0$ and at the other walls $U = V = 0, \frac{\partial T}{\partial N} = 0$

At the inside and on the wall of enclosure fluid pressure $P = 0$

3. NUMERICAL PROCEDURE

The governing equations of this physical problem are transferred to the non-dimensional form. It is assumed that the fluid inside the cavity is viscous and incompressible. It is further assumed that the right and left wall will be insulated and top wall will be cold, while the bottom wall as well as object inside the cavity will be heated. To handle the cavity situation, the finite element method (FEM) will be considered. The discretized energy and momentum equations subjected to the boundary conditions simultaneously will be solved using (FEM) [13]. The numerical technique based on the Galerkin weighted residual method of finite element formulation is used in this study. The solution method has been chosen to solve the governing equations, which are linearized implicitly with respect to the equation's dependent variable. Velocity distribution as well as temperature profiles will be shown graphically.

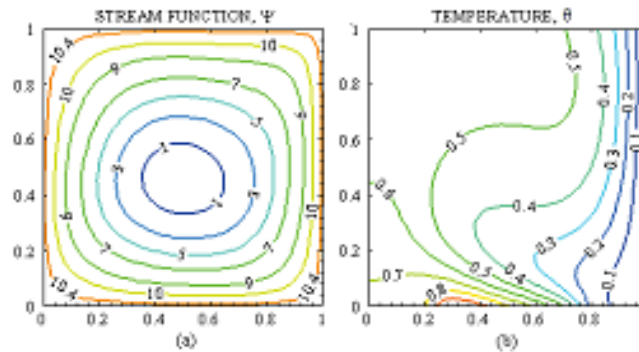


Fig. 2(a). Obtained results by Santosh [6]

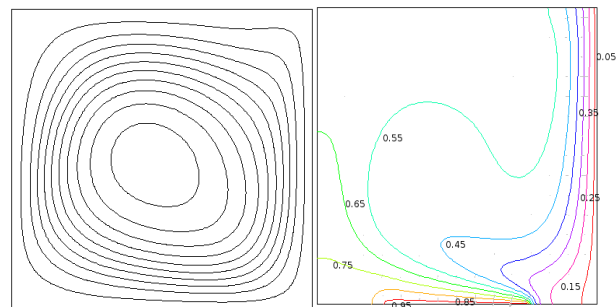


Fig. 2(b). Obtained results by Present work

4. CODE VALIDATION

Validation of the code was done by comparing streamlines and isotherms with results shown in Fig. 2(a) and Fig. 2(b) by Santosh et al. [6] while $Pr=0.71$, $Ra=10^5$. As seen from this figure the obtained results show good agreement.

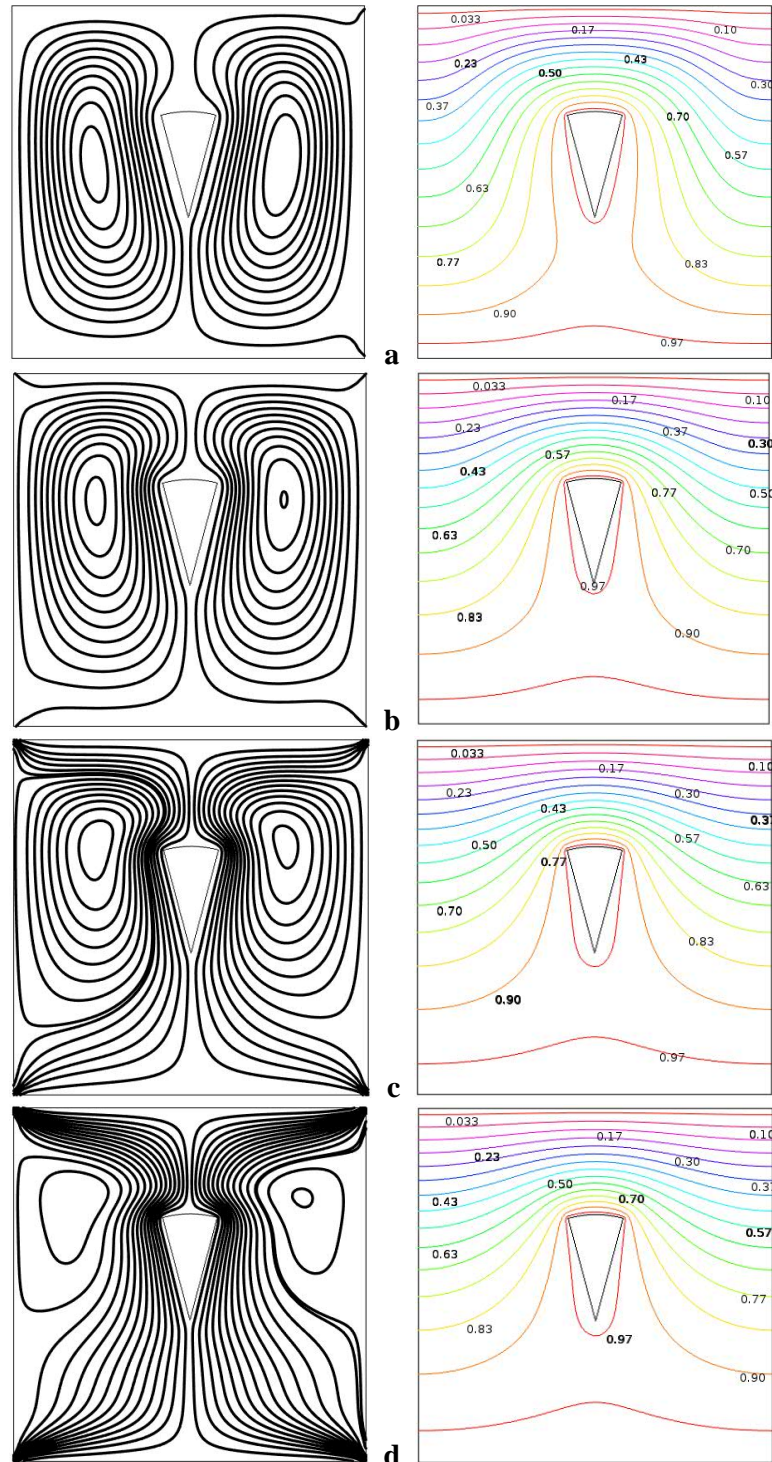


Fig. 3. Streamlines (left column) and isotherms (right column) for $AR=0.4$, $Pr=0.71$ and $Ra=10^4$: (a) $Ha=0$; (b) $Ha=20$; (c) $Ha=50$; (d) $Ha=100$

5. RESULTS

A numerical analysis has been performed in this work to investigate the effects of magnetic field in a square cavity inside heated solid block of different aspect ratio (AR). The ranges AR and Ha for this investigation vary from 0.4 to 4 and 0 to 100 respectively whereas other parameters are fixed at Ra = 10⁴ and Pr = 0.71. In this section the influence of the Hartmann number (Ha =0, 20, 50, 100) on the flow and temperature fields for Ra=10⁴ and three values of the aspect ratio (AR=0.4, 1, 4) are presented.

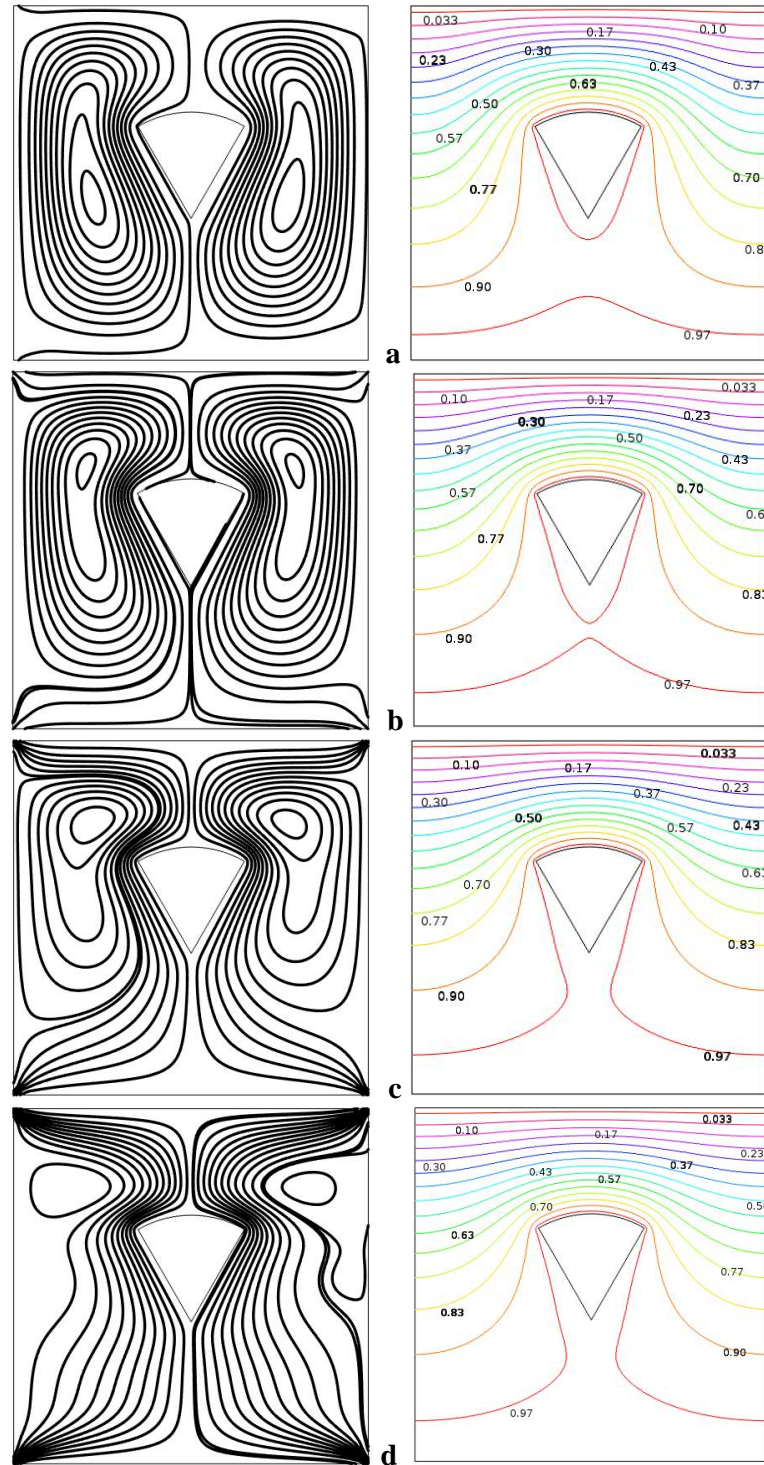


Fig. 4. Streamlines (left column) and isotherms (right column) for AR=1, Pr=0.71 and Ra=10⁴:
(a) Ha=0; (b) Ha=20; (c) Ha=50; (d) Ha=100

Fig. 3 shows the streamlines and isotherms for AR=0.4. In the absence of the magnetic field, almost elliptic size two vortices are generated left and right side of the heated solid block due to buoyancy force. As the Hartmann number increases shape of the vortices changes and move to the top side. Less bend of the isotherms lines is observed as the Hartmann number increases. Fig. 4 shows the streamlines and isotherms for AR=1. In the absence of the magnetic field, two vortices are appearing clearly left and right side of the heated solid block due to buoyancy force.

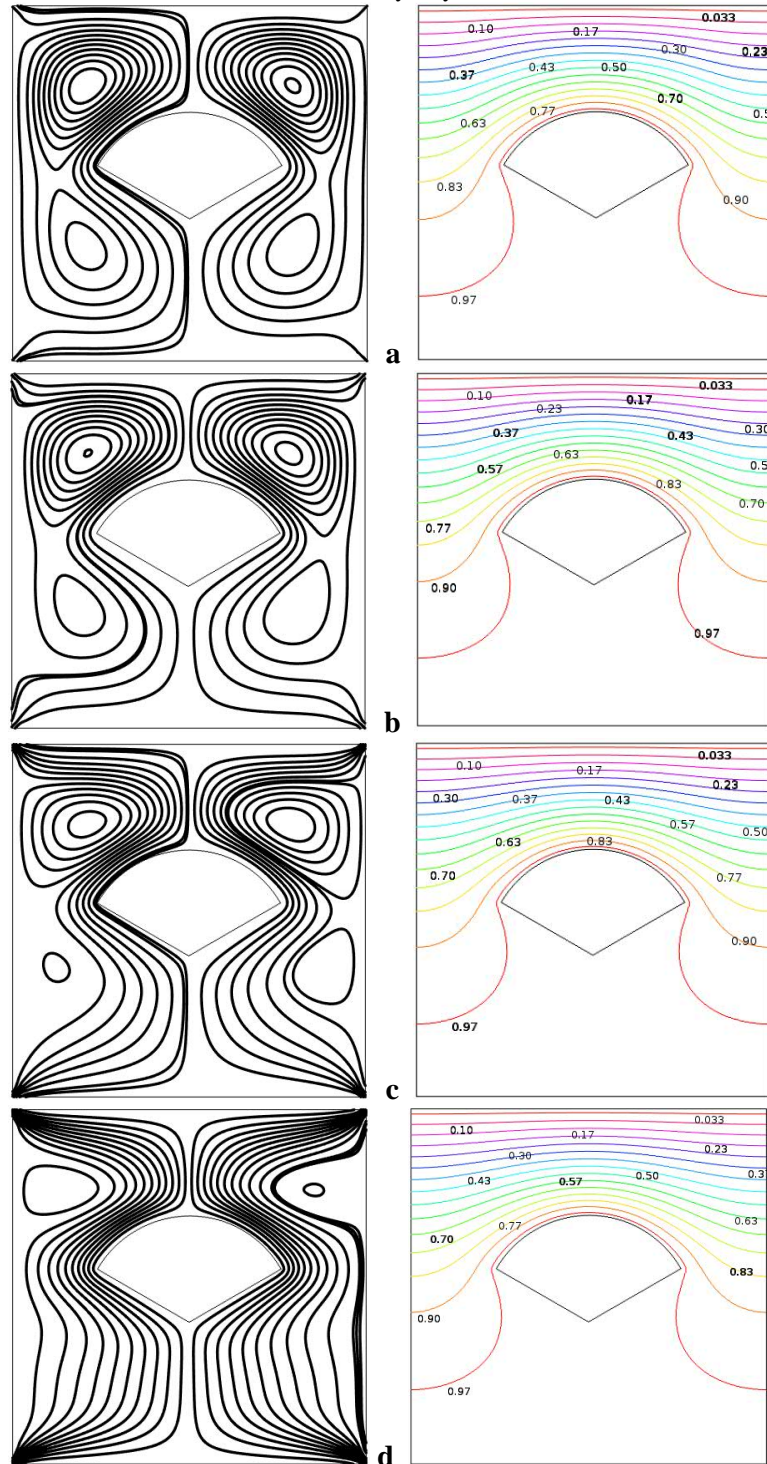


Fig. 5. Streamlines (left column) and isotherms (right column) for AR=4, Pr=0.71 and Ra=10⁴: (a) Ha=0; (b) Ha=20; (c) Ha=50; (d) Ha=100

As the Hartmann number increases shape of the vortices changes and move to the top side faster than $AR=0.4$. Bending of the isotherms lines are a lesser amount of with increasing Hartmann number. Fig. 5 illustrates the streamlines and isotherms for $AR=4$, where the buoyancy effects dominate the flow field in the cavity and the heat transfer is mainly due to natural convection. The results show that the buoyancy induced vortices in the cavity in the absence of the magnetic field ($Ha = 0$). Four vortices are evident inside of the cavity for $Ha = 0$. When the Hartmann number increases, two of them are reduced and finally disappear due to the effect of the magnetic field. The isotherms distribution is also affected by the effect of the magnetic field. The average Nusselt number is plotted as a function of Hartmann number as shown in Fig. 6 for five different aspect ratio ($AR=0.4, 1, 2, 4, 8$) while $Pr=0.71$ and $Ra=10^4$. The maximum heat transfer rate is obtained for the lowest Ha . This is because the magnetic field retards the flow.

6. CONCLUSION

The effects of natural convective flow on the thermal phenomena in an enclosure have been investigated. This study presents important fundamental aspects of natural convection in an enclosure. From the present investigation the following conclusions may be drawn: the average Nusselt number decreases when aspect ratio of the solid block increases and heat transfer rate from the cavity decreases with increasing magnetic field.

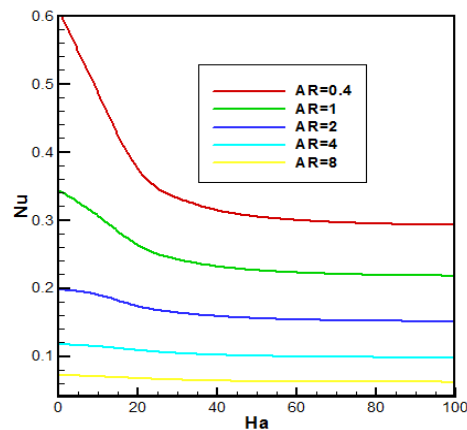


Fig. 6. Effect of AR and Ha on Nu while $Pr=0.71$ and $Ra=10^4$

REFERENCES

- [1] M. A. Taghikhani, H. R. Chavoshi, "Two Dimensional MHD Free Convection with Internal Heating in a Square Cavity", *Thermal Energy and Power Engineering*, vol. 2, pp. 22-28, 2013.
- [2] Y. Bakhshan and H. Ashoori, "Analysis of a Fluid Behavior in a Rectangular Enclosure under the Effect of Magnetic Field", *World Academy of Science, Engineering and Technology*, vol. 61, pp. 637-641, 2012.
- [3] F. Hakan Öztöp and Khaled Al-salem, "Effects Of Joule Heating On MHD Natural Convection In Non-Isothermally Heated Enclosure", *Journal of Thermal Science and Technology*, vol. 32, pp. 81-90, 2012.
- [4] S. Parvin, R. Nasrin, "Analysis of the flow and heat transfer characteristics for MHD free convection in an enclosure with a heated obstacle", *Nonlinear Analysis: Modeling and Control*, vol. 16, No. 1, pp. 89-99, 2011.
- [5] M. M. Mousa, "Modeling of Laminar Buoyancy Convection in a Square Cavity Containing an Obstacle", *Mathematics Subject Classification: 65M60, 76D05, 80A20*, 2010.
- [6] B. Santosh, G. Archana, Aswatha and K. N. Seetharamu, "Natural convection in a square cavity localized heating from below", the 37th National & 4th International Conference on Fluid Mechanics and Fluid Power December 16-18, 2010, IIT Madras, Chennai, India.
- [7] M. C. Ece and E. Büyüç, "Natural convection flow under a magnetic field in an inclined rectangular enclosure heated and cooled on adjacent walls", *Fluid Dyn. Res.*, vol. 38, pp. 564-590, 2006.
- [8] S. Roy and Basak Tanmay, "Finite element analysis of natural convection flows in a square cavity with non-uniformly heated wall(s)", *Int. J. of Engineering Science*, Vol. 43, pp. 668-680, 2005.

- [9] M. Rahman and M.A.R. Sharif, "Numerical study of laminar natural convection in inclined rectangular enclosures of various aspect ratios", Numer. Heat Transf. Part A, vol. 44, pp. 355-373, 2003.
- [10] O. Aydin, J. Yang, "Natural convection in enclosures with localized heating from below and symmetrically cooled from side walls", Int. J. Numer. Methods Heat Fluid Flow, vol. 10, pp. 518-529, 2000.
- [11] S. Kimura and A. Bejan, "Natural convection in a differentially heated corner region", Phys. Fluids, vol. 28, pp. 2980-2989, 1995.
- [12] M. M. Ganzarolli and L. F. Milanez, "Natural convection in rectangular enclosure heated from below and symmetrically cooled from the sides", Int. J. Heat Mass Transf., vol. 38, pp. 1063-1073, 1995.
- [13] J. N. Reddy, An introduction to Finite element method, McGraw-Hill, New York, 1993.

ENHANCEMENT OF HEAT TRANSFER BY USING DIFFERENT TYPES OF FIN AT CONSTANT TEMPERATURE

Md. Arefin Kowser¹, Md. Omar Faroque Sarker²

¹Associate Professor, Department of Mechanical Engineering, Dhaka University of Engineering & Technology (DUET), Gazipur-1700, Bangladesh. Email: nadimduet@yahoo.com

² M.Sc. Student, Department of Mechanical Engineering, Dhaka University of Engineering & Technology (DUET), Gazipur-1700, Bangladesh. Email: f.sarker@yahoo.com

ABSTRACT: The research is to design, construct, and determine the performance of different types of fin. The fin is an extended surface that accelerates the heat transfer rate to cool a heated body quickly. It has wide application in heat transfer engineering such as: motor, generator, transformer, and automotive engines and so on. The performance of fin depends upon different parameters like: geometrical shape, kinds of materials, base thickness, fin height, fin spacing, surface finish etc. by considering rectangular, triangular and parabolic fins. Theoretical analysis and experiment showed that parabolic fin transferred maximum amount of heat among three types of fin profiles at constant temperature. Heat transfer can be studied either by maintaining constant temperature or constant heat flux. This project work is carried out only at constant temperature. By comparing the effect of fin height for different ratios ($L/B = 0.875$ to 1.35) of fin height to fin base, it was noticed that smallest one transferred the highest amount of heat among parabolic fin. In the research work, the experimental values of convective heat transfer coefficient for rectangular and parabolic fins are compared with theoretical ones and presented. Optimum ratio of fin height to fin base length (L/B) are not achieved but predicted from the nature of heat released (Q) versus (L/B) ratio curve. Experiment showed that more heat transfer for smaller L/B ratio than larger ratio.

Keywords: Rectangular fins, Triangular fins, Parabolic fins, Constant temperature, Fin Length (height) to Fin Base ratios (L/B ratios), Mass of Condensate and Heat Transfer.

1. INTRODUCTION

The optimal fin literature mainly deals with the problems of finding the maximum heat dissipation for given mass of fin. While the bulk of the work deals with single fin, some work has been done with arrays. Most of the previous work in fin optimization employed one dimensional lumping [1, 2] to allow for the approximation of unidirectional heat flow in these fins. Usually, the temperature is assumed to be uniform over the base of fin, however as shown by suryanarayana [3]. This may not be true in real fins. For a conductive fin with convective boundary conditions, Schmidt [4] proposed the first optimal fin solution by assuming that the temperature profile is a linear function of distance from the root of the fin. Using variation method Duffin [5] proved that Schmidt's assuming was correct. Wilkins [6] showed that for a minimum mass fin a linear temperature profile was only true for the case of pure convection with constant thermal conductivity and heat transfer co efficient. Cobble [7] found the optimal profile for a fin subject too simultaneous convection and radiation occurring along the boundary. By assuming that the temperature profile followed a power law and that both the convective heat transfer coefficient and thermal conductivity were constant, the resulting profile for the optimal fin was a concave function, with a sharp edge. In the manufacture of fins there are practical design constraints that must be satisfied. One could select a desired shape and then find the optimal dimensions for the profile. For example: ravel and Imaret [8] require that their annular fin have a trapezoidal profile with only convective heat dissipation. Razelos and Imare deals with circular fins exclusively but allowed for a variable heat transfer co-efficient and thermal conductivity. Another form of constraint requires a minimum material thickness. Branes [9] used a variational formulation to study the effects of constraints on the maximum and minimum thickness of a convective fin. Dhar and Arora [10] discuss arrays of fins, where the formulation includes the effects of the space between the fins. Aram and little [11] have studied the temperature gradients dt/dy and dt/dx in thick fins of rectangular profile. Carrier and Anderson [12] have presented open solutions in terms of infinite series for circular fins of rectangular and parabolic profile. Grader [13] has generalized the extended surface problem by deriving general equation and solution. Zabronsky [14] has presented an exact solution for the efficiency of square fins on round tubes. All four rectangular fin edges are considered adiabatic, as would occur in a heat exchanger, where a

symmetrically spaced bank of normal tubes penetrates a large single fin sheet. The efficiency of such fins found to be nearly identical with that of a circular fin of the same surface area. The works accomplished in the area of natural convection heat transfer from the fins or fins arrays has increased over five folds in the last 35 years. Natural convection heat transfer find important applications in the cooling of small energy conversion devices, in room air heating and for special heat exchange conditions where trouble free and noiseless operation are desired. Although a lot of investigations have been conducted with fin of different profiles, but very little attention has been paid to study the heat transfer behavior from arrays of triangular, rectangular, and parabolic fins. Considering the above the present work has been selected for further study. The laws which govern heat transmission are very important to the engineer in the design, construction, testing and operating of heat transfer apparatus. Fins find numerous applications in mechanical engineering in the field of cooling of internal combustion engines, refrigeration and air conditioning and so on. Fins are also used in electrical apparatus in which generated heat must be efficiently dissipated. Example: motor, generator, transformer etc. the application of fin is equally important in the field of other branches of engineering.

2. MATHEMATICAL MODEL

2.1 DIFFERENT HEAT TRANSFER EQUATIONS

1. Conduction heat transfer, $q = -KA \frac{dt}{dx}$
- Here, K is the thermal conductivity
2. Convection heat transfer, $q = hA(T_w - T_\infty)$
3. Radiation heat transfer, $q = \sigma A(T_1^4 - T_2^4)$
4. If mass of water condensed is m(kg) and latent heat of condensation becomes L (kJ/kg), then heat transfer during condensation process, $Q = mL/t$ (kJ/sec).
5. Fin efficiency = actual heat transferred/ heat which would be transferred if entire fin area at base temperature.
6. Fin effectiveness = heat with fin /heat without fin.

2.2 MATHEMATICAL ANALYSIS OF RECTANGULAR FIN

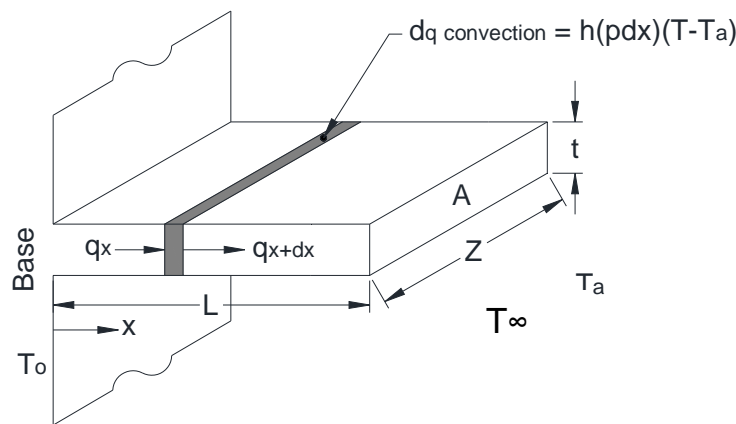


Fig.2.1: One dimensional conduction & convection heat transfer through a Rectangular fin.

Now the energy balance:

Energy in left face = Energy in right face + Energy lost by convection

The equation for the convective heat transfer

$$q = hA\Delta T = h(pdx)(T - T_\infty) \dots \dots \dots (2.1)$$

Where

h = heat transfer co- efficient

p = perimeter

T = temperature at any point

Energy in left face, $q_x = -KA \frac{dT}{dx}$

Energy in right face, $q_{x+dx} = -KA \left[\frac{dT}{dx} + \frac{d}{dx} \left(\frac{dT}{dx} \right) dx \right]$
 $= -KA \left[\frac{dT}{dx} + \frac{d^2T}{dx^2} dx \right]$

From energy balance equation (i) we get by putting the values,

$$-KA \frac{dT}{dx} = -KA \frac{dT}{dx} - KA \frac{d^2T}{dx^2} dx + h(pdx)(T - T_\infty)$$

$$\Rightarrow KA \frac{d^2T}{dx^2} dx = h(pdx)(T - T_\infty)$$

$$\Rightarrow KA \frac{d^2T}{dx^2} = hp(T - T_\infty)$$

$$\Rightarrow \frac{d^2T}{dx^2} = \frac{hp}{KA} (T - T_\infty)$$

$$\Rightarrow \frac{d^2T}{dx^2} - \frac{hp}{KA} (T - T_\infty) = 0 \dots \dots \dots (2.2)$$

(T - T_∞) is a variable, Let (T - T_∞) = θ

$$\therefore \theta = T - T_\infty$$

$$\Rightarrow \frac{d\theta}{dx} = \frac{dT}{dx} \quad [\because T_\infty = c]$$

$$\therefore \frac{d^2\theta}{dx^2} = \frac{d^2T}{dx^2}$$

From (ii)

$$\Rightarrow \frac{d^2T}{dx^2} - \frac{hp}{KA} \theta = 0$$

$$\Rightarrow \frac{d^2\theta}{dx^2} - \frac{hp}{KA} \theta = 0$$

General boundary condition:

$$\theta = \theta_0 = T_0 - T_\infty \text{ at } x = 0$$

Other boundary condition:

For the fin is of finite length and losses heat by convection from its end.

$$\text{at } x = 0, \quad \theta = T_0 - T_\infty = \theta_0$$

$$-KA \frac{dT}{dx} = hA\Delta T$$

$$\text{at } x = L, \quad -KA \frac{d\theta}{dx} = hA\theta$$

$$\Rightarrow \text{at } x = L, \quad K \frac{d\theta}{dx} + h\theta = 0$$

Let $\frac{hp}{KA} = m^2$ and obtain the equation as

$$\frac{d^2\theta}{dx^2} - m^2\theta = 0 \dots \dots \dots (2.3)$$

Therefore general solution of the given differential equation:

$$0 = C_1 e^{-mx} + C_2 e^{mx}$$

at $x = 0, \theta = \theta_0 \therefore \theta_0 = c_1 + c_2 \dots \dots \dots (2.4)$

at $x = L, K \frac{d\theta}{dx} + h\theta = 0$

$$\Rightarrow \frac{d\theta}{dx} = -\frac{h}{k}\theta$$

Then

$$\theta = C_1 e^{-mx} + C_2 e^{mx}$$

$$\therefore \frac{d\theta}{dx} = -mC_1 e^{-mx} + mC_2 e^{mx}$$

Applying $x=L$

$$\Rightarrow -C_1 m e^{-mL} + C_2 m e^{mL} = -\frac{h}{k} (C_1 e^{-mL} + C_2 e^{mL})$$

$$\Rightarrow m[-C_1 e^{-mL} + C_2 e^{mL}] = -\frac{h}{k} (C_1 e^{-mL} + C_2 e^{mL})$$

From equation (vi) $\Rightarrow C_2 = \theta_0 - C_1$

From equation (viii) no. equation,

$$\Rightarrow m[-C_1 e^{-mL} + (\theta_0 - C_1) e^{mL}] = -\frac{h}{k} [C_1 e^{-mL} + (\theta_0 - C_1) e^{mL}]$$

$$\Rightarrow mC_1 e^{-mL} - m\theta_0 e^{mL} + mC_1 e^{mL} = \frac{h}{k} C_1 e^{-mL} + \frac{h}{k} \theta_0 e^{mL} - \frac{h}{k} C_1 e^{mL}$$

$$\Rightarrow mC_1 e^{-mL} + mC_1 e^{mL} - \frac{h}{k} C_1 e^{-mL} + \frac{h}{k} C_1 e^{mL} = \frac{h}{k} \theta_0 e^{mL} + m\theta_0 e^{mL}$$

$$\Rightarrow C_1 \left\{ m e^{-mL} + m e^{mL} + \left(-\frac{h}{k} e^{-mL} + \frac{h}{k} e^{mL} \right) \right\} = \theta_0 \left[\frac{h}{k} e^{mL} + m e^{mL} \right]$$

$$\therefore C_1 = \frac{\theta_0 \left(\frac{h}{k} e^{mL} + m e^{mL} \right)}{(e^{-mL} + e^{mL}) + \left(\frac{h}{mk} \right) (e^{mL} - e^{-mL})}$$

Putting C_1 & C_2 in the general solution

We have,

$$\theta = \theta_0 \frac{\cosh m(L-x) + \left(\frac{h}{mk} \right) \sinh m(L-x)}{\cosh(mL) + \left(\frac{h}{mk} \right) \sinh(mL)}$$

This is the temperature distribution equation.

Heat flow:

$$q = -KA \left. \frac{d\theta}{dx} \right|_{x=0}$$

$$q = -KA\theta_0 \frac{-m \sinh(mL) - \left(\frac{h}{mk} \right) m \cosh(mL)}{\cosh(mL) + \left(\frac{h}{mk} \right) \sinh(mL)}$$

$$= \sqrt{hpKA}\theta_0 \frac{-m \sinh(mL) - \left(\frac{h}{mk} \right) m \cosh(mL)}{\cosh(mL) + \left(\frac{h}{mk} \right) \sinh(mL)}$$

$$= \sqrt{hpKA}(T_0 - T_\infty) \frac{\tanh(mL) + \frac{h}{mK}}{1 + \frac{h}{mK} \tanh(mL)} \dots \dots \dots (2.5)$$

This is the heat flow equation.

2.3 MATHEMATICAL ANALYSIS OF TRIANGULAR FIN

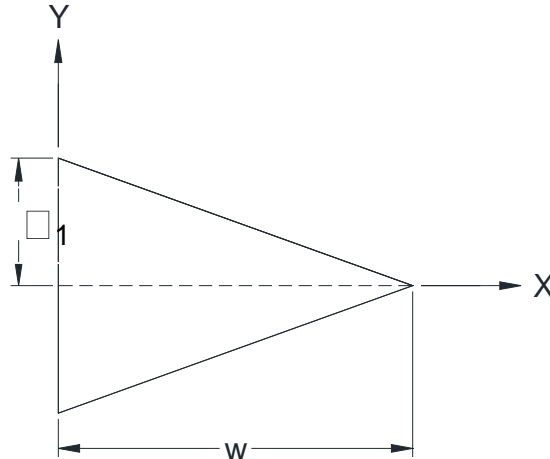


Fig.2.2: Straight Triangular fin profile

The generalized differential equation for temperature distribution is:

$$y_x \frac{d^2T}{dx^2} + \frac{dy_x}{dx} \cdot \frac{dT}{dx} - \frac{h}{K} T = 0 \dots \dots \dots (2.6)$$

Considering the straight fin of triangular profile, since x = 0 is chosen at fin tip and maximum thickness at base x = w is 2δ₁, then y_x = δ₁ (x/w), and the general differential equation

(2.6) reduces to

$$x \frac{d^2T}{dx^2} + \frac{dT}{dx} - N^2 w T = 0 \dots \dots \dots (2.7)$$

This is distinguished from Bessel's equation and comparing it with the generalized Bessel's equation and solution. We determine its general solution as,

$$T = C_1 J_0(2iN\sqrt{wx}) + C_2 Y_0(2iN\sqrt{wx}) \dots \dots \dots (2.8)$$

Where the J₀ and Y₀ are zero order Bessel functions of the first and second order respectively.

The integration constant C₁ and C₂ are to be determined such that T satisfies the required boundary conditions

T = T₀ at x = w,

dT/dx = 0 at x = 0

It is seen that J₁(0) = 0 and Y₁(0) = -∞

So on applying the second boundary condition as

$$\left(\frac{dT}{dx} \right)_0 = 0 = -C_1 iN \sqrt{\frac{w}{x}} J_0(2iN\sqrt{wx}) \Big|_{x=0} - C_2 iN \sqrt{\frac{w}{x}} Y_1(2iN\sqrt{wx}) \Big|_{x=0}$$

We find that C₂=0 and the general solution must then be represented by

$$T = C_1 J_0(2iN\sqrt{wx})$$

The evaluation of C₁ by application of the first boundary condition leads to the particular solution for T which reads,

$$\frac{t - t_g}{t_0 - t_g} = \frac{J_0(2iN\sqrt{wx})}{J_0(2iNw)} \dots \dots \dots (2.9)$$

The rate of heat dissipation from the surfaces of the straight triangular fin is computed according to (2.9) as

$$q = 2h \int_0^w T dx = \frac{2hT_0}{J_0(2iNw)} \int_0^w J_0(2iN\sqrt{wx}) dx$$

To perform this integration, we expand the J_0 function according to the Bessel's series and then integrate term by term, as

$$\int_0^w J_0(2iN\sqrt{wx}) dx = \int_0^w \left(1 + N^2wx + \frac{N^4w^2x^2}{2^2} + \dots \dots \dots \right) dx$$

$$= w \left(1 + \frac{N^2w^2}{2} + \frac{N^4w^2}{2^2 \cdot 3} + \dots \dots \dots \right)$$

On computing this with the J_1 series as

$$j_1(2iN\sqrt{wx}) = iNw \left(1 + \frac{N^2w^2}{2} + \frac{N^4w^2}{2^2 \cdot 3} + \dots \dots \dots \right)$$

We have,

$$\int_0^w J_0(2iN\sqrt{wx}) dx = \frac{-l}{N} j_1(2iNw)$$

Where with,

$$q = \frac{-2ihT_0}{N} \cdot \frac{j_1(2iNw)}{j_0(2iNw)} \dots \dots \dots (2.10)$$

This is the heat flow equation

2.4 MATHEMATICAL ANALYSIS OF PARABOLIC FIN

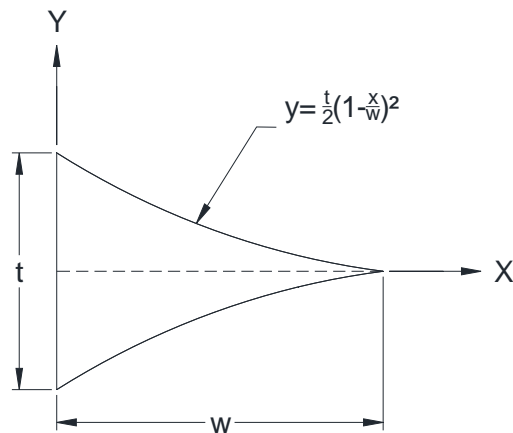


Fig.2.3: straight parabolic fin profile

The profile equation,

$$y_x = \delta_1 \frac{w}{\left(5\frac{1}{2} - x\right)}$$

Here

δ_1 = semi thickness of fin profile = $2''$

W = length across X axis = $5''$

$$y_x = \delta_1 \frac{w}{(5\frac{1}{2} - x)} \quad y_x = \delta_1 \frac{w}{(5\frac{1}{2} - x)}$$

Now, differential equation for temperature distribution is

$$y_x \frac{d^2 T}{dx^2} + \frac{dy_x}{dx} \cdot \frac{dT}{dx} - \frac{h}{k} T = 0$$

$$\Rightarrow \delta_1 \frac{5}{(5\frac{1}{2} - x)} \cdot \frac{d^2 T}{dx^2} + \delta_1 \frac{5}{(5\frac{1}{2} - x)} \cdot \frac{dT}{dx} - \frac{h}{k} T = 0$$

$$\frac{5}{(5\frac{1}{2} - x)} \cdot \frac{d^2 T}{dx^2} + \delta_1 \frac{5}{(5\frac{1}{2} - x)} \cdot \frac{dT}{dx} - \frac{h}{5\delta_1 k} T = 0 \dots \dots \dots (2.11)$$

Taking $(5\frac{1}{2} - x) = u - dx = du \therefore -\frac{d}{dx} = d/du$

And

$$a = \frac{h}{5\delta_1 k}$$

Where $1 > a > 0$

Now the equation becomes,

$$\frac{1}{u} \frac{d^2 T}{du^2} - \frac{1}{u^2} \frac{dT}{du} - aT = 0$$

$$\Rightarrow u \frac{d^2 T}{du^2} - \frac{dT}{du} - u^2 aT = 0$$

By Frobenius method,

We have obtained the solution of equation... .. (2.11)

$$T = A \left[1 + \frac{au^3}{1.3} + \frac{a^2 u^6}{1.3.4.6} + \dots \right] + B \left[u^2 + \frac{au^2}{3.5} + \frac{a^2 u^8}{3.5.6.8} + \dots \right]$$

Boundary condition:

$T = T_0$ when $x = 5$ or $u = 1/2$

$dT/dx = 0$ when $x = 0$ or $u = 5\frac{1}{2}$

$T_0 \simeq A + 1/4B$

$$\frac{dT}{du} = A \left[au^2 + \frac{a^2 u^5}{1.3.4} + \dots \right] + B \left[2u + \frac{au^4}{3} + \frac{a^2 u^7}{3.5.6} + \dots \right]$$

$$A \left[au_0^2 + \frac{a^2 u_0^5}{12} + \dots \right] + B \left[2u_0 + \frac{au_0^4}{3} + \frac{a^2 u_0^7}{90} + \dots \right] = 0$$

$$\left(T_0 - \frac{1}{4}B \right) A \left[au_0^2 + \frac{a^2 u_0^5}{12} + \dots \right] + B \left[2u_0 + \frac{au_0^4}{3} + \frac{a^2 u_0^7}{90} + \dots \right] = 0$$

$$T_0 \left[au_0^2 + \frac{a^2 u_0^5}{12} + \dots \right] = B \left[\frac{a}{4} u_0^2 + \frac{a}{48} u_0^5 + \dots - \left\{ 2u_0 + \frac{au_0^4}{3} + \frac{a^2 u_0^7}{90} \right\} \right]$$

$$B = T_0 \frac{au_0^2 + \frac{a^2 u_0^5}{12} + \dots}{\frac{a}{4} u_0^2 + \frac{a}{48} u_0^5 - 2u_0 + \frac{au_0^4}{3} + \frac{a^2 u_0^7}{90}}$$

$$\begin{aligned}
 T &= T_0 \left[1 + \frac{au^3}{3} + \frac{a^2u^6}{72} + \dots \right] \\
 &\quad + B \left[u^2 + \frac{au^2}{15} + \frac{a^2u^8}{720} + \dots - \frac{1}{4} \left\{ 1 + \frac{au^3}{3} + \frac{a^2u^6}{72} + \dots \right\} \right] \\
 \left(\frac{dT}{du} \right)_{u=\frac{1}{2}} &\cong A \left[\frac{a}{4} \right] + B = \left(T_0 - \frac{1}{4}B \right) \cdot \frac{a}{4} + B \\
 &= \frac{a}{4}T_0 + \left(1 - \frac{a}{16} \right) B \cong \frac{a}{4}T_0 + \left(1 - \frac{a}{16} \right) \left(-\frac{1}{2}au_0T_0 \right) \\
 &= \frac{a}{4}T_0 - \frac{1}{2}au_0T_0 = \frac{a}{4}T_0(1 - 2u_0) \\
 \text{Putting, } u_0 &= 5 \left(\frac{dT}{du} \right)_{u=\frac{1}{2}} \cong -\frac{9}{4}aT_0 \text{ where } a = \frac{h}{5\delta_1 k} \ll 1 \\
 \therefore \left(\frac{dT}{du} \right)_{u=\frac{1}{2}} &\cong -\frac{9}{4} \frac{h}{5\delta_1 k} T_0 = \frac{9}{20} \frac{h}{\delta_1 k} T_0 \dots \dots \dots (2.12)
 \end{aligned}$$

2.5 FIN EFFICIENCY

To indicate the effectiveness of a fin in transferring a given quantity of heat, a new parameter called fin efficiency is defined by
For above case, the fin efficiency becomes

$$\eta_f = \frac{\sqrt{hpk}\theta_0 \tanh mL}{hpL\theta_0} = \frac{\tanh mL}{mL}$$

The fins discussed above were assumed to be sufficiently deep that the heat flow could be considered one-dimensional. The expression for mL may be written

$$mL = \sqrt{\frac{hp}{KA}} L = \sqrt{\frac{h(2z + 2t)}{Kzt}} L$$

Where Z is the depth of fin and t is the thickness. Now, if the fin is sufficiently deep, the term 2z will be large compared with 2t, and

$$mL = \sqrt{\frac{2hz}{Ktz}} L = \sqrt{\frac{2h}{Kt}} L$$

Multiplying numerator and denominator by $L^{\frac{3}{2}}$ gives

$$mL = \sqrt{\frac{2h}{KLt}} L^{\frac{3}{2}}$$

Lt is the profile area of the fin, which are defined as

$$A_m = Lt$$

So that final equation can be presented as

$$mL = \sqrt{\frac{2h}{KA_m}} L^{\frac{3}{2}} \dots \dots \dots (2.13)$$

3. EXPERIMENTAL MODEL

Different fin profiles are shown in Figs.3.1-3.4 and the complete experimental set-up is presented in Fig.3.4.

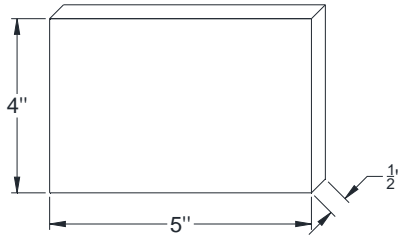


Fig.3.1: Rectangular Fin profile

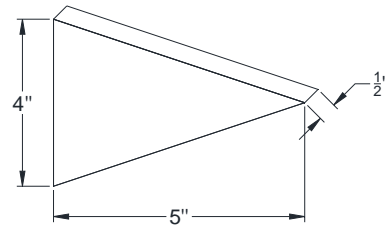


Fig.3.2: Triangular Fin profile

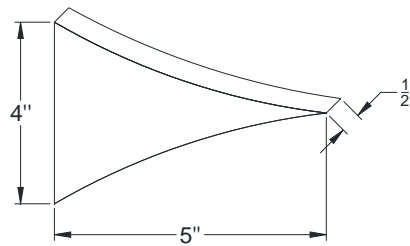


Fig.3.3: Parabolic Fin profile

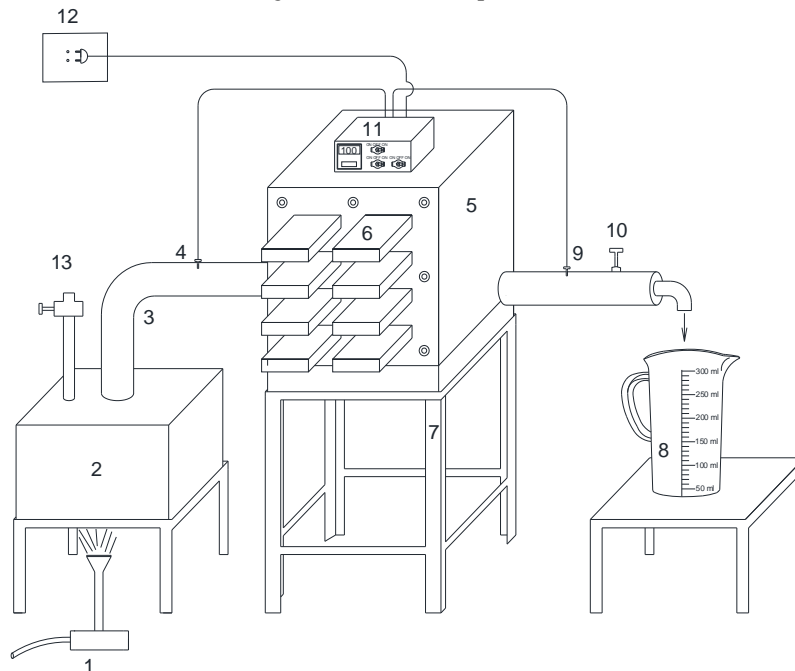


Fig.3.4: Arrangement of experiment set-up for Constant Temperature

Elements of Experiment Set Up: Elements of experimental set-up is listed below:

- 1) Burner
- 2) Steam generating unit
- 3) GI pipe
- 4) Thermocouple
- 5) Rectangular box
- 6) Aluminium plate attached with fins
- 7) Stand
- 8) Condensate water pot (Beaker)
- 9) Thermocouple Temperature Sensor port
- 10) Valve
- 11) Display unit
- 12) Electric Source
- 13) Pressure relief valve

4. WORKING PROCEDURE

It is known that temperature remains constant during latent heat of condensation. Thus in this project work the principle of latent heat of condensation was applied for maintaining constant temperature at the plate.

The steam was generated in a container by applying heat was supplied to a rectangular metallic box through an inlet pipe. The temperature of inlet steam was measured by a thermocouple placing at the inlet pipe. Fins were attached with the box by nut and bolt and were sealed by using gasket. There were 9 plates along with different types of fin. The plate could be easily removed and might set up another plate in the box. By placing a certain plate in the box, **100°C** steam was supplied in the box. The fin received heat from steam and transferred heat to atmosphere. As a result the steam got condensed due to the release of latent heat of condensation. The condensed water was delivered by outlet pipe and collected in a beaker. By measuring the mass of condensed water, the heat transfer rate of fin was obtained by applying the following formula: $Q = mL/t(\text{Watt})$

5. RESULTS

Comparison of Heat Transfer with various fin profiles using different L/B ratio is presented in Figs. 5.1-5.3. Comparison of Heat Transfer with various L/B ratios for different fins are shown in Figs. 5.4-5.6.

L/B = 0.875

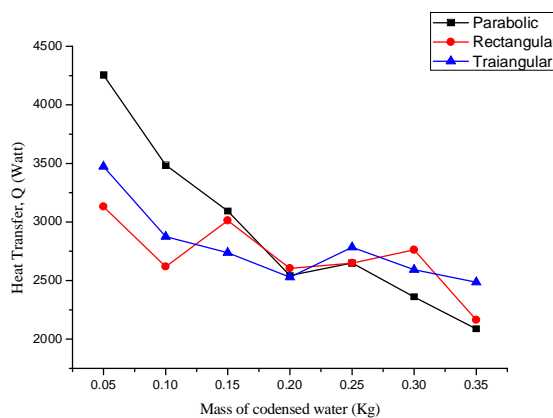


Fig.5.1: Heat Transfer Vs Mass of condensed water curve

L/B = 1.25

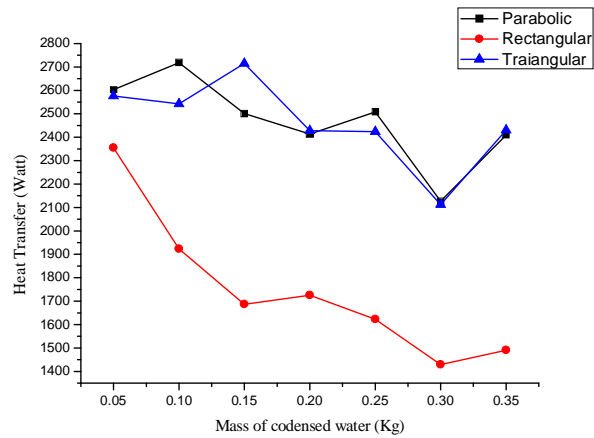


Fig.5.2: Heat Transfer Vs Mass of condensed water curve

L/B = 1.35

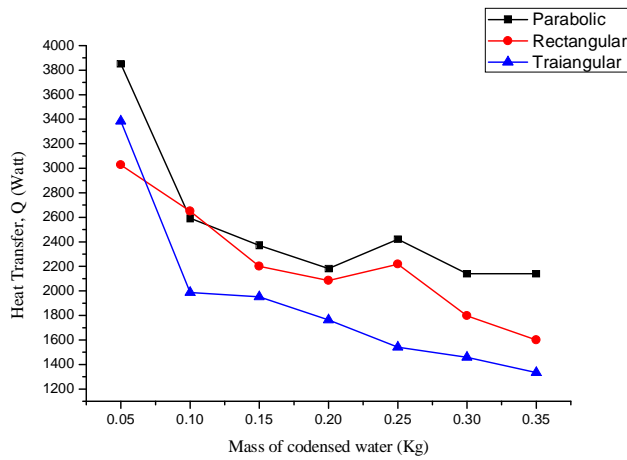


Figure 5.3 Heat Transfer Vs Mass of condensed water curve

For Parabolic Fin profile:

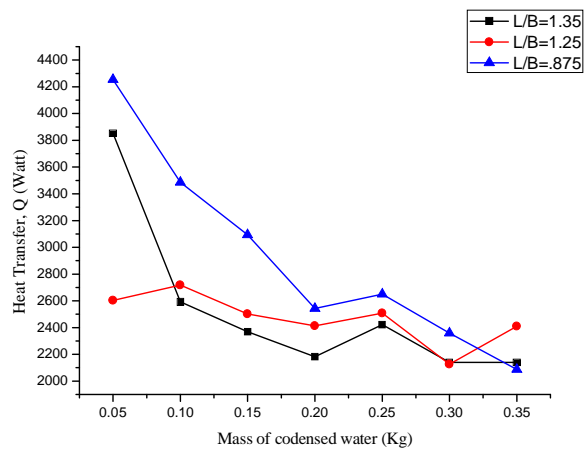


Figure 5.4 Heat Transfer Vs Mass of condensed water curve

For Triangular Fin profile:

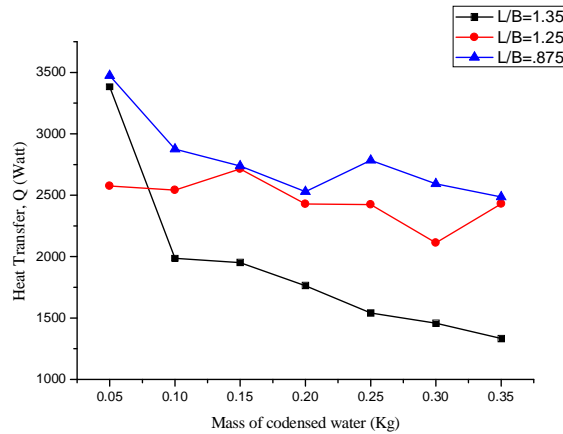


Fig.5.5: Heat Transfer Vs Mas of condensed water curve

For Rectangular Fin profile

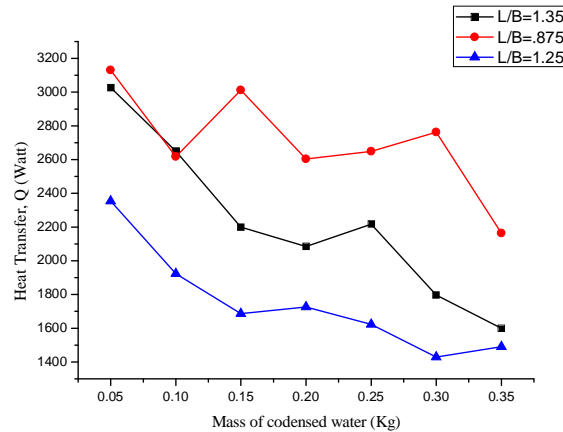


Fig.5.6: Heat Transfer Vs Mass of condensed water curve

6. DISCUSSIONS

The project work was carried out for determining the performance of different type of fins for free convection. The performance of fin depends upon different parameters like: Fin spacing dominant role in the transfer of heat. Radiation from one effects another and with the change of spacing for each fin size, shape factor changed. Moreover spacing controlled heat transfer for horizontal orientation. For simplicity and time limitations of the project work, only the effect of fin height, fin material and different geometrical shapes were considered in this project. Base areas for all type of fins were kept constant. For selecting the best geometrical shape, we considered rectangular, triangular and parabolic fins and the highest heat transfer were received from the parabolic fin among three types of fin profiles. For comparing the effect of fin height, different heights $L= 3.5, 5, 5.4$ of parabolic fin were considered keeping the base length (B) constant. From the project work, it was noticed that the smallest ratio transferred maximum amount if heat for parabolic fin constant base thickness, maximum heat transfer might be found for different L/B ratio for another of parabolic fin.

The project work was carried out by placing the fins in horizontal position for comparing the heat transfer rate in both cases. The physical mechanism of heat transfer at the wall was conduction. Since on the surface of fin, fluid particles remained at constant, conduction of heat took place from the

surface to the fluid micro layer. Particles of this micro layer then moved upward causing convection current.

Density of heated air was lighter than surrounding air. So, it tend to move upward. In horizontal orientation of fins, heat was transferred by convection process from the upper surface of fin due to buoyant force. The heated air under the bottom surface could not escape away. So heat was transferred from the bottom surface of a horizontal fin by conduction process. For multiple horizontal fins, one just above another, the heated air from the lower fin was trapped by the bottom surface of the upper fin and made an interruption of heat transfer by convection. The heat air was plumed upward by the both sides of the upper fins due to buoyant force of air. In vertical orientation of multiple fins, a large portion of total convection area transferred heat with less interruption. Only the bottom surface of fins made an interruption for its horizontal orientation, which was not emphasized, due to its smaller area as compared with total convective surface for parabolic fins.

In this project work, the experimental value of heat transfer co- efficient was compared with theoretical ones. For rectangular fin Optimum ratio (L/B) for which maximum heat dissipation was likely to correspond even at lower (L/B) ratio. For constant temperatures experiment showed slightly variation of temperatures in outlet and inlet system.

7. CONCLUSION

After performing the project and researches the following statements may be concluded

1. Parabolic fin transferred 1.05% more heat than triangular one and 9.56% more than rectangular of the ratio $L/B = 1.25$ at constant temperature.
2. Highest heat transfer obtained from parabolic fin of the ratio $L/B = 0.875$ at constant temperature.
3. Optimum ratio of fin height to fin base length (L/B) were not achieve but predicted from the nature of heat released (Q) versus (L/B) ratio curve, lower L/B ratio released higher heat than higher ratio.
4. Parabolic fin transferred more amount heat.
5. At constant Heat Flux Parabolic fin also transferred more heat and Numerical Nodal Analysis satisfied exactly by the Fin of the ratio $L/B = 1.25$.

REFERENCES

- [1] A.vrami,M. and little, J.B., "Diffusion of Heat Through a Rectangular bar and the Cooling and Insulating of Fins." Journal of Applied Physics, Vol.13, 1942 pp.621-631.
- [2] Barnes, E.R., "A Variational Problem Arising in the Design of Cooling Fins," Quarterly Journal of Applied Mathematics, Vol. 34, 4976, pp. 1-17.
- [3] Carrier W.H. and Anderson, S.W. "The Resistance to Heat Flow Through Finned Tubing"
- [4] Cobble, M.H., "Optimum fin Shape," Journal of the Franklin Institute, Vol. 91, 1971, pp.283-292.
- [5] Dhar, P.L and Arora, C.P., "Optimum Design of Finned Surfaces" Journal of the Franklin Institute, Vol.301, 1976, pp.379-392.
- [6] Duffin, R.J., "A Variational Problem Relating to Cooling Fins," Journal of Mathematics and Mechanics, Vol. 8, 1959, pp.47-56.
- [7] Gardner K.A., "Efficiency of Extended Surface Trans", ASME Vol.67, No.8, 1945, pp.621-631.
- [8] HOLMAN, J.P. "HEAT TRANSFER" Ninth Edition in SI units pp-13, 44-50, 83-88,341.
- [9] Incropera, Frank.P. and Dewitt, David. P. "Introduction to Heat Transfer" Third Edition in S.I unit's pp. 110-130.
- [10] Kern, D.Q., and Kraus, A.D., Extended Surface Heat Transfer, McGraw-Hill, New York, 1972.
- [11] Ozisik, M.N., Basic Heat Transfer, McGraw-Hill, New York, 1977.
- [12] Razelos, P., and Imre, k., "The Optimum Dimensions of Circular Fins with Variable Thermal Parameters," ASME Journal of Heat Transfer, Vol. 102, 1980, pp.420-425.
- [13] ROY, P.N., "Manufacturing Technology, Foundry and Welding" First Edition.
- [14] Schmidt, E., "Die Waer Meuebertragung DurchRippen," Zeitschriftdes Vereines Deutscher Ingenieure, Vol. 70, 1926, pp. 885-889,947-951.

- [15] Suryanarayana, N.V., "Two-Dimensional Effects on Heat Transfer Rates from an Array of Straight Fins," ASME Journal OF Heat Transfer, Vol.97, 1977, pp.129-132.
- [16] Wilkins, J.E., "Minimum-Mass Thin Fins and Constant Temperature Gradients," SIAM Journal, Vol.10, 1962, pp.62-73.
- [17] Zabronsky, H., "Efficiency of a Heat Exchanger using Square Fins on Round Tubes" USAEC, L-29, Oak Ridge Technical Information Service, August,1952

METHOD FOR PREDICTING NUCLEATE BOILING CURVE OF PURE REFRIGERANT ON A POROUS SURFACE

¹Ashok K Dewangan, ²Ravi Kumar, ³Anil Kumar

Indian Institute of Technology Roorkee, Uttarakhand, 247667

ashokiitr2012@gmail.com, ravikfme@iitr.ernet.in, anilkfme@iitr.ernet.in

ABSTRACT: This paper proposes a numerical method for the nucleate pool boiling heat transfer of R-134a (1, 1, 1, 2-tetrafluoroethane) on a thin porous layer over a copper tube placed horizontal. The governing equations have been used to explain heat transfer characteristics in the liquid and vapor on a porous horizontal heating surface. A numerical method (Finite difference method) has been employed for analysis of steady state, one dimensional heat and mass transfer in a porous surface saturated with the liquid and vapor phases of working fluid. The effect of surface structure characteristics (porosity, porous layer thickness, particle diameter and thermal conductivity) and fluid properties for boiling within the porous layer were included. A commercially available Matlab software package has been used for analyzing the boiling heat transfer and fluid flow in the sintered porous surface. At present numerical investigation revealed that at low heat flux, porous layer with a low porosities yield better boiling heat transfer performance, whereas at high heat flux porous layer with high porosities do better due to the necessity of the high rate of liquid evaporation. The present numerical model matches well with experimental results and literature data on pool boiling over coated surface, thus validating the present approach.

Keywords: Heat transfer; Pool boiling; R-134a; Coated surface, Numerical method.

1. INTRODUCTION

Pool boiling heat transfer characteristic is influenced by the surface distinctiveness of the boiling region. Porous surface is being widely used to enhance boiling heat transfer in the industry. In recent years, significant progresses in technology have demanded new and improved heat transfer systems. The Pool boiling heat transfer is one of the most intense ways of heat transfer in many engineering problems as power or chemical plants. For this reason, numerous investigations have been reached on how to further enhance this kind of heat transfer. Boiling heat transfer with porous surface has been of considerable research interest due to its effectiveness and several applications. The porous layer coatings can be manufactured by various methods such as sintering, brazing, flame spraying, metallic coating to foam substrate, electrolytic deposition [1] etc. The enhanced boiling heat transfer on porous coated surfaces may be attributed much more effective nucleation sites, continuous evaporation inside the pore structure with significant reduction of wall superheat at boiling incipience and enhance the associated heat transport. The thin porous coating can promote nucleation and hence, intensify the heat transfer at low heat flux. The effect of geometric parameters such as coating layer thickness, porosity, particle diameter and material on pool boiling of refrigerants on enhanced surfaces have been discussed in various fields. The structure of porous layer is dependent on the application process. For smooth surfaces or roughened surfaces, the rate of heat transfer is mainly depends on the rate of vapor production. On the other hand, porous coated surfaces are composed of randomly arranged particles, producing pores and interconnecting channels providing flow paths of liquid supply and vapor escape, where the intensity of heat transfer depends on the ability of the coating to transmit vapor [2].

The development of the porous layer coating began as early as 1947 at Union Carbide and was later known by its trade name High Flux. Milton [3] was the first one to patent a porous layer coating. Milton and Gottzmann [4] applied high flux coated surface in air-separation plants for producing the larger heat transfer coefficient (HTC). Starner and Cromis [4] compared the high flux coating with finning tube and took note that the enhanced surface has 6 times higher HTC than those of fin tube. Polezhaev and Kovalev [4] proposed a model that the distance between vapor columns decreased as compared with the smooth surface and the heat transfer would be increased. O'Neill et al. [5] proposed a model that predicts the required wall superheat for given coating porosity and observed that the surface tension and thermal conductivity are main thermo-physical parameters for optimum porous structure. Ovodkov and Kovalev [5] modeled porous layer coating and explained its

mechanism. Bukin et al. [4, 5] applied three different methods for making the porous layers and noticed an optimum coating thickness for sintered particles. Lu and Chang [6] explained as the thickness of the porous layer increases, the heat transfer is enhanced in the low heat flux region and diminished in the high heat flux zone. R Chang [7] suggested a comprehensive model of nucleate boiling heat transfer of methanol on a porous surface of various thicknesses and shown larger boiling heat transfer coefficient in the region of low heat flux. Nishikawa [8] et al. developed an empirical correlation for the boiling coefficient and also investigated copper and bronze particles and the effect of particle size and coating thickness on the boiling co-efficient and obtained an optimum coating thickness approximately four times of particle diameter.

Webb [9] also found that the coating thickness is around four particle diameters. Fujii, et al. [10] determined the optimum particle diameter for varying the porous layer thickness and powder sizes. Kovalev et al. [11] developed a model to describe the effects of coating porosity and material conductivity on the shape and position of the boiling curve. Hsieh and Weng [12] considered the key parameters affecting boiling on porous coated surfaces. Hsieh and Yang [13] concluded that pore diameter and porous layer thickness are the strongest factors for cavity flooding. The purpose of this study is to identify the effects of numerical investigation the pool boiling heat transfer characteristics of the copper porous coated tube using the refrigerant R-134a at the saturation temperature of 6 °C. The effects of porosity, porous layer thickness and particle diameter are included. The numerical results are also trying to compare and their validation with data from experiments and empirical correlations.

2. PROPOSED MODEL AND GOVERNING EQUATIONS

Boiling with a porous layer at 6°C saturation on a copper heating tube of 150 mm diameter and 100 mm long has been analyzed numerically using a commercially available Matlab software package. The heat transfer surface is made of copper, where spherical copper powders sintered on a horizontal heating surface. The working fluid is R-134a and saturated vapor at system pressure of 3.62 bar, where this fluid enters into porous structure and is driven by capillary forces.

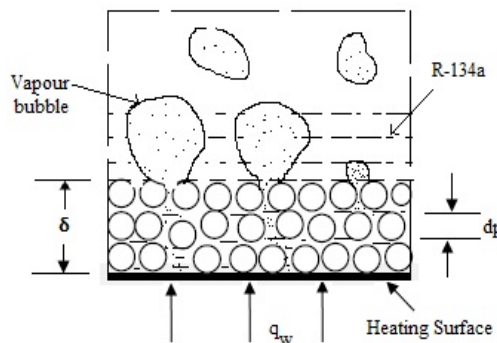


Fig.1: Model of a porous boiling surface

Due to a continuation of growth and detachment of bubbles, pumping force is generated, and fluid is sucked into the porous structure [14]. This superheated liquid is heated, vaporized and spread along interconnected capillary passages of porous structure. The heat transfer mechanisms are conducted through a test section and conduction across the liquid film as shown in figure 1. During this process vapor passage is covered by liquid film and dominant heat transfer mechanisms which are assumed [6] to be: (1) Conduction heat transfer through the solid wall of the test section (2) Conduction heat transfer for separating the bubble from top surface of the test section, and (3) Evaporation of the micro-layer (thin liquid film). The saturated liquid flows out due to the force generated by vapor in the porous structure, resulting counter-current liquid and vapor flows within the porous structure. The thermo-physical properties of the working fluid and the condition of heated wall are listed below in table 1. To analyze this purpose, heat transfer, mass transfer and liquid saturation formulated through finite difference technique has been used to solve the differential equations and code is generated by

commercial available Matlab software. The result obtained by numerical method is validated through the data from experiments and empirical correlations.

Table 1. Thermo-physical properties of R-134a at 6 °C [data from ASHRAE]

Properties	Liquid	Vapor
Density(kg/m ³)	1274.7	17.73
Enthalpy(kJ/kg)	208.11	402.06
Viscosity(μPas)	251.2	10.98
Thermal conductivity(w/mK)	89.4	12.04

2.1. Governing Equations

The governing equations [6, 7] for boiling flows are the conservation of mass, momentum and energy equations. These equations are:

$$\frac{d(\rho u)}{dy} = \pm q_g \quad (1)$$

where positive and negative sign indicates for vapor and liquid. The rate of heat generation of vapor per unit volume of porous structure is:

$$q_g = \frac{(q_p A_p)}{h_{fg}} \quad (2)$$

where $q_p = K_l \frac{T - T^i}{\delta}$ and $A_p = \frac{\delta(1-\epsilon)}{d_p}$ (3)

$$T^i = T_{sat} [1 + \frac{1}{\rho_v h_{fg}} \sigma \sqrt{\frac{\epsilon}{K}} J(x)] \quad (4)$$

Momentum Equations:

$$\frac{d(\frac{\rho}{\epsilon} + \beta u)}{dy} = \left(\frac{\rho u}{K K_r} + \frac{\beta u^2}{K K_r} \right)_{1,V} \quad (5)$$

where $\beta = \frac{1.75(1-\epsilon)}{150 D_p}$ (6)

$$K = \frac{D_p^2 \epsilon^3}{150(1-\epsilon)^2} \quad (7)$$

$$K_{rl} = x^4, K_{rv} = (1-x)^2(1-x^2) \quad (8)$$

The saturation [6] can be determined the equation is given by

$$\frac{dK}{dy} = \left(\left(\frac{\rho u}{K K_r} \right)_V - \left(\frac{\rho u}{K K_r} \right)_L + \left(\frac{\beta \rho u^2}{K K_r} \right)_V - \left(\frac{\beta \rho u^2}{K K_r} \right)_L - \frac{(\rho_l - \rho_v) g K \frac{dJ}{dx}}{\sigma \sqrt{\epsilon}} \right) \quad (9)$$

The relative permeability's are chosen for typical porous medium [6,7] Conduction heat is transferred from the test section to thin liquid film, therefore energy transfer from a solid wall of the test section can be written as:

$$k_e \frac{d^2 T}{dy^2} = A_p q_p \quad (10)$$

with the following boundary conditions:

at $y = 0$ $u = 0$ (11)

$-k_e \frac{dT}{dy} = q_w$ (12)

at $y = \delta$ $u = \frac{q_w}{\rho_v h_{fg}}$ (13)

$-k_e \frac{dT}{dy} = h(T - T_{sat})$ (14)

$x = x$ (15)

The capillary pressure generates discontinuity between vapor and liquid and it is directly proportional to the surface tension and inversely proportional to the meniscus radius of the vapor liquid interface. The liquid distribution in porous medium must satisfy the following equation [5]:

$$P_c = P_v - P_l = \frac{\sigma}{\sqrt{K/\epsilon}} J(x) \tag{16}$$

where $J(x)$ is the Leverett function [5] for different porosity media and it can be written as:

$$J(x) = 1.42 (1 - x) - 2.12 (1 - x)^2 + 1.26 (1 - x)^3 \tag{17}$$

The Leverett function is a dimensionless function describing the capillary pressure. The fluid saturation can be obtained using this function.

3. RESULTS AND DISCUSSIONS

The surface characteristics which involve complicated parameters such as marangoni flow induced by surface tension gradients, the capillary force, porosity, particle diameter, thickness etc. will significantly influence the critical heat flux (CHF). In this section, the effects of these parameters on the wall superheat and the liquid saturation are examined.

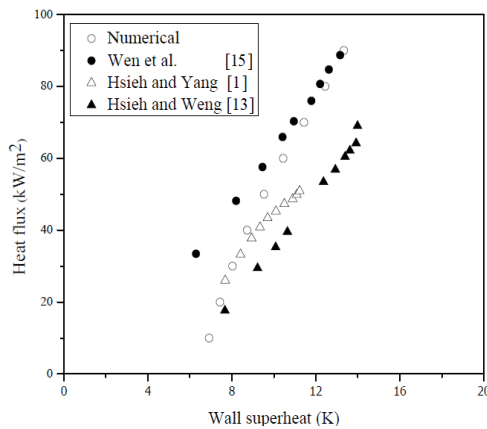


Fig.2: Boiling curve of R-134a

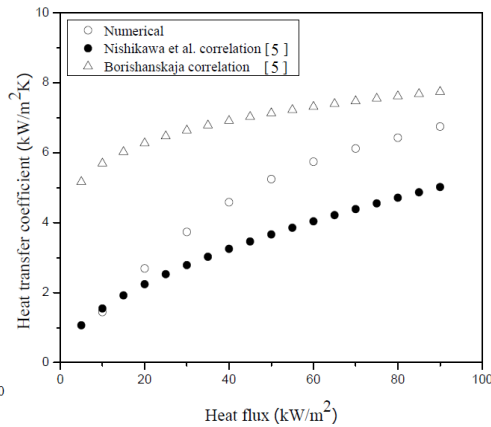


Fig.3: Heat transfer coefficient of R-134a

The numerical analysis and parametric study may provide general guidelines for the optimum design of cooling systems where thin porous layers are proposed to be coated on the heating surface to enhance the heat transfer under boiling conditions. The lower wall superheat is required, when the surface coated with a copper porous material, and gives better boiling heat transfer capability than smooth surface [15]. The degree of enhancement in heat transfer is mainly dominated by the vaporization at the liquid vapor interface; the turbulence induced by bubble generation and detachment and depends on the thickness of a porous layer. When the results of a numerical investigation were analyzed, it was noticed that boiling on the current model surface was similar to the experimental and empirical correlation results.

The hysteresis effect of the coated surface predicted from the numerical model at 6°C saturation condition of R-134a and the results from experimental [12, 13, 16] and empirical correlation [5,17] for pool boiling over a horizontal heating tube are presented in Fig. 2 and Fig. 3 for validation. Figure 2 shows that the wall superheat increases with increasing heat flux. The required super-heat from the numerical model is slightly lower than those from Weng and Yang experimental results below CHF. Due to lower porosity at the substrate surface, the minimum wall superheat was observed from Wen’s work of the horizontal coated tube. An increase of coating thickness leads to decrease the number of emittable vapor bubbles, increases of intensity of the recirculation rate due to capillary structure and decrease the heat flow rate by conduction from a substrate surface to various coating layers due to continuous replacement of R-134a by vapor in porous structure. An increase in heat flux raises the number of nucleation sites to form large population of vapor bubbles which in turn, causes high heat transfer rate and thereby high heat transfer coefficient. The test tube coated with copper (independently of the method of fabrication), an increase in the value of heat transfer

rate as compared with the data of empirical correlations of various investigators [5] as depicted in Fig 3. Figure 4 exhibits the influence of HTC of the boiling characteristics due to porosity at different heat flux levels in R-134a obtained from the present study and empirical correlation [5].

The effects associated with increasing porosity are (a) the completing void space increase. As a result, both the liquid and vapor move more easily, which reduces the wall superheats and (b) leads to smaller internal phase change surfaces per unit volume, which tends to cause an increase of the wall superheat. The porosity of coating surface significantly affects the boiling HTC and its hysteresis phenomenon. The comparison of present numerical model with Nishikawa et al. [5] correlation shown in Fig.4 reveals that the porosity increases at low heat flux; it affects the hydrodynamics of the vapor phase.

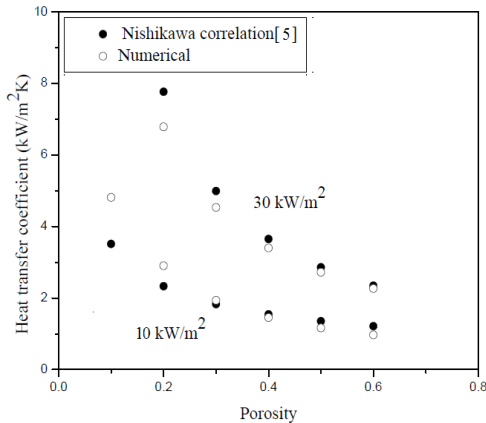


Fig.4: Influence of porosity on heat transfer

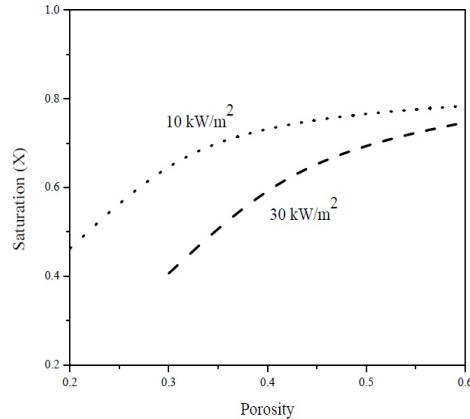


Fig.5: Effect of porosity on minimum coefficient saturation

It implies that the porous layer coating makes resistance to vapor flow away from the heating surface. Also at high heat flux, tube with high porosities shows better heat transfer performance due to the demand of the high rate of liquid evaporation. The interconnecting void space increases with increasing porosity; as a consequence, both liquid and vapor move more easily, which causes a decrease in the wall superheats. As the porosity increases, the saturation level inside the porous structure also increase has been depicted in Fig. 5. The trend in Fig. 5 also indicates that the CHF increases with increasing porosity. The larger porosity gives more void space for liquid flowing towards the heating surface and the vapor to escape easily from a porous surface.

4. CONCLUSIONS

Pool boiling heat transfer of sintered copper porous surface was numerically investigated and the following conclusions were drawn:

- The porous coated surface leads to enormous enhancement in nucleate boiling heat transfer.
- The boiling heat transfer performance of the copper coated tube depends on the heat flux and geometrical coating parameters such as the coating thickness and pore size distribution.
- An important condition of increase in critical heat-flux density is to have good attachment of the porous coating to the heating surface.
- For coating made of high thermal conductivity copper particles, the particle diameter had a negligible effect on the heat transfer performance.
- Porosity and coating thickness are the main parameters of the porous coated tube that acts upon the boiling heat transfer independent of the fabrication method.
- The present numerical results were found to be qualitatively in good accord with empirical results.

5. NOMENCLATURE

A	specific surface area (m^2/m^3)	Δ	liquid film thickness
d	diameter (m)	<i>Subscripts</i>	
K	permeability (dimensionless)	V	vapor
J	leverett function (dimensionless)	l	liquid
P	pressure (N/m^2)	p	particle
X	scaled liquid saturation (dimensionless)	cs	coating surface
T	Temperature (K)	w	wall
g	gravity (m/s^2)	i	interface
h_{fg}	latent heat of vaporization (J/kg)	c	capillary
h	heat transfer coefficient ($\text{W}/\text{m}^2\text{K}$)	r	relative
k	thermal conductivity ($\text{W}/\text{m-K}$)	e	effective
K	permeability	g	generation
q	heat flux (W/m^2)	sat	saturation
u	superficial velocity (m/s)		
y	position (mm)		
<i>Greek Symbols</i>			
ρ	density (kg/m^3)		
μ	viscosity (N-s/m)		
ν	kinematic viscosity ((m/s)		
ϵ	porosity (dimensionless)		
δ	porous layer thickness (mm)		

ACKNOWLEDGEMENTS

This numerical work has been carried out in the Refrigeration and Air-conditioning Lab of Mechanical and Industrial Engineering Department at the Indian Institute of Technology, Roorkee, Uttarakhand, India under the Research Fellowship from MHRD which is gratefully acknowledged.

REFERENCES

- [1] Cieslinski, J.T., "Nucleate Pool Boiling on Porous Metallic Coatings". Experimental Thermal and Fluid Science, Vol. 25, pp. 557-564, 2002.
- [2] Polyakov, V. M., and Kichatov, B. V. "Boiling of Solutions on Porous Surfaces". Theoretical Foundations of Chemical Engineering, Vol. 34, No. 1, pp. 22-26, 2000.
- [3] Milton, R. M., "Heat Exchange System". U.S. Patent 3,384,154, 1968.
- [4] Yang, J., "Development of Heat Transfer Enhancement Techniques for External Cooling of an Advanced Reactor Vessel". PhD. Thesis, Pennsylvania State University the Graduate School College of Engineering
- [5] Hsieh, S.S., and Weng, C.J., 1997. "Nucleate pool boiling from coated surfaces in saturated R-134a and R-407c". Int. J. Heat Mass Transfer. Vol. 40, No. 3, pp. 519-532, 2005.
- [6] Poniewski, P.E. and Thome, J.R., Nucleate Boiling on Micro-structured Surfaces, Heat Transfer Research, Inc. (HTRI), 150 Venture Drive, College Station, TX 77845, USA, pp. 55-70, 2005.
- [7] Lu, S.M., and Chang R.H., "Pool Boiling from a Surface with a Porous Layer". A.I.Ch.E.J., Vol. 33, No. 11, pp. 1813-1828, 1987.
- [8] Chang, R.H., "A Comprehensive Model of Nucleate Boiling from a Surface with a Porous Layer". Proceedings Symposium on Transport Phenomena and Applications, pp. 131-138, 1991.
- [9] Nishikawa, K., Ito, T., and Tanaka, K., "Enhanced Heat Transfer by Nucleate Boiling on a Sintered Metal Layer". Heat Transfer Jap. Res., 8, No. 2, pp. 65-81, 1979.
- [10] Webb, R. L., "Nucleate Boiling on Porous Coated Surfaces". Heat Transfer Engineering, Vol. 4, No. 3-4, pp. 71-82, 1983,
- [11] Fujii, M., "Nucleate Pool Boiling Heat Transfer from a Porous Heating Surface (Optimum Particle Diameter)". Heat Transfer Jap. Res., Vol. 13, No. 1, pp.76-91 1984.
- [12] Kovalev, S. A., Solov'yev, S. L., and Ovodkov, O. A., "Liquid Boiling on Porous Surfaces". Heat Transfer Sov. Res., Vol. 19, No. 3, pp. 109-120, 1987.
- [13] Hsieh, S.S., and Weng, C.J., "Nucleate pool boiling from coated surfaces in saturated R-134a and R-407c". Int. J. Heat Mass Transfer. Vol. 40, No. 3, pp. 519-532, 1997.

- [14] Hsieh, S.S., Yang T.Y., “Nucleate Pool Boiling From Coated and Spirally Wrapped Tubes in Saturated R-134a and R-600a at Low and Moderate Heat Flux”. *Journal of Heat Transfer*, Vol. 123, pp. 257-270, 2001.
- [15] Wu, W., Du, J.H., Hu, X.J., and Wang, B.X., “Pool Boiling Heat Transfer and Simplified One Dimensional Model for Prediction on Coated Surfaces with Vapour Channels”. *Int. J. of Heat and Mass Transfer*, Vol. 45, pp. 1117-1125, 2002.
- [16] Chai, L.H. and Wen, D.S., “Theoretical Analyses on Boiling Critical Heat Flux with Porous Media”. *Int. J. of Heat Mass Transfer*, Vol. 41, pp.780–784, 2005.
- [17] Wen, T., J., Zhi, G. Q., Zeng, Y. L., Jian, F. G., Ding, Z., and Wen, Q. T., “Pool boiling heat transfer of R134a on single horizontal tube surfaces sintered with open celled copper foam”. *Int. J. of Thermal Sciences*, Vol.50, pp. 2248-2255, 2011.
- [18] Sarbu, I., Stefan V.E., “Correlation for Boiling Heat Transfer on Porous Surfaces Tubes”. *The Romanian Academy, Series A, Volume 12, Number 4*, pp. 332–338, 2011.

DESIGN CONSTRUCTION AND PERFORMANCE TEST OF A CROSS FLOW HEAT EXCHANGER

*Dipayan Mondal, Md. Fazla Rabbi, Prof. Dr. Md. Nawsher Ali Moral

Department of Mechanical Engineering, Khulna University of Engineering & Technology (KUET)
Khulna-9203, Bangladesh. Email: dip.kuet@gmail.com

ABSTRACT: A characteristic of heat exchanger design is the procedure of specifying a design, heat transfer area and pressure drops and checking whether the assumed design satisfies all requirements or not. The purpose of this project is how to design the heat exchanger especially for cross flow water to air heat exchanger which is the majority type of liquid to air heat exchanger. Here cross flow heat exchanger was chosen because of occupying less space and better performance. Fundamental heat transfer concepts and complex relationships involved in such exchanger are also presented in this report. This project addresses design of Heat Exchanger with the basics of thermal design, covering topics such as components of heat exchangers, classification of heat exchanger, data considered for design. The primary aim of this design is to obtain a high heat transfer rate without exceeding the allowable pressure drop. The type of design that is utilized determines the coefficient of heat transfer and thus has an effect upon the surface area needed to obtain the desired level of heat exchange. The flow pattern through most heat exchangers is a combination of counter flow, cross flow and parallel flow. But in this case cross flow are considered. Within the experimental limit the gain in temperature was to a maximum value of 10⁰C, for water flow rate of 0.014 kg/sec and air flow rate of 0.01 kg/sec. Within the experimental limit the logarithmic mean temperature difference (LMTD) was found from 34.63⁰C to 8.37⁰C. The efficiency and effectiveness were found to maximum of 23.11% and 0.96 respectively and overall heat transfer coefficient was found to a maximum value of 157.67w/m²⁰C.

Keywords: Cross flow; Water to air heat exchange; LMTD; effectiveness; efficiency; Temperature distribution.

1. INTRODUCTION

Heat exchangers are devices that facilitate heat transfer between two or more fluids at different temperatures. Heat transfer may occur between a solid surface and a fluid, or between solid particulates and a fluid at different temperatures and in thermal contact. Typical applications involve heating or cooling of a fluid stream of concern and evaporation or condensation of single or multi component fluid streams. In a few heat exchangers, the fluids are in direct contact for exchanging heat. In most heat exchangers, heat transfer between fluids takes place through a separating wall or into and out of wall in a transient manner. In many heat exchangers the fluids are separated by a heat transfer surface and ideally they do not mix or leak. Such exchangers are referred to as indirect transfer type heat exchanger. They are referred to as surface heat exchanger. The example of such heat exchanger is automobile radiators. In the direct contact heat exchangers, heat transfer takes place between two immiscible fluids such as a gas and a liquid [1].

There could be internal thermal energy source in the exchanger such as in electric heater or nuclear fuel elements. Combustion and chemical reaction may take place within the exchanger such in boiler fired heaters and fluidized bed exchangers [12-13]. Mechanical devices may be used in some exchangers such as in the scraped surface exchangers, agitated vessels and stirred tank reactors. Heat transfer in the separating wall of a recuperator generally takes place by conduction [4]. In general if the fluids are immiscible, the separation wall may be eliminated and the interface between the fluids replaces a heat transfer surface as in a direct contact heat exchanger. A heat exchanger consists of heat elements such as a core of a matrix containing the surface and fluid distribution such as headers manifolds, tank and inlet or outlet nozzle. Usually there are no moving parts in a heat exchanger. However there are exceptions such as a rotary regenerative exchanger, scraped surface heat exchanger [9].

Common appliances containing a heat exchanger include air conditioners, refrigerators, and space heaters. These devices are also used in chemical processing and power production. Perhaps the most

commonly known heat exchanger is a car radiator, which cools the hot radiator fluid by taking advantage of airflow over the surface of the radiator [2].

In the cross-flow heat exchanger, the two fluids usually flow at right angles, i.e., the hot and cold fluids are flows at the right angle to each other. Unlike a rotary heat exchanger, a cross-flow heat exchanger does not exchange humidity and there is no risk of short-circuiting the airstreams [1].

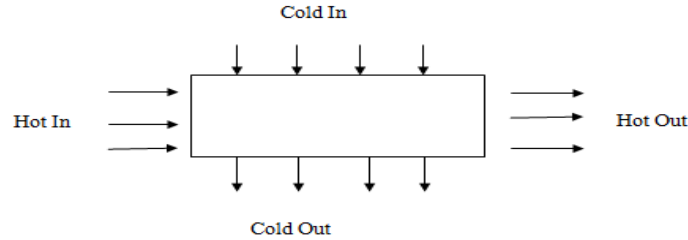


Fig.1: Cross flow arrangement

2. MATERIALS AND DESIGN CRITERIA

2.1. Materials used and stepwise construction

At first copper tube was bended using sand and then the copper tube was placed into the wooden frame. Galvanized Iron pipe was holed by 1.5mm drill bit. Then it was hanged up along the copper tube surrounding the sheet metal with the wooden frame. Separate thermocouple wires were used to determine the temperature of the different position of the copper tube. An overhead tank was made for the storage of hot water. A gate valve was used through which the mass flow rate of hot water from the tank to the galvanized iron pipe. A blower was connected with the copper tube for the supply of air to the tube. Cotton and polythene were used as insulation.

2.2. Design condition

The design conditions are usually specified for estimating heat transfer between inside and outside. It was desired to determine the exit temperatures of the fluids for various entrance conditions. Particular set of conditions depends on many factors other than heat transfer aspects- like cost, space requirements, personal opinions of the designer etc.

2.3. Selection of Fluid

Two kinds of fluid both of unmixed are used in where the cold fluid, supply air passes inside the copper tube and at every point it gains heat. The supply hot water enters the galvanized iron pipe at a certain higher temperature and exit the pipe at a certain lower temperature.

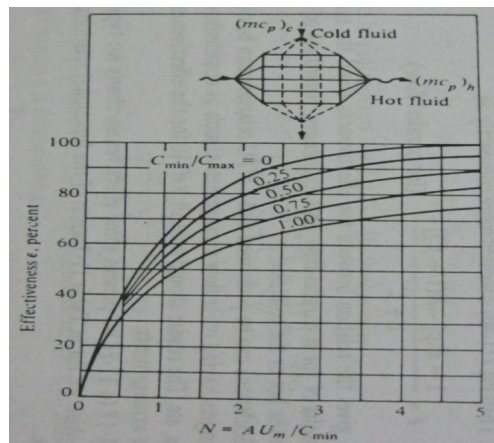


Fig. 2: Effectiveness for a cross flow heat exchanger, both fluids unmixed [5] & [8].

2.4. Theoretical aspects

The total amount of heat transfer [1] is denoted by;

$$Q = mC_p \Delta T$$

Where, m is total mass flow, $\text{kg}\cdot\text{s}^{-1}$; C_p is the specific heat of the fluid, $\text{J}\cdot\text{kg}^{-1}\cdot\text{K}^{-1}$; ΔT is the temperature difference in heat exchanger, $^{\circ}\text{K}$. The overall heat transfer coefficient U is calculated with the following relations [6]; $Q = UA\Delta T_{\text{ln}}$

Where, Q = Total heat transfer (W); U = Overall heat transfer coefficient ($\text{W}/(\text{m}^2\cdot\text{K})$); A = Heat transfer surface area (m^2); ΔT_{ln} = log mean temperature difference ($^{\circ}\text{K}$)

Heat transfer for pulsating flow in a curved pipe was numerically studied by Guo et al. for fully developed turbulent flow for the Reynolds number range of 6000 to 18000 [1]. The Nusselt No. is given below; $Nu = 0.328\text{Re}^{0.58} \text{Pr}^{0.4}$ Again for forced convection and flow inside the cylinder, Nusselt number is given by $Nu = 0.023\text{Re}^{0.8} \text{Pr}^{0.4}$. This equation is called Dittus-Boelter equation which can be used only when $\text{Re} > 10000$. For forced convection and flow over the cylinder,

Nusselt number is given by $Nu = (0.04\text{Re}^{0.5} + 0.06\text{Re}^{2/3})\text{Pr}^{0.4}$.

This equation is called Whitaker correlation which can be used only when $40 < \text{Re} < 100000$ [1]. The heat transfer coefficient (h) [6] is calculated from the relation below; $Nu = \frac{h \times D_m}{k}$ where, D_m = diameter of copper tube. The LMTD is calculated from the expression [10];

$$\Delta T = \frac{\Delta T_i - \Delta T_e}{\ln\left(\frac{\Delta T_i}{\Delta T_e}\right)}$$

Where, the grouping of terms $N = NTU = \frac{UA}{C_{\text{min}}}$ is called the number of transfer units (NTU) and

$$C = \frac{C_{\text{min}}}{C_{\text{max}}}$$

2.5. Summary of Design

Assumptions:

Inlet and outlet temperatures of hot water of the pipe respectively, $T_{h1} = 80^{\circ}\text{C}$ & $T_{h2} = 65^{\circ}\text{C}$

Inlet and outlet temperatures of cold air of the pipe respectively, $T_{c1} = 30^{\circ}\text{C}$ & $T_{c2} = 40^{\circ}\text{C}$

Arbitrary selections:

Diameter of the copper tube, $D_m = 0.013\text{m}$

Number of holes on the galvanized iron pipe = 3 Row each of 18 holes

Diameter of the each hole = 0.0015m

Mass flow rates of hot water and cold air respectively, $m_h = 0.027\text{kg/s}$ & $m_c = 0.00564\text{kg/s}$

For film temperature of water;

If drill bit diameter is d then,

$$u = \frac{4 \times m}{12 \times \pi \times \rho \times d^2} = \frac{4 \times 0.027}{12 \times \pi \times 979.77 \times 0.0015^2} = 1.27\text{m/s}^2$$

$$R_e = \frac{u \times D_m}{\nu} = \frac{1.27 \times 0.013}{0.421 \times 10^{-6}} = 39216.15$$

Whitaker correlation; $Nu = \left(0.04Re^{0.5} + 0.06R^{2/3}\right) Pr^{0.4}$ & $Nu = \frac{h_i \times D_m}{k}$; and then

find $h_i = 76580.02 w / m^2 . ^\circ C$ Again for cold air; $Re = \frac{4m_c}{\pi D_m \mu} = 30594.85$ Dittus-Boelter correlation;

$Nu = 0.023Re^{0.8} Pr^{0.4} = 80.49$ & $Nu = \frac{h_o \times D_m}{k}$; and then find $h_o = 160.98 w / m^2 . ^\circ C$

Now, $U = \frac{1}{\left(\frac{1}{h_i}\right) + \left(\frac{1}{h_o}\right)} = 154.48 w / m^2 . ^\circ C$ & $\Delta T = \frac{\Delta T_i - \Delta T_e}{\ln\left(\frac{\Delta T_i}{\Delta T_e}\right)} = 37.44 ^\circ C$

Again, $Q = m_h C_{ph} (T_{h1} - T_{h2}) = 1697.09 w$ and using Correction factor, $F = 0.96$ with the help of $Q = FAU\Delta T_{in} = F(\pi D_m L)U\Delta T_{in}$ it is found $L = 7.51 m$;

A suction type air blower having capacity $1hp, 5200rpm$

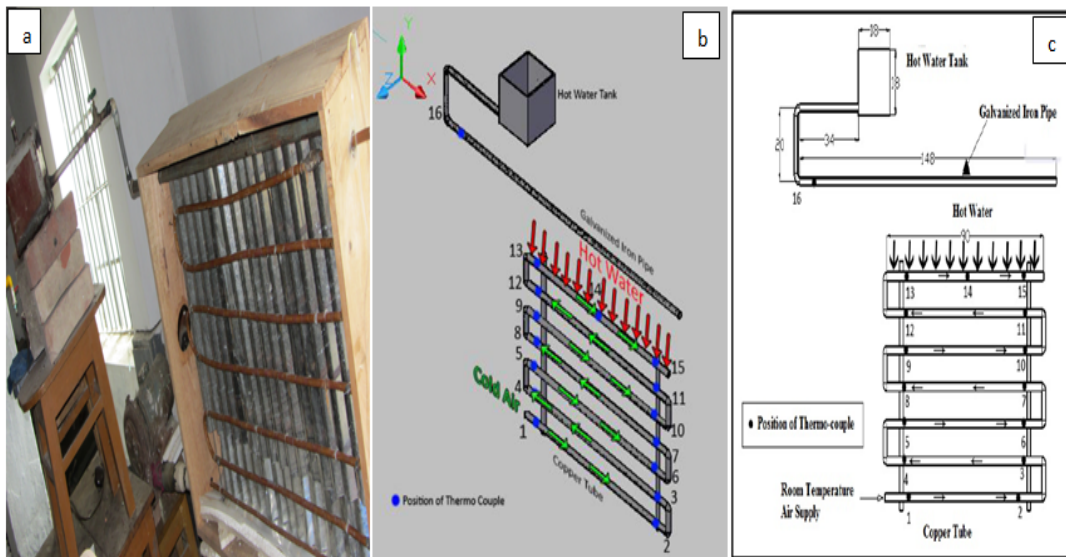


Fig. 3: (a) Isometric view (Constructional); (b) Isometric view; (c) Schematic diagram for cross flow heat exchanger.

3. PRESENTATION OF DATA

The recorded data are measured by experimentally and hence inlet and outlet temperatures are found from inlet and outlet sections respectively. Again from T_2 to T_7 temperatures are measured as average of 2-3, 4-5, 6-7, 8-9, 10-11, 12-13 points temperatures respectively as per above drawings.

Table1: Experimental data for cross flow heat exchanger for case I

No. of obs	Flow Rate of hot water m_h (kg/s)	Flow Rate of cold air m_c (kg/s)	Type of fluids	Inlet Temp. T_1 (°C)	T_2 (°C)	T_3 (°C)	T_4 (°C)	T_5 (°C)	T_6 (°C)	T_7 (°C)	Outlet Temp. T_8 (°C)
1	0.0120	0.01	Hot water	75							65
			Cold air	30	32	34	35	37	37	39	39
2	0.0074	0.01	Hot water	70							58
			Cold air	30	30	32	33	35	36	37	37
3	0.0063	0.01	Hot water	64							43
			Cold air	29	29	31	33	34	34	36	37
4	0.0061	0.01	Hot water	60							42
			Cold air	28	29	31	32	34	34	35	36
5	0.0082	0.01	Hot water	57							40
			Cold air	28	32	32	32	35	35	37	38
6	0.0110	0.01	Hot water	50							39
			Cold air	28	29	31	32	34	35	36	37
7	0.0070	0.01	Hot water	48							37
			Cold air	28	29	31	32	34	35	35	36

Table2: Experimental data for cross flow heat exchanger for case II

No. of obs	Flow Rate of hot water m_h (kg/s)	Flow Rate of cold air m_c (kg/s)	Type of fluids	Inlet Temp. T_1 (°C)	T_2 (°C)	T_3 (°C)	T_4 (°C)	T_5 (°C)	T_6 (°C)	T_7 (°C)	Outlet Temp. T_8 (°C)
8	0.0140	0.01	Hot water	63							54
			Cold air	29	32	33	34	35	35	36	38
9	0.0089	0.01	Hot water	59							49
			Cold air	29	30	30	32	33	35	36	37
10	0.0078	0.01	Hot water	56							48
			Cold air	29	29	31	32	33	34	35	35
11	0.0125	0.01	Hot water	50							41
			Cold air	30	31	31	33	34	35	36	37
12	0.0090	0.01	Hot water	48							39
			Cold air	28	31	33	33	34	35	36	36
13	0.0110	0.01	Hot water	45							40
			Cold air	27	28	30	31	31	32	32	33

4. RESULTS AND DISCUSSIONS

Table 3 Result for cross flow heat exchanger for case I

No. of obs.	Effectiveness ε	LMTD ($^{\circ}\text{C}$)	Efficiency, η (%)	Overall heat transfer coefficient $\text{w/m}^2\cdot^{\circ}\text{C}$
1	0.94	34.63	18.03	157.67
2	0.91	29.49	18.95	157.67
3	0.87	17.11	16.08	157.67
4	0.86	18.55	18.5	157.67
5	0.91	15.23	17.25	157.67
6	0.92	11.97	17.26	157.67
7	0.96	10.87	13.6	157.67

Table 4: Result for cross flow heat exchanger for case II

No. of obs.	Effectiveness	LMTD ($^{\circ}\text{C}$)	Efficiency, η (%)	Overall heat transfer coefficient $\text{w/m}^2\cdot^{\circ}\text{C}$
8	0.96	25.16	13.35	157.67
9	0.94	19.64	21.61	157.67
10	0.91	19.15	23.11	157.67
11	0.95	9.94	14.96	157.67
12	0.94	8.37	17.81	157.67
13	0.95	10.89	17.48	157.67

Temperature distribution curves and performance curves

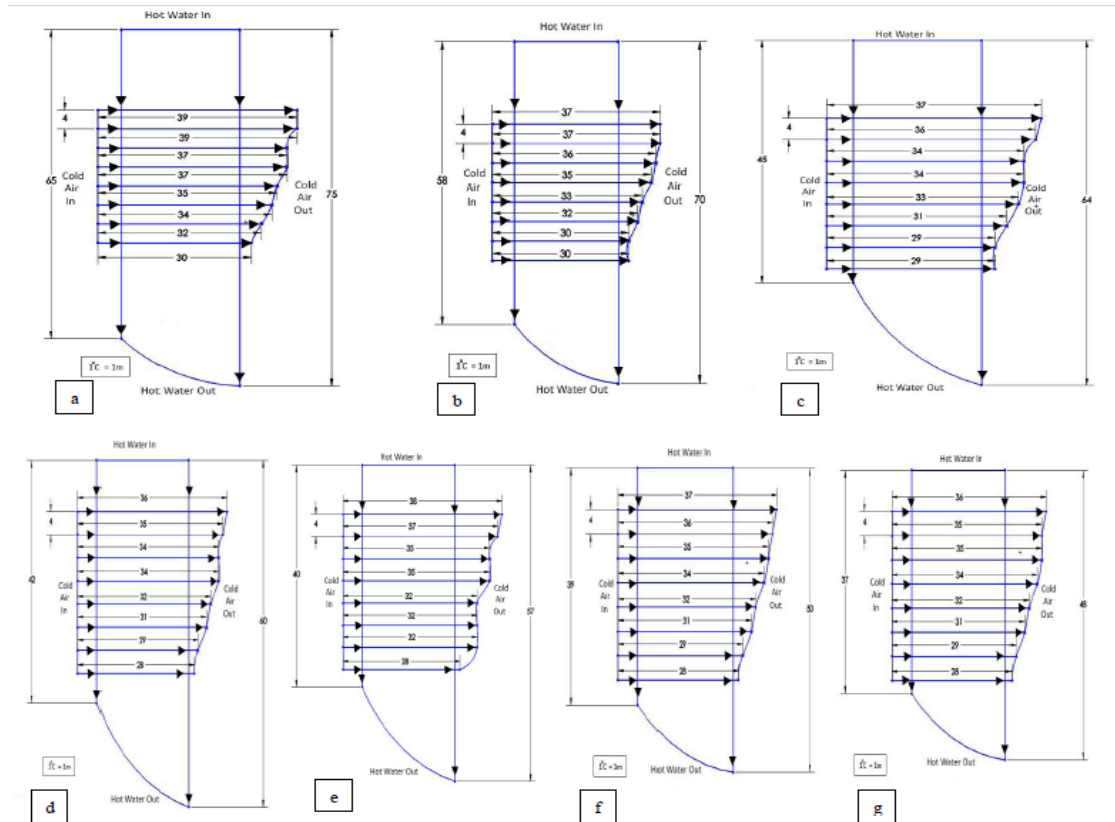


Fig. 4: (a to g) Temperature distribution curve for observation 1 to 7 for the case I

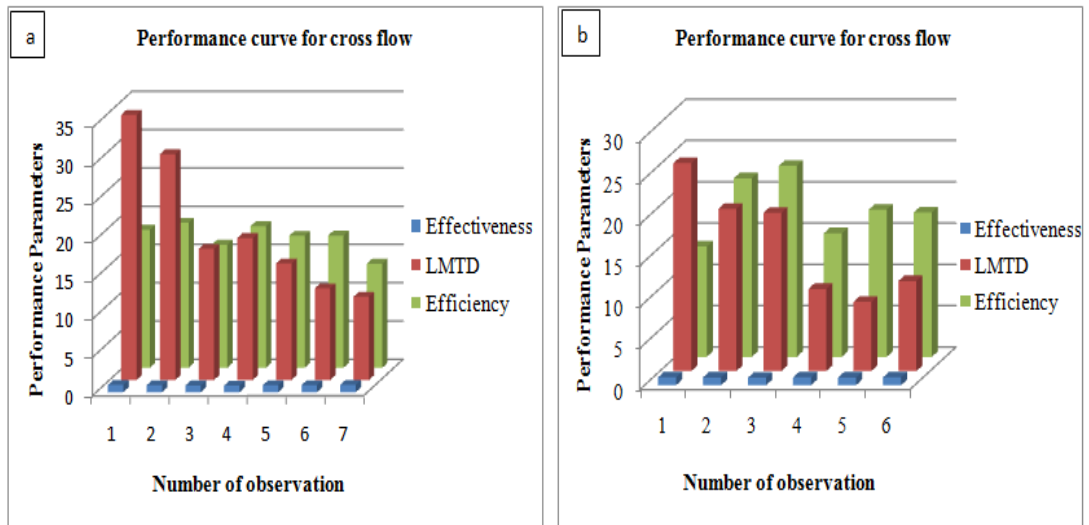


Fig. 5: Performance curves (a) for cross flow heat exchanger for case I; (b) for counter flow heat exchanger for case II.

Under the steady condition, data were collected and recorded and hence the mass flow rate of hot water was varied and the mass flow rate of cold air was fixed. The hot water varied from 0.012 kg/sec to 0.0061 kg/sec and mass flow rate of cold air kept constant at 0.01 kg/sec. From Table-1 &

Fig. 4, it is observed that during flow the temperature of hot water was varied from 75⁰C to 48⁰C and the cold air temperature was varied from 30⁰C to 28⁰C and it was also observed that to pass the entire length of copper tube, the hot water temperature was decreased from 65⁰C to 37⁰C and air temperature was increased from 33⁰C to 38⁰C. From Table-3. and Fig.5 (a), it is observed that the calculated LMTD was varied from 34.63⁰C to 10.87⁰C, efficiency was varied from 18.95% to 13.6% and effectiveness was varied from 0.96 to 0.86.

Again from Table-2, it is observed that during flow the temperature of hot water was varied from 63⁰C to 45⁰C and the cold air temperature was varied from 29⁰C to 27⁰C and it was also observed that to pass the entire length of copper tube, the hot water temperature was decreased from 54⁰C to 40⁰C and air temperature was increased from 33⁰C to 38⁰C. From Table 3. and Fig.5 (b), it is observed that the calculated LMTD was varied from 25.16⁰C to 8.37⁰C, efficiency was varied from 23.11% to 13.35% and effectiveness was varied from 0.96 to 0.91.

The designed value that was assumed was not obtained during experiment. It was deviated. The mass flow rate of hot water was not maintained as the assumed value due to the low head tank. The mass flow rate of air was obtained by calibrating with previous data which was not maintained as the assumed value. The hot water was flow over the copper tube from the galvanized iron pipe which was not contacted all the portion of the copper tube due to the alignment problem. So the temperature difference was not obtained as the assumed value. And the result of this experiment was fluctuated from the design result.

5. CONCLUSION

On the basis of the experimental the gain in temperature was to a maximum value of 10⁰C, for water flow rate of 0.014 kg/sec and air flow rate of 0.01 kg/sec. Within the experimental limit LMTD was found from 34.63⁰C to 8.37⁰C. The efficiency, effectiveness and the LMTD were found to a maximum value of 23.11%, 0.96 and 34.63⁰C respectively. Overall heat transfer coefficient was found to a maximum value of 157.67 w/m².⁰C

REFERENCES

[1] Ozisik, M.N; “Heat Transfer, A Basic Approach.” International Edition, 1985; Tata McGraw-Hill Publishing Company Limited; New Delhi
 [2] <http://1heatexchanger.info/2009/10/what-is-a-heat-exchanger-2/>
 [3] http://www.engineersedge.com/heat_transfer/parallel_counter_flow_designs.htm
 [4] http://en.wikipedia.org/wiki/Heat_exchanger/Plate_heat_exchanger
 [5] Kays, W.M., and A. L. London: Compact Heat Exchangers, 2nd edition, McGraw-Hill, New York, 1964
 [6] http://en.wikipedia.org/wiki/Heat_transfer_coefficient
 [7] http://en.wikipedia.org/wiki/Log_mean_temperature_difference
 [8] <http://en.wikipedia.org/wiki/Effectiveness>
 [9] Nag, P.K; “Heat and Mass Transfer,” Second Edition; Tata McGraw-Hill Publishing Company Limited; New Delhi
 [10] Holman, J.P; “Heat Transfer”, Ninth Edition, 2004; Tata McGraw-Hill Publishing Company Limited; New Delhi
 [12] <http://www.genemco.com/alo/movingheatexchanger.gif>
 [13] http://www.tpub.com/content/doe/h1018v1/css/h1018v1_77.htm

Nomenclature					
Symbols	Meaning	Unit	Symbols	Meaning	
D _i & d _o	Inside & outside diameter of the small tube	m	Re	Reynolds number	
d _i & d _o	Inside & outside diameter of the large tube	m	Nu	Nusselt number	

m_h & m_c	Mass flow rate of hot water & cold air	kg/s	Pr	Prandalt number
h	Convective heat transfer coefficient	$w/m^2 \cdot ^\circ C$	Q	Total heat transfer rate
w				
U	Overall heat transfer coefficient	$w/m^2 \cdot ^\circ C$	D_m	Effective diameter
m				
ΔT_{lm}	Logarithmic Mean Temperature Difference (LMTD)	$^\circ C$	K	Thermal conductivity
$w/m \cdot ^\circ C$				

EFFECTS OF VISCOUS DISSIPATION AND HEAT GENERATION ON NATURAL CONVECTION FLOW ALONG A VERTICAL WAVY SURFACE

Nazma Parveen and Sujon Nath*

Department of Mathematics, Bangladesh University of Engineering and Technology
Dhaka-1000, Bangladesh, nazma@math.buet.ac.bd

*M.Phil student, Department of Mathematics, Bangladesh University of Engineering and
Technology Dhaka-1000, Bangladesh, sujon.buet@yahoo.com

ABSTRACT: This paper is devoted to the study of viscous dissipation effects on natural convection flow of viscous incompressible fluid along a uniformly heated vertical wavy surface in the presence of heat generation. Adopting a suitable transformation, the governing nonlinear partial differential equations with their corresponding boundary conditions are first converted to non-dimensional form. The equations are mapped into the domain of a vertical flat plate and then solved numerically employing the implicit finite difference method with Keller-box scheme. Effects of various parameters on the surface shear stress in terms of the skin friction coefficient, the rate of heat transfer in terms of local Nusselt number, the streamlines as well as the isotherms are shown graphically for different values of parameters entering into the problem. It is shown that the numerical results are substantially dependent on the set of parameters.

Keywords: Viscous dissipation, Heat generation, Natural convection, Uniform surface temperature, Keller-box method, Wavy surface.

1. INTRODUCTION

The study of viscous dissipation in incompressible fluid is very important as it has many practical applications in different areas such as oil products transportation through ducts, glass-fiber, paper production, cooling of metallic sheet or electronic chip and so on. It is also necessary to justify the effect of viscous dissipation in presence of heat generation through an irregular surface because irregular surfaces are often present in many applications, such as radiator, heat exchangers and heat transfer enhancement devices.

From the very beginning Yao [1–2] first investigated the natural convection heat transfer from an isothermal vertical wavy surface and used an extended Prandtl's transposition theorem and a finite-difference scheme. Vajravelu and Hadjinolaou [3] studied the heat transfer characteristics in the laminar boundary layer of a viscous fluid over a stretching sheet with viscous dissipation or frictional heating and internal heat generation. In this study they considered that the volumetric rate of heat generation, $q''' [W/m^3]$, should be $q''' = Q_0(T - T_\infty)$, for $T \geq T_\infty$ and equal to zero for $T < T_\infty$, where Q_0 is the heat generation/absorption constant. Natural and mixed convection heat and mass transfer along a vertical wavy surface have been checked by Jang et al. [4]. Molla et al. [5] studied natural convection flow along a vertical wavy surface with uniform surface temperature in presence of heat generation/absorption. Alam et al. [6] investigated viscous dissipation effects on MHD natural convection flow over a sphere in the presence of heat generation. Mamun et al [7] analyzed MHD-conjugate heat transfer analysis for a vertical flat plate in presence of viscous dissipation and heat generation. Few years ago, Anjali Devi and Kayalvizhi [8] presented viscous dissipation and radiation effects on the thermal boundary layer flow with heat and mass transfer over a non-isothermal stretching sheet with internal heat generation embedded in a porous medium. Recently, Parveen and Alim [9] have observed the effects of MHD natural convection flow along a vertical wavy surface in presence of heat generation/absorption with viscosity dependent on temperature.

In all the aforementioned analyses it is demanded to research for justifying the effects of viscous dissipation and heat generation on natural convection flow along a vertical wavy surface and the present work demonstrates the issue.

2. FORMULATION OF THE PROBLEM

The boundary layer analysis outlined below allows $\bar{\sigma}(X)$ being arbitrary, but our detailed numerical work assumed that the surface exhibits sinusoidal deformations. The wavy surface may be described by

$$Y_w = \bar{\sigma}(X) = \alpha \sin\left(\frac{n\pi X}{L}\right) \quad (1)$$

where L is the wave length associated with the wavy surface. The geometry of the wavy surface and the two-dimensional cartesian coordinate system are shown in Fig. 1.

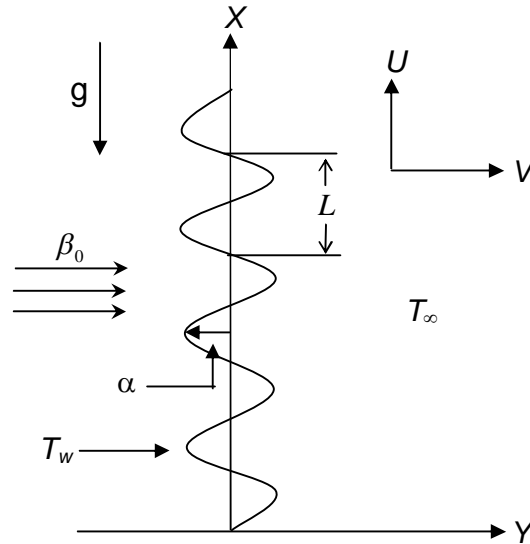


Fig.1: The coordinate system and the physical model.

The conservation equations for the flow characterized with steady, laminar and two-dimensional boundary layer; under the usual Boussinesq approximation, dimensionless form of the continuity, momentum and energy equations can be written as:

$$\frac{\partial u}{\partial x} + \frac{\partial v}{\partial y} = 0 \quad (2)$$

$$u \frac{\partial u}{\partial x} + v \frac{\partial u}{\partial y} = -\frac{\partial p}{\partial x} + Gr^{1/4} \sigma_x \frac{\partial p}{\partial y} + (1 + \sigma_x^2) \frac{\partial^2 u}{\partial y^2} + \theta \quad (3)$$

$$\sigma_x \left(u \frac{\partial u}{\partial x} + v \frac{\partial u}{\partial y} \right) = -Gr^{1/4} \frac{\partial p}{\partial y} + \sigma_x (1 + \sigma_x^2) \frac{\partial^2 u}{\partial y^2} - \sigma_{xx} u^2 \quad (4)$$

$$u \frac{\partial \theta}{\partial x} + v \frac{\partial \theta}{\partial y} = \frac{1}{Pr} (1 + \sigma_x^2) \frac{\partial^2 \theta}{\partial y^2} + Q\theta + N \left(\frac{\partial u}{\partial y} \right)^2 \quad (5)$$

where $Pr = \frac{C_p \mu}{k}$ is the Prandtl number, $Q = \frac{Q_0 L^2}{\mu C_p Gr^{1/2}}$ is the heat generation parameter and

$N = \frac{\nu^2 Gr}{L^2 C_p (T_w - T_\infty)}$ is the viscous dissipation parameter.

Using Prandtl's transposition theorem to transform the irregular wavy surface into a flat surface as extended by Yao [2] and boundary-layer approximation, the following dimensionless variables are introduced for non-dimensionalizing the governing equations,

$$x = \frac{X}{L}, \quad y = \frac{Y - \bar{\sigma}}{L} Gr^{\frac{1}{4}}, \quad p = \frac{L^2}{\rho v^2} Gr^{-1} P$$

$$u = \frac{L}{v} Gr^{-\frac{1}{2}} U, \quad v = \frac{L}{v} Gr^{-\frac{1}{4}} (V - \sigma_x U),$$

$$\theta = \frac{T - T_\infty}{T_w - T_\infty}, \quad \sigma_x = \frac{d\bar{\sigma}}{dX} = \frac{d\sigma}{dx}, \quad Gr = \frac{g\beta(T_w - T_\infty)}{v^2} L^3$$

where θ is the non-dimensional temperature function and (u, v) are the dimensionless velocity components.

It can easily be seen that the convection induced by the wavy surface is described by equations (2)–(5). We further notice that, equation (11) indicates that the pressure gradient along the y -direction is $O(Gr^{-\frac{1}{4}})$, which implies that lowest order pressure gradient along x -direction can be determined from the inviscid flow solution. For the present problem this pressure gradient ($\partial p / \partial x = 0$) is zero. Equation (4) further shows that $Gr^{\frac{1}{4}} \partial p / \partial y$ is $O(1)$ and is determined by the left-hand side of this equation. Thus, the elimination of $\partial p / \partial y$ from equations (3) and (4) leads to

$$u \frac{\partial u}{\partial x} + v \frac{\partial u}{\partial y} = (1 + \sigma_x^2) \frac{\partial^2 u}{\partial y^2} - \frac{\sigma_x \sigma_{xx}}{1 + \sigma_x^2} u^2 + \frac{1}{1 + \sigma_x^2} \theta \quad (6)$$

The corresponding boundary conditions for the present problem are:

$$\left. \begin{aligned} u = v = 0, \quad \theta = 1 \quad \text{at} \quad y = 0 \\ u = \theta = 0, \quad p = 0 \quad \text{as} \quad y \rightarrow \infty \end{aligned} \right\} \quad (7)$$

Now we introduce the following transformations to reduce the governing equations to a convenient form:

$$\psi = x^{\frac{3}{4}} f(x, \eta), \quad \eta = yx^{-\frac{1}{4}}, \quad \theta = \theta(x, \eta) \quad (8)$$

where $f(\eta)$ is the dimensionless stream function, η is the pseudo similarity variable and ψ is the stream function that satisfies the Eq. (2) and is defined by

$$u = \frac{\partial \psi}{\partial y}, \quad v = -\frac{\partial \psi}{\partial x} \quad (9)$$

Introducing the transformations given in Eq. (8) and into Eqs. (6) and (5) the following system of non linear equations are obtained,

$$(1 + \sigma_x^2) f''' + \frac{3}{4} f f'' - \left(\frac{1}{2} + \frac{x \sigma_x \sigma_{xx}}{1 + \sigma_x^2} \right) f'^2 + \frac{1}{1 + \sigma_x^2} \theta = x \left(f' \frac{\partial f'}{\partial x} - f'' \frac{\partial f}{\partial x} \right) \quad (10)$$

$$\frac{1}{Pr} (1 + \sigma_x^2) \theta'' + \frac{3}{4} f \theta' + x^{\frac{1}{2}} Q \theta + N x f''^2 = x \left(f' \frac{\partial \theta}{\partial x} - \theta' \frac{\partial f}{\partial x} \right) \quad (11)$$

The boundary conditions (7) now take the following form:

$$\left. \begin{aligned} f(x, 0) = f'(x, 0) = 0, \quad \theta(x, 0) = 1 \\ f'(x, \infty) = 0, \quad \theta(x, \infty) = 0 \end{aligned} \right\} \quad (12)$$

In the above equations prime denote the differentiation with respect to η .

The local skin friction coefficient C_{fx} and the rate of heat transfer in terms of the local Nusselt number Nu_x takes the following form:

$$C_{fx} (Gr/x)^{1/4} / 2 = \sqrt{1 + \sigma_x^2} f''(x, 0) \quad (13)$$

$$Nu_x (Gr/x)^{-1/4} = -\sqrt{1 + \sigma_x^2} \theta'(x, 0) \quad (14)$$

3. NUMERICAL PROCEDURE

The transformed boundary layer equations are solved numerically with the help of implicit finite difference method together with the Keller-box scheme [10]. To begin with the partial differential equations (10) and (11) are first converted into a system of first order differential equations. Then these equations are expressed in finite difference forms by approximating the functions and their derivatives in terms of the central difference approximations. The above central difference approximations reduces the system of first order differential equations to a set of non-linear difference equations for the unknown at x_i in terms of their values at x_{i-1} . The resulting set of non-linear difference equations are solved by using the Newton's quasi-linearization method. The Jacobian matrix has a block-tridiagonal structure and the difference equations are solved using a block-matrix version of the Thomas algorithm.

4. RESULTS

Here we have shown the combined effects of viscous dissipation and heat generation on natural convection flow of viscous incompressible fluid along a uniformly heated vertical wavy surface. The skin friction coefficient C_{fx} , the rate of heat transfer in terms of Nusselt number Nu_x , the streamlines as well as the isotherms are shown graphically in Figs. 2-7 for different values of the aforementioned physical parameters.

The variation of local skin friction C_{fx} and the rate of heat transfer in terms of the local Nusselt number Nu_x against x from the wavy surface while $\alpha = 0.3$, $Q = 0.5$, and $Pr = 1.73$ are illustrated in Fig. 2(a) and 2(b) respectively. Since the higher value of N accelerates the fluid flow and increases the temperature so from the figure it is noted that for the viscous dissipation parameter $N = (0.0, 0.5, 1.0, 2.0)$, the skin friction coefficient increases along the upstream direction of the surface and to decrease of the heat transfer rates.

The influence of the parameter Q , on the skin friction coefficient C_{fx} and local rate of heat transfer Nu_x are illustrated in Figs 3(a) and 3(b) respectively while $\alpha = 0.3$, $N = 0.5$ and $Pr = 1.73$. From those it is observed that an increase in the heat generation parameter $Q = (0.0, 0.4, 0.8, 1.0)$ leads to increase the local skin friction coefficient C_{fx} and decrease the local rate of heat transfer Nu_x at different position of x . These are happened, since the heat generation mechanism creates a layer of hot fluid near the surface and finally the resultant temperature of the fluid exceed the surface temperature and temperature gradient decreases. For this reason the rate of heat transfer decreases. Increasing temperature increases the viscosity of the fluid. Hence the corresponding shearing stress in terms of local skin friction coefficient increases.

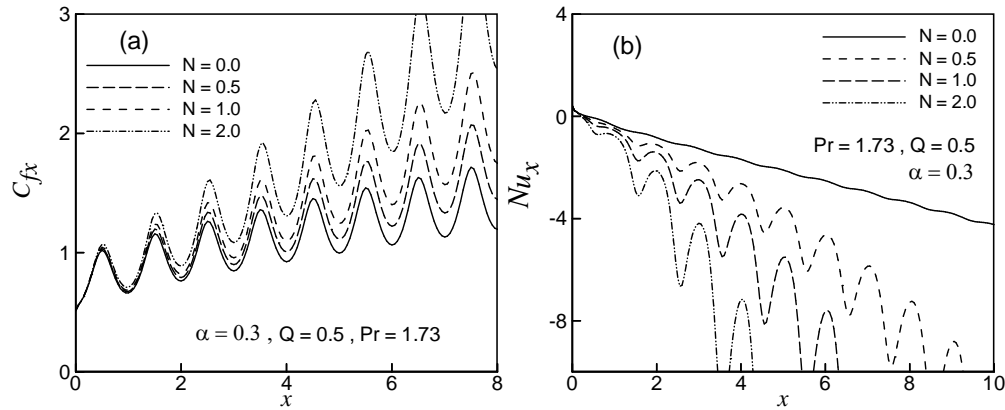


Fig. 2: Effect of N on (a) skin friction coefficient C_{fx} and (b) rate of heat transfer Nu_x .

Fig. 4 and Fig. 5 show the effect of viscous dissipation parameter $N = (0.0, 0.5, 1.0, 2.0)$ on the formulation of streamlines and isotherms respectively while $Pr = 1.73, Q = 0.5$ and $\alpha = 0.3$. We find that for $N = 0.0$ the value of ψ_{max} is 12.52, for $N = 0.5$ ψ_{max} is 13.25, for $N = 1.0$ ψ_{max} is 14.29 and for $N = 2.0$ ψ_{max} is 15.82. From Fig. 4, it is seen that the effect of viscous dissipation parameter N , the flow rate in the boundary layer increases. From Fig 5, it is also observed that due to the effect of N , the thermal state of the fluid increases. Finally, the thermal boundary layer becomes thicker.

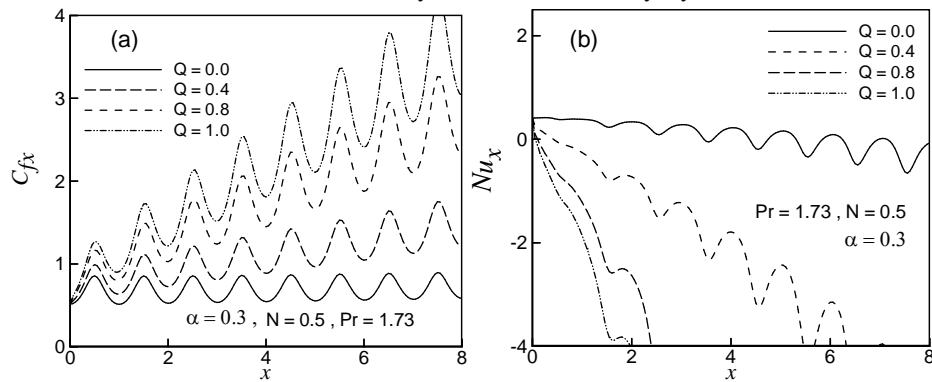


Fig. 3: Effect of Q on (a) skin friction coefficient C_{fx} and (b) rate of heat transfer Nu_x .

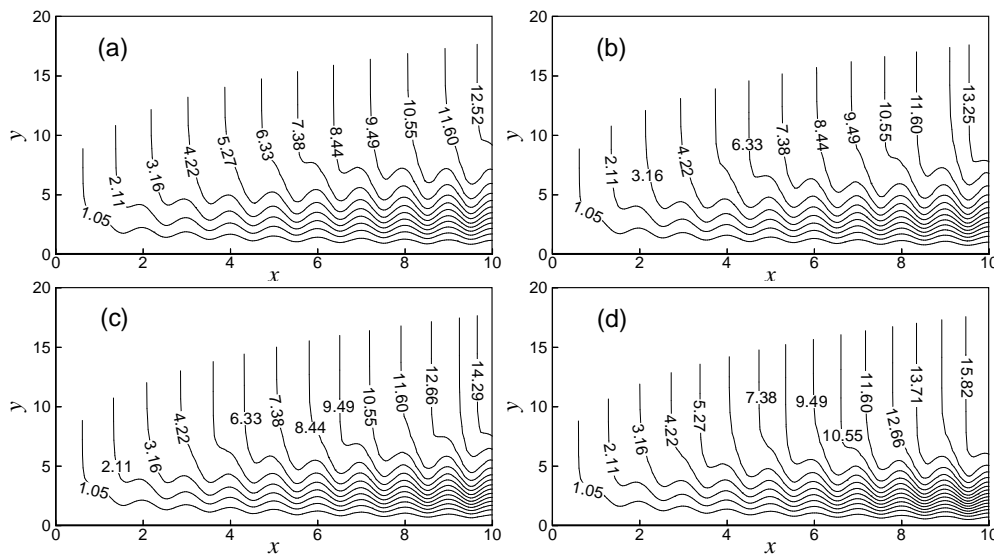


Fig. 4: Streamlines for (a) $N = 0.0$ (b) $N = 0.5$ (c) $N = 1.0$ and (d) $N = 2.0$ while $Pr = 1.73, Q = 0.5$ and $\alpha = 0.3$.

The effect of variation of the Q equal to 0.0, 0.4, 0.8 and 1.0 on the streamlines and isotherms are depicted by the Fig. 6 and 7 respectively while $\alpha = 0.3$, $N = 0.5$ and $Pr = 1.73$. Figure 6 depicts that the maximum values of ψ increases while the values of Q increases that is ψ_{max} are 7.72, 11.76, 16.17 and 17.63 for $Q = 0.0, 0.4, 0.8$ and 1.0 respectively. It is noted from Fig. 7 that as the value of Q increases the thermal boundary layer becomes thicker gradually. So the isotherms increases while the values of Q increases.

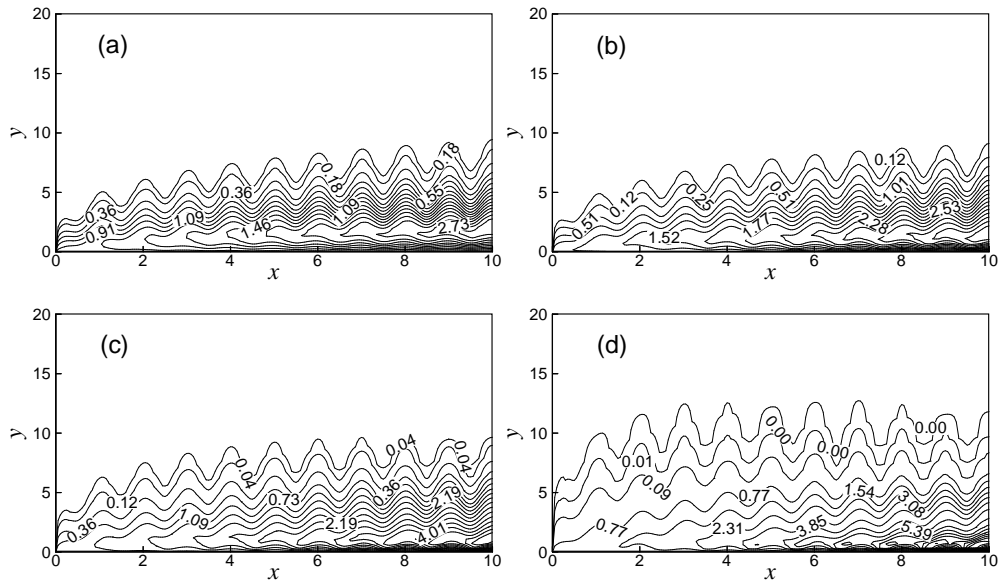


Fig. 5: Isotherms for (a) $N = 0.0$ (b) $N = 0.5$ (c) $N = 1.0$ and (d) $N = 2.0$ while $Pr = 1.73$, $Q = 0.5$ and $\alpha = 0.3$.

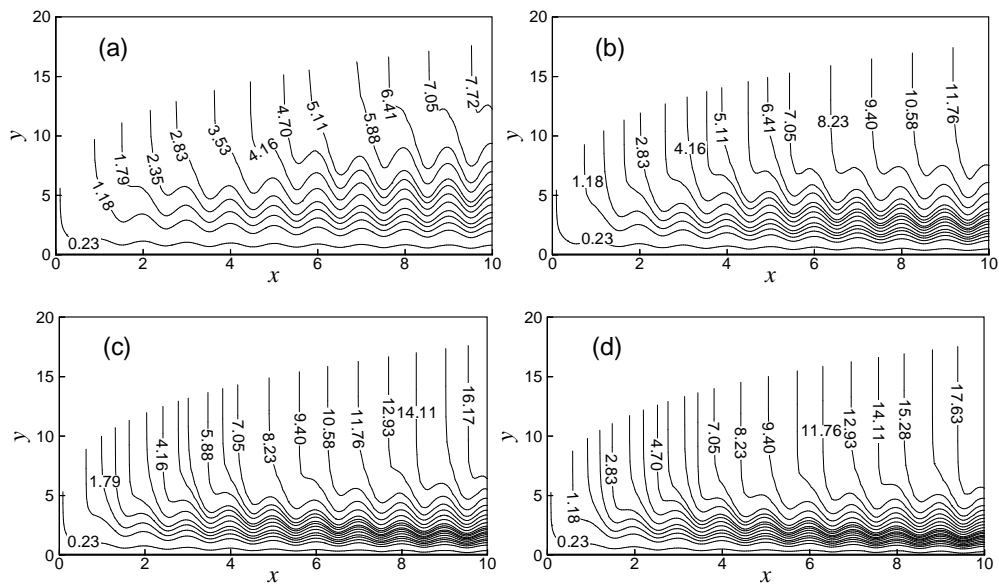


Fig. 6: Streamlines for (a) $Q = 0.0$ (b) $Q = 0.4$ (c) $Q = 0.8$ and (d) $Q = 1.0$ while $Pr = 1.73$, $N = 0.5$ and $\alpha = 0.3$.

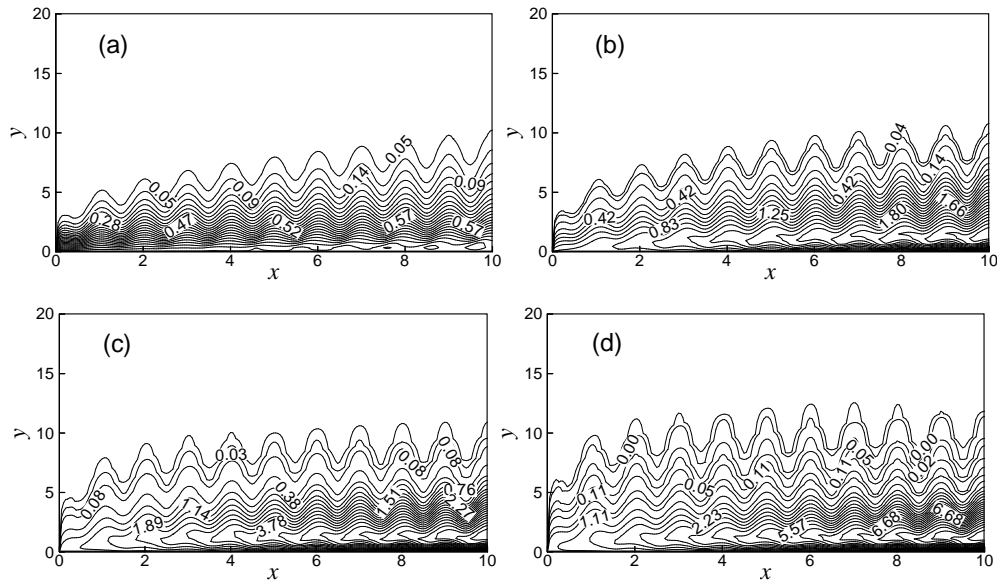


Fig. 7: Isotherms for (a) $Q = 0.0$ (b) $Q = 0.4$ (c) $Q = 0.8$ and (d) $Q = 1.0$ while $Pr = 1.73$, $N = 0.5$ and $\alpha = 0.3$.

5. CONCLUSION

The combined effects of viscous dissipation and heat generation on natural convection flow along a vertical wavy surface have been studied. From the present investigation the following conclusions may be drawn:

- The skin friction coefficient C_{fx} has increased and the rate of heat transfer in terms of Nusselt number Nu_x has decreased for the effect of viscous dissipation parameter N and heat generation parameter Q .
- Streamlines have changed slightly too upper and the same results are observed for thermal boundary layer thickness with the increasing values of viscous dissipation parameter N and heat generation parameter Q .

6. REFERENCES

[1] L. S. Yao, Natural Convection along a Vertical Wavy Surface, *ASME J. Heat Transfer*, 105, pp. 465–468, 1983.

[2] L. S. Yao, A note on Prandtl's Transposition Theorem, *ASME J. Heat Transfer*, 110, pp. 503–507, 1988.

[3] K. Vejravelu and A. Hadjinicolaou, Heat transfer in a viscous fluid over a stretching sheet with viscous dissipation and internal heat generation, *Int. comm. Heat Transfer*, 20, pp. 417-430, 1993.

[4] J. H. Jang, W. M. Yan and H. C. Liu, Natural Convection Heat and Mass Transfer along a Vertical Wavy Surface, *Int. J. Heat Mass Transfer*, 46, pp. 1075–1083, 2003.

[5] M. M. Molla, M. A. Hossain and L. S. Yao, Natural Convection Flow along a Vertical Wavy Surface with Uniform Surface Temperature in Presence of Heat Generation/Absorption, *Int. J. Therm. Sci.*, 43, pp. 157-163, 2004.

[6] M. M. Alam, M.A. Alim and M. M. K. Chowdhury, Viscous Dissipation Effects on MHD Natural Convection Flow over a Sphere in the Presence of Heat Generation, *Nonlinear Analysis: Modelling and Control*, 12, No.4, 447-459, 2007

[7] A. A. Mamun, Z. R. Chowdhury, M. A. Azim and M. M. Molla, MHD-Conjugate Heat Transfer Analysis for a Vertical Flat Plate in Presence of Viscous Dissipation and Heat Generation, *Int. comm. Heat Transfer*, 35, pp. 1275-1280, 2008.

[8] S. P. A. Devi and M. Kayalvizhi, Viscous Dissipation and Radiation effects on the Thermal Boundary Layer Flow with Heat and Mass transfer over a Non-Isothermal Stretching Sheet with

internal Heat Generation embedded in a Porous Medium, Int. J. Energy Technology, 2(20), pp. 1-10, 2010.

[9] N. Parveen and M. A. Alim, MHD natural convection flow along a vertical wavy surface in presence of heat generation/absorption with viscosity dependent on temperature, Journal of Mechanical Engineering, Vol. ME 42 (1), pp. 47-55, 2012.

[10] H. B. Keller, Numerical Methods in Boundary Layer Theory, Ann. Rev. Fluid Mech., vol. 10, pp. 417-433, 1978.

DESIGN & OPTIMIZATION OF A RADIAL FLOW HEAT SINK UNDER FREE CONVECTION AT STEADY STATE CONDITION

¹M.M.Rahman, ²H.Bhowmik and ³M.Kamruzzaman

¹Lecturer and ^{2,3} Associate Professor

Department of Mechanical Engineering, DUET, Gazipur, Bangladesh.

Email: mostafiz00360@duet.ac.bd

Abstract: Three dimensional numerical models were developed to make prediction free convection heat transfer at steady state condition from radial flow heat sink. The air was considered as the medium of heat transfer. In radial flow heat sink, heat conducts through base in radial pattern and is uniformly transported to the fins. The Tagucy method was used to investigate the effect of several design parameters such as fin length, fin height, number of fins and heat sink base radius on heat transfer. There are five factors and four levels on each factor were chosen. Sixteen types of model were analyzed to obtain total heat transfer for each model. The result was used to estimate the optimum designed values of the parameters affecting the heat sink efficiency. The reproducibility of the optimum design value was verified. The average rate of heat transfer of optimum model was increased by more than 50 % than the reference model. Finally, the heat transfer data of radial flow heat sink were correlated of several outer radius by an equation.

Keywords: Natural convection, Laminar flow, Radial flow, Heat transfer, Optimization

1. INTRODUCTION

Natural convection heat transfer from finned surface is used for the thermal management of low power-density devices. Radial flow heat sink with finned surfaces has been extensively used in many applications. These types of heat sinks can be a very successful solution for LED application and processor based desktop computer. The heat sink with radial fin orientation provides uniform temperature distribution at equilateral distances from the base, which enhances the thermal performance. All these imported issues provided motivation of the present study.

The performance analysis and optimization of conventional heat sinks were studied by many researchers both experimentally and numerically [1-7]. A theoretical and experimental study was conducted by Kobus and Oshio [1], to study the effect of various geometries on thermal resistance of the heat sink. In the natural convection region, the author obtained the improved performance at the increased fin length, while the fin spacing was constant. Huang et al. [2] investigated the orientation effect of square pin fin on natural convection heat transfer and obtained the high heat transfer coefficient at the upward and sideward facing orientation. Zografos and Sunderland [3] analyzed the heat transfer performance of inline and staggered pin fins and obtained better performance from inline fins compared to the staggered fins. Sparrow and Vemuri [4] investigated the effect of heat transfer on the fin orientation and obtained the highest heat transfer coefficient at the upward facing orientation. The authors also optimized the fin density and height. Inada et al. [5] investigated experimentally the effects of vertical fins with constant height on heat transfer rate. The authors also investigated the effects of flow orientation and obtained an enhanced heat transfer rate at the upward flows.

As this survey shows, many of the analyses were based on the heat transfer from the rectangular plate fin heat sink, and completely ignored the transfer of heat for the radial fluid flow conditions and optimization of such types of heat sink. The present analysis simulated the natural convection heat transfer from an array of aluminum rectangular fins that were oriented radially on a horizontal circular base plate. Parametric studies were performed in order to determine the optimum heat sink. The optimum design value of each parameter was presented, and the reproducibility of the results was discussed. Finally, the heat transfer data at different outer radius were correlated.

2. DESCRIPTION OF THE GEOMETRY

Geometric dimension of the heat sink

The radial flow heat sink with rectangular fins is arrayed as shown in Figure 1. The baseline design consisted of long, medium and short fins, arranged radially along the flow direction.

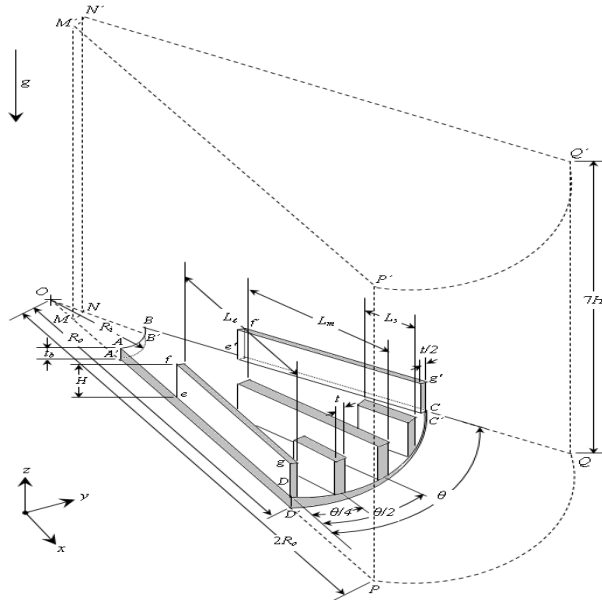


Fig.1: Schematic diagram of the heat sink

To increase the surface area for heat transfer, compared to the case with only long fins, the medium and short fins were introduced. The heat sink base and fins were made of Aluminum of thermal conductivity, 202.4 W/(m·K). The considered heat transfer medium was air (Pr = 0.7). Heat sink geometry was described by the fin lengths L_l, L_m, L_s , fin height H , fin thickness t , heat sink base thickness t_b and the angle between two long fins θ . The H, t, t_b were chosen as constant, i.e. $H = 21.3$ mm, $t = t_b = 2$ mm. The inner radius (R_i) was kept constant as 10 mm and the outer radius (R_o) of the heat sink varied from 75 mm to 115 mm. The surrounding air temperature was maintained constant as 303 K. The base temperature of the heat sink was varied from 330 K to 350 K.

3. MODELING APPROACH AND GOVERNING EQUATIONS

The modeling was approached based on the assumptions, i.e. the flow velocity was steady and laminar natural convection [6], Radiation heat loss was neglected [7], all the properties of air except density were assumed constant and the properties were assumed constant for the fin material, Aluminium. Three dimensional steady-state laminar flow model was selected to simulate the flow and heat transfer from the heat sink. The CFD package FLUENT, based on finite-volume method was employed to solve the fluid flow and heat transfer problems. A segregated solver was used to work out the governing integral equations for the conservation of mass, momentum, and energy. The preprocessor GAMBIT was used to create a computational geometry. After specifying the geometry, ANSYS ICEM was used for the boundary conditions and to create the computational mesh. The meshes were then exported to the software FLUENT to carry out the numerical simulation. The finite volume technique and the semi-implicit method for pressure-linked equation (SIMPLE) were used to solve the basic conservation Eqs. (1) to (5), in three dimensional Cartesian coordinates.

The continuity equation:

$$\frac{\partial(\rho u)}{\partial x} + \frac{\partial(\rho v)}{\partial y} + \frac{\partial(\rho w)}{\partial z} = 0 \quad (1)$$

The momentum equation in the x, y, z directions:

$$\frac{\partial(\rho u^2)}{\partial x} + \frac{\partial(\rho uv)}{\partial y} + \frac{\partial(\rho uw)}{\partial z} = -\frac{\partial P}{\partial x} + \mu \left(\frac{\partial^2 u}{\partial x^2} + \frac{\partial^2 u}{\partial y^2} + \frac{\partial^2 u}{\partial z^2} \right) \quad (2)$$

$$\frac{\partial(\rho vu)}{\partial x} + \frac{\partial(\rho v^2)}{\partial y} + \frac{\partial(\rho vw)}{\partial z} = -\frac{\partial P}{\partial y} + \mu \left(\frac{\partial^2 v}{\partial x^2} + \frac{\partial^2 v}{\partial y^2} + \frac{\partial^2 v}{\partial z^2} \right) \quad (3)$$

$$\frac{\partial(\rho wu)}{\partial x} + \frac{\partial(\rho wv)}{\partial y} + \frac{\partial(\rho w^2)}{\partial z} = -\frac{\partial P}{\partial z} + \mu \left(\frac{\partial^2 w}{\partial x^2} + \frac{\partial^2 w}{\partial y^2} + \frac{\partial^2 w}{\partial z^2} \right) + g(\rho - \rho_a) \quad (4)$$

The energy equation:

$$\frac{\partial(\rho u T)}{\partial x} + \frac{\partial(\rho v T)}{\partial y} + \frac{\partial(\rho w T)}{\partial z} = \frac{k_{fin}}{c_p} \left(\frac{\partial^2 T}{\partial x^2} + \frac{\partial^2 T}{\partial y^2} + \frac{\partial^2 T}{\partial z^2} \right) \quad (5)$$

For the fin material, temperature distribution was modeled by Fourier's heat conduction equation:

$$\left(\frac{\partial^2 T}{\partial x^2} + \frac{\partial^2 T}{\partial y^2} + \frac{\partial^2 T}{\partial z^2} \right) = 0 \quad (6)$$

For an incompressible flow, the solver computed the density according to the ideal gas law:

$$\rho = \frac{p}{\frac{R_c}{M_w} T_a} \quad (7)$$

3.1 Boundary conditions

Figure 1 illustrates the computational domain, where the fin base surface A'B'C'D'A' was held at constant temperature, T_{base} and constant heat flux, q'' . The surrounding air temperature was assumed constant, T_a . The Periodic boundary conditions were applied at the surfaces ADD'A'A, efgDe, MA'AefgDD PP'MM, and at the back BCC'B'B, e'f'g'Ce', NB'Be'f'g'CC'QQ'N'N. FLUENT treated the flow at a periodic boundary as though the opposing periodic plane was a direct neighbor of the cells adjacent to the first periodic boundary. The Pressure inlet boundary condition was applied at the surfaces MNB'A'M, DPQC'D', and PQQ'P'P, and the pressure outlet boundary condition was applied at the surfaces MP'Q'N'M' and MNN'M'M.

3.2 Calculation of numerical data

The thermo physical properties were evaluated at the film temperature, $T_f = (T_{base} + T_a)/2$.

The total heat transfer, q_T from the rectangular fins and un-finned base was calculated as

$$q_T = h_{avg} (A_{fin} + A_b) \theta_T \quad (8)$$

where, A_{fin} and A_b were the fin area and base area, available for heat transfer. The A_{fin} and A_b were calculated as

$$A_{fin} = (n_l L_l + n_m L_m + n_s L_s)(t + 2H) + 2Ht(n_l + n_m + n_s) \quad (9)$$

$$A_b = \pi(R_o^2 - R_i^2) + 2\pi t_b(R_o + R_i) - t(n_l L_l + n_m L_m + n_s L_s) \quad (10)$$

The number of fins was calculated as

$$n_l = n_m = n_s / 2 = 360^\circ / \theta \quad (11)$$

4. RESULTS AND ANALYSIS

4.1 Model validation

Numerical results of the reference model, $\theta = 18^\circ$, $R_o = 75$ mm, $L_l = 55$ mm, $L_m = 40$ mm, $L_s = 15$ mm, was compared with experimental data. The experiment was performed at the surrounding air temperature of $T_a = 292.4$ K. The constant heat flux, $q'' = 371.6$ W/m² was maintained at the base of the heat sink. Four type-T thermocouples were attached on the base of the heat sink to measure temperatures at different points. The average of the four temperatures was yielded the temperature of the heat sink. It was obtained that the difference between the experimental and numerical result was 1.74°C that showed a reasonably good agreement. However, our model was definitely able to reproduce qualitative data, as will be described in the following sections.

4.2 Optimization of geometric parameters

For the present radial flow heat sink, the heat transfer rate depends mainly on the diameter of the heat sink, number of fins and the lengths of the long, medium and short fins. The effects of geometric parameters, namely outer radius of the heat sink, number of fins, lengths of the long, medium, short fins on heat sink performance were analyzed simultaneously using the Taguchi method [8]. The orthogonal array (OA) was adopted for the scheme design, of which the schemes of experiments were determined. For the present study, four geometric parameters as A, L, M and S were promoted as control factors, and each control factor having four levels as listed in Table 1.

As for orthogonal array method, the orthogonal table $L_{16}(4^4)$ needed 16 test cases, which was based on four factors and four levels on each factor. The average heat transfer coefficient, h_{avg} data were obtained

from the simulation calculation for the each sample. Then the heat transfer rate, q_T was calculated according to Eq. (8).

In order to select the levels and control factors more efficiently, the heat transfer data were converted into the signal-to-noise (SN) ratio [9]. A larger SN ratio was preferred and was defined by the following equation representing the static characteristics [10]

$$SN = -10 \log_{10} \left[\frac{1}{N} \sum_{i=1}^N \frac{1}{(q_T)_i^2} \right] \quad (12)$$

Here, N is the number of design point, i.e. $N = 1$. The SN ratios for sixteen cases were obtained based on the outer radius, $R_o = 75, 95, 115$ mm. The factorial effect and contribution ratio of each factor from those SN ratios were calculated. The SN ratios of levels on each factor in Table 2, for $R_o = 75$ mm were calculated from the arithmetic average of SN ratios corresponding to each level [11].

The contribution ratio (CR) means the effect of each factor on heat transfer rate, q_T , i.e. the performance characteristics of a heat sink. This was calculated using D that indicated the difference between maximum and minimum SN ratios on each factor. The contribution ratio of each factor was obtained from the ratio of the D corresponding to each factor to the total D [11]. For example, the effect of each factor on heat transfer rate was obtained as 81.24% for angle A, and 3.61%, 1.22%, 13.93% for L, M, S, respectively, for $R_o = 75$ mm as presented in Table 2. It was also found that the contribution ratio of factor A decreased with increasing radius R_o , whereas the contribution ratios of factors L, M, S increased with increasing radius R_o . Thus, all these factors significantly affected the heat transfer performance of the heat sink.

Table 1. Levels of each control factor in this study

Factors	Base model	Levels of each factor				
		L-1	L-2	L-3	L-4	
A	Angle, θ	18	12	15	18	20
L	L_ℓ/R_o	0.733	0.65	0.7	0.75	0.8
M	L_m/L_ℓ	0.727	0.65	0.7	0.75	0.8
S	L_s/L_ℓ	0.273	0.15	0.2	0.25	0.3

Table 2. Effect of factors and contribution ratio

Level	Control Factors				
	A	L	M	S	
SN	1	15.204	18.783	18.680	19.266
	2	18.169	18.786	18.759	18.753
	3	20.344	18.780	18.761	18.606
	4	21.153	18.521	18.671	18.246
D		5.949	0.264	0.0892	1.020
CR		81.24	3.61	1.22	13.93

In order to select the optimum condition, the SN ratios could be plotted for the four factors (A, L, M, S), as shown in Figure 2. The largest SN ratio of the four levels on each factor might be the best thermal performance, i.e. the optimum condition, as can be conjectured from Eq. (12). As far as the angle was concerned, the angle 20° was the best for $R_o = 75, 95, 115$ mm for the increased rate of heat transfer. According to SN comparisons in Figure 2, the optimum condition was obtained by a combination of levels showing the largest SN ratio in each control factor, as A_4, L_2, M_3 and S_1 for the radius $R_o = 75, 95, 115$ mm.

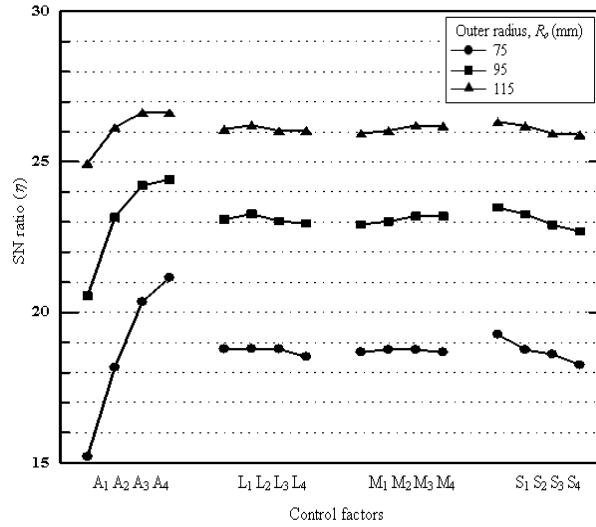


Figure 2. SN ratio on each factor

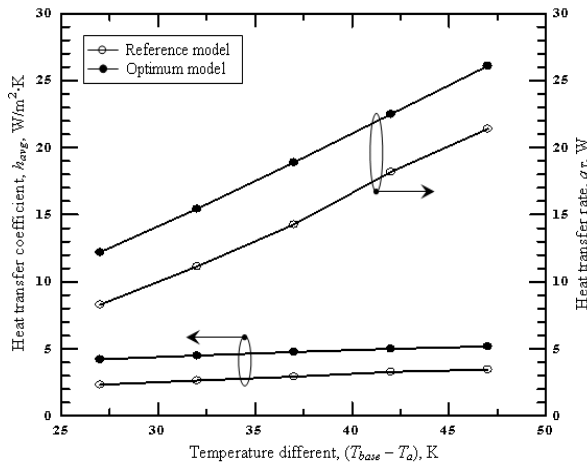


Fig.3: Variations of h_{avg} and q_T of two models

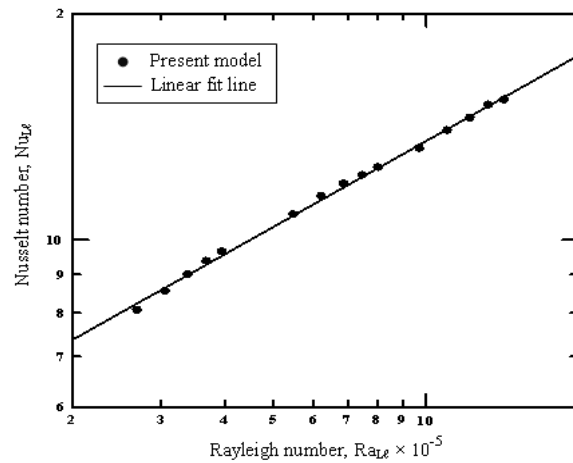


Figure 4. Variations of $Nu_{L\ell}$ with $Ra_{L\ell}$

4.3 Confirmation test of the optimum model

The test samples were designed by combining the optimum level on each factor as described above, i.e. $\theta = 20^\circ$, $L_d/R_o = 0.7$, $L_m/L_f = 0.75$ and $L_s/L_f = 0.15$. The heat transfer data was obtained from the sample and the reproducibility of the result was tested as follows for $R_o = 75$ mm. The presumed SN ratio of the optimum model obtained from Table 2 was compared with the SN ratio of the optimum sample. The presumed SN ratio, η_{pre} was calculated using the SN ratio corresponding to the optimum level on each factor as [9,11]

$$\begin{aligned}\eta_{pre} &= \eta_{A4} + \eta_{L2} + \eta_{M3} + \eta_{S1} - (m - 1) \bar{\eta} \\ &= 21.153 + 18.786 + 18.761 + 19.266 - 3 \times 18.718 \\ &= 21.812\end{aligned}\tag{13}$$

Here, the values of η_{A4} , η_{L2} , η_{M3} , η_{S1} were obtained from Table 2, m indicated the total number of factors, i.e. four, and $\bar{\eta}$ was the average SN values of the four factors. The SN ratio of the optimum sample ($\theta = 20^\circ$, $L_d/R_o = 0.7$, $L_m/L_f = 0.75$ and $L_s/L_f = 0.15$) was calculated as 21.724 for $R_o = 75$ mm. This value was in good agreement (within 1%) with the presumed value in Eq. (13), which ensured the reproducibility of the optimum condition. Similarly, the reproducibility of the optimum test samples for $R_o = 95$ and 115 mm were tested and obtained good agreement (within 2% for $R_o = 95$ and 115 mm) with the presumed values.

The average heat transfer coefficient and total heat transfer rate of the optimum model ($\theta = 20^\circ$, $L_d/R_o = 0.7$, $L_m/L_f = 0.75$ and $L_s/L_f = 0.15$) were compared with the reference model ($\theta = 18^\circ$, $R_o = 75$ mm, $L_d/R_o = 0.733$, $L_m/L_f = 0.727$ and $L_s/L_f = 0.273$). Figure 3 represents the variations of the average heat transfer coefficient and the total heat transfer rate of the reference model and the optimum model. For $R_o = 75$ mm, the average heat transfer coefficient and the heat transfer rate of the optimum model was higher by 38% and 23%, respectively than the reference model over the test range ($T_{base} = 330$ K to 350 K). It was also obtained that the total heat transfer rate per unit fin area of the optimum model ($R_o = 75$ mm) increased of about 40% than the reference model. Among the optimum models, the heat transfer rate increased of about 26% and 42%, for $R_o = 95$ and 115 mm, respectively, than that of $R_o = 75$ mm.

4.4 Correlation Equation

It was obtained that the average heat transfer coefficient and the heat transfer rate of the optimum heat sink increased with increasing the outer radius of the heat sink. However, at the optimum condition, the heat transfer data obtained from $R_o = 75$, 95 and 115 mm could be correlated by an equation. The variation of the Nusselt number (Nu_{Lt}) with Rayleigh number (Ra_{Lt}) of the optimum models at different outer radius (75, 95, 115 mm) over the test region ($T_{base} = 330$ K to 350 K) is shown in Figure 4. The relation between Nusselt and Rayleigh numbers is given by the linear fit method as

$$Nu_{Lt} = 0.072 Ra_{Lt}^{0.38}\tag{14}$$

5. CONCLUSIONS

A steady-state 3D analysis of radial flow heat sink was performed. The model described the effects of various design parameters, namely the lengths of long, medium and short fins, number of fins, and heat sink base radius on heat transfer rate using the Taguchi method. It was obtained that these parameters significantly affected the heat transfer performance of the heat sink. It was also noted that the performance of the optimum heat sink showed superior characteristics compared to the reference heat sink. The design parameters of the optimum heat sink were obtained as $\theta = 20^\circ$, $L_d/R_o = 0.7$, $L_m/L_f = 0.75$ and $L_s/L_f = 0.15$, for the $R_o = 75$, 95, 115 mm. The factor related to the heat sink surface area, i.e. outer radius, showed significant influence on the heat transfer performance of the heat sink and the heat transfer data at different outer radius were correlated by Eq. (14). These results might be useful to thermal optimization of the radial flow heat sink.

NOMENCLATURE

c_p	coefficient of heat capacity, J/(kg·K)
h_{avg}	heat transfer coefficient, W/(m ² ·K)

k	thermal conductivity of air, W/(m·K)
k_{fin}	thermal conductivity of fin, W/(m·K)
L_l, L_m, L_s	length of the long, medium, short fins, mm
M_w	the molecular weight of the air
Nu_{Ll}	Nusselt number, $h_{avg}L_l/k$
n_l, n_m, n_s	no. of the long, medium, short fins
p	Pressure, Pa
Pr	Prandtl number, ν/α
R_c	the universal gas constant
SN	signal-to-noise
Ra_{Ll}	Rayleigh number, $g\beta\rho^2c_p(T_{base}-T_a)L_l^3/(k\mu)$
u, v, w	x, y, z -components of velocity, m/s

Greek symbols

α	thermal diffusivity, m ² /s
μ	dynamic viscosity, N·s/m ²
ν	kinematic viscosity, μ/ρ , m ² /s
ρ	density of fluid, kg/m ³
β	thermal expansion co-efficient, 1/K
θ_T	$(T_{base} - T_a)$, K

REFERENCES:

- [1] Kobus, C.J. and Oshio, T. (2005): "Development of a theoretical model for predicting the thermal performance characteristics of a vertical pin-fin array heat sink under combined forced and natural convection with impinging flow". *International Journal of Heat and Mass Transfer*, Vol. 48, pp. 1053-1063.
- [2] Huang, R.T., Sheu, W.J. and Wang, C.C. (2008): "Orientation effect on natural convection performance of square pin fin heat sinks". *International Journal of Heat and Mass Transfer*, Vol. 51, pp. 2368-2376.
- [3] Zografos, A.I. and Sunderland, J.E. (1990): "Natural convection from pin fin arrays". *Experimental Thermal and Fluid Science*, Vol. 3, pp. 440-449.
- [4] Sparrow, E.M. and Vemuri, S.B. (1986): "Orientation effects on natural convection/radiation heat transfer from pin-fin arrays". *International Journal of Heat and Mass Transfer*, Vol. 29, pp. 359-368.
- [5] Inada, S., Taguchi, T. and Yang, W.J. (1999): "Effects of vertical fins on local heat transfer performance in a horizontal fluid layer". *International Journal of Heat and Mass Transfer*, Vol. 42, pp. 2897-2903.
- [6] Al-Arabi, M. and El-Riedy, M.K. (1976): "Natural convection heat transfer from isothermal horizontal plates of different shapes". *International Journal of Heat and Mass Transfer*, Vol. 19, pp. 1399-1404.
- [7] Leung, C. W. and Probert, S. D. (1989): "Heat exchanger performance: effect of orientation". *Applied Energy*, Vol. 33, pp. 235-252.
- [8] Taguchi, G. (1991): "Taguchi on robust technology development", *Bring Quality Engineering (QE)* Upstream ASME.
- [9] Taguchi, G., Elsayed, A.E. and Thomas, C.H. (1989), "Quality Engineering in Production Systems", McGraw-Hill, New York.
- [10] Lochner J.H. and Matar, J.E. (1990), "Designing for Quality", ASQC Quality Press.
- [11] Yun, J.Y. and Lee, K.S. (2000): "Influence of design parameters on the heat transfer and flow friction characteristics of the heat exchanger with slit fins". *International Journal of Heat and Mass Transfer*, Vol. 43, pp. 2529-2539.

DESIGN, FABRICATION AND PERFORMANCE ANALYSIS OF AN EVAPORATIVE COOLER

Mohammad Zoynal Abedin* and Mohammed Moinul Islam

Department of Mechanical Engineering, Dhaka University of Engineering and Technology,
Gazipur-1700, Bangladesh

Correspondence Email: abedin.mzoynal@gmail.com

Tel: + 88-02-9204734-43, Fax: + 88-02-9204701-2

ABSTRACT: The paper presents a state-of-the-art evaporative cooler with its design, fabrication and performance evaluation. The evaporative cooler, often known as desert cooler or swamp cooler, is designed for the application in the desert environment where the ambient temperature is high and humidity is low. The shape of the cooler is like a unitary type air-conditioner mounted on the wall in which the atmospheric air drawn by a fan passes through the media situated inside the cooler and the media is always kept wet by circulating water (which works as a refrigerant) with the help of a submersible pump (HD12127: [Hydor SELTZ L20 Pump 185 gph](#)). To get the maximum output of the cooler and to maintain the comfortable environment such as low temperature and moderate humidity in the conditioned space where the cooler is installed, the media such as the coconut strips, jute products and clothes are used. Based on the data recorded from April to August in Dhaka city, Bangladesh, the results show that the performance of the cooler is higher for the case in which the coconut strips are used as media when compared with those of others, and the efficiency of the cooler with coconut strips can be increased as high as about 70% for the comparable working condition.

Keywords: Evaporative Cooler, Efficiency, Design, Fabrication, Performance Evaluation

1. INTRODUCTION

Evaporative cooler is of particular importance in the application of many engineering problems such as a sole cooling system in a home, as a substitute to a conventional air conditioner, or in combination with a conventional refrigerated air conditioning system. Evaporative cooling ensures not only the reduction in air temperature but also increase in air humidity that occurs when water evaporates, consequently creating the cooling effect. Evaporative coolers can be not only economically manufactured and but also operated more easily when compared with the conventional air conditioner. Usually, the coolers do not use refrigerants like chlorofluorocarbons (CFCs) and hydro chlorofluorocarbons (HCFCs) that can harm the ozone layer. Rather, it uses non-harmful water as a refrigerant. The coolers can improve the indoor air quality inside a home by drawing a large supply of fresh outdoor air. With evaporative cooling, a complete air change occurs every one to three minutes, offering a great health benefit over traditional refrigerated air conditioning, which recirculates house air repeatedly.

The research of evaporative cooler was started in the beginning of nineteenth century, although the art of air conditioning dated back to the earlier ages of the Ancient Rome. [Franklin](#) and [Hadley](#) (1758) conducted an experiment to explore the principle of evaporation as a means to rapidly cool an object. According to their report, evaporation of highly volatile liquids such as alcohol and ether could be used to drive down the temperature of an object past the freezing point of water. They conducted their experiment with the bulb of a mercury thermometer as their object and with a bellows used to quicken the evaporation. They lowered the temperature of the thermometer bulb down to 7°F while the ambient temperature was 65°F. They passed the freezing point of water (32°F) in a thin film of ice formed on the surface of the thermometer's bulb and that the ice mass was about a quarter inch thick when they stopped the experiment upon reaching 7°F. On the other hand, Jones (2007) reported that in 1842, [Florida](#) physician [John](#) Gorrie used compressor technology to create ice, which he used to cool air for his patients in his hospital in [Apalachicola, Florida](#). In addition, Gorrie hoped eventually to use his ice-making machine to regulate the temperature of buildings. He even envisioned centralized air conditioning that could cool entire cities.

The experimentation with air conditioning was first performed by the American Inventor [Willis Haviland Carrier](#) in [Buffalo, New York](#).¹ According to his experimental research, an option was explored to control not only [temperature](#) but also [humidity](#). To control the temperature and humidity as whole in a system, the phenomenon of evaporative cooling was materialized, although the research for the improved efficiency of the evaporative cooler is awaited. The efficiency of the evaporative cooler influenced with various parameters has been described by many researchers (Luikov et al., 1973; Erens and Dreyer, 1993; Fisenko et al. 2004; Kaiser et al. 2005). In some of the researches, it is found that the strong influence of the average water drop size on efficiency of the system and also revealed the effect of other variables like wet bulb temperature, water mass flow to air mass flow ratio and temperature gap between water inlet temperature and wet bulb temperature (Kaiser et al. 2005).

In the present study, we have performed the design and fabrication of an evaporative cooler and also analyzed the performance evaluation of the cooler by using different media such as coconut strips, jute products and cotton clothing.

2. DESIGN AND FABRICATION

The schematic drawing of an evaporative cooler is shown in Fig. 1. The cooler is designed like a shape as a unitary window type air-conditioner to easily mount on the wall. The cooler has mainly three supporting structures which are fabricated with GI sheet of 18 gauge and each of which has a dimension of 20"×20". One structure holds a drag forced fan installed at the middle of the cooler. The fan is attached with the frame by bolts and screws, and is positioned at the upstream of the media which drags atmospheric air into the media. The upstream position of the fan is due to the reason to keep the fan free from the moist air, which might corrode the blades of the metallic frame, that in turn, reducing the durability and efficiency of the cooler. The other two structures are installed at the front and back of the cooler. The three structures are fixed into their positions by welding them with four "L" shaped angles which are made of the same quality GI sheet of 18 gauges and each of them is of 28" long.

The cover of the cooler, the top and the bottom trays are fabricated with the GI sheet of 26 gauges. The cover of the cooler is attached with the main structure by bolts and screws. The top tray is attached with the cover by gas welding and the clearance between the tray and the cover is sealed with putty. The structure to hold the bottom tray in which the tray slides in and out is fabricated with GI sheet of 18 gauges. This structure is attached to the main structure of the cover by gas welding. A submersible water pump is positioned into the bottom tray so that it can pump water in order to reach out to the top tray by a hose pipe from the bottom tray (not shown in figure). This type of arrangement of pump confirms a constant water circulation from bottom tray to top tray.

In the front and back side of the cooler, there are safety covers which are made of nets. The meshing of the nets is chosen in a way that the pressure drops across the nets are negligible. These covers are also attached with the main frame of the cooler by the screws and bolts. The frame that holds the media has one layer of media and two layers of net, and the media is sandwiched between the two net layers. A provision is kept to change the media in such a way that the frame can be slide into and out of the cooler on a cross slide attached in the cooler. A frame holding the media is just placed below the top fixed tray so that the water coming from the bottom tray can easily reach out to the media. This keeps the media always wet with water and it ensures that the incoming air always come in contact with water.

3. EXPERIMENTAL PROCEDURE

At first the fan is allowed to run and it makes the circulation of an atmospheric air from outside to the inside of the room. The pump installed in the bottom tray is used to pump water and later the energized water is allowed to pass to the top tray through a hose pipe. From the top tray, the water falls into the media and help the media become wet wherein the atmospheric hot and dehumidified

¹ http://en.wikipedia.org/wiki/Air_conditioning

air is allowed to pass through the media by the help of a fan. The water in the media absorbs heat from the hot atmospheric air and become vapor by taking the latent heat of evaporation. In the meantime, the hot air becomes cold by releasing heat to water, and turns into the humidified air by absorbing water vapor, as well. The cold and humidified air entered from the cooler into the confined space may be treated as the conditioned air having the characteristics of thermal comfort. The temperature and humidity of the incoming air from the cooler may be controlled further according to the design conditions in the confined space.

4. MATHEMATICAL METHOD

In the present study, we have performed first the cooling load calculation of a room where the cooler is installed by using the conventional method of the load calculation. In the method of the load calculation, we have analyzed the following categories of heat gain phenomena such as (1) instantaneous solar radiation heat gain through glass, (2) transmission heat gain, (3) internal heat gain, and (4) heat gain due to the ventilation and infiltration of air. Furthermore, we have illustrated the following parameters required for the load calculation and cooler efficiency like as (1) geographical location of the room such as latitude and longitude, (2) design time and month, (3) outside and inside design conditions along with the daily range of temperature, (4) number of peoples, and (5) various loads of the electrical and electronic appliances inside the room. In the calculation, the various temperature and humidity of air are measured with the help of the hygrometer which help find out the different humidity from the Psychometric chart. The incoming air velocity is measured with the help of an anemometer (Model: AR816; Wind speed measuring range: 0.3 to 30m/s). We have recorded the following parameters to carry out the performance evaluation of the cooler as: (i) average velocity of air, (ii) cross-sectional area of cooler, (iii) air temperatures (dry bulb and wet bulb) inside the cooler, (iv) air temperatures (dry bulb and wet bulb) outside the cooler, (v) humidity ratio at the inlet condition of cooler, (vi) humidity ratio at the outlet condition of cooler.

We have illustrated the different parameters of the cooler such as mass of air handled by the cooler, volume of water vapor absorbed by air, cooling effect of the cooler, and efficiency of the cooler. The mass of air (M_{air}) handled by the cooler can be expressed as follows.

$$M_{air} = \text{volumetric flow rate} \times \text{density of air}$$

The volumetric flow rate (Q_{air}) can be expressed as the product of the velocity of the incoming air after the cooler and the cross sectional area of the cooler.

Therefore, the volumetric flow rate (Q_{air}) can be written as follows.

$$Q_{air} = \text{velocity of the incoming air after the cooler} \times \text{cross sectional area of the cooler}$$

The volume of water vapor (Q_w) added to the air can be written as follows:

$$Q_w = \text{mass of air} \times \text{change of humidity between cooler inlet and outlet condition} / \text{density of water}$$

The cooling effect ($C.E.$) of the cooler can be expressed as follows:

$$C.E. = \text{mass of water vapor} \times \text{latent heat of vaporization}$$

The efficiency (η) of the cooler can be defined as the ratio of the difference between the dry bulb temperature of atmospheric air at inlet and dry bulb temperature of conditioned air at outlet of the cooler to the difference between the dry bulb and wet bulb temperatures of atmospheric air at inlet of the cooler. In the mathematical form, the efficiency (η) of the cooler can be expressed as follows:

$$\eta = (T_{dbi} - T_{dbo}) / (T_{dbi} - T_{wbi})$$

Here T_{dbi} , T_{dbo} and T_{wbi} represent dry bulb temperature of atmospheric air at inlet, dry bulb temperature of conditioned air at outlet and web bulb temperature of atmospheric air at inlet, respectively. The sample calculations for the performance parameters of the cooler like as mass of air handled by the cooler, volume of water vapor absorbed by air, cooling effect of the cooler, and

efficiency of the cooler are provided in the Appendix, However, the sample load calculation of the room where the cooler is installed is not provided. Moreover, the calculated efficiency of the cooler is provided in the Table 1 shown in the following section.

5. RESULTS AND DISCUSSION

We have evaluated the efficiencies (η) of the cooler from April to August by using coconut strips, jute products and cotton clothing. Figures 2-4 show the efficiency of cooler from April to August for coconut strips, jute product and cotton clothing, respectively. It is seen that the efficiencies of the cooler calculated in June increase as much as 70%, 58% and 40%, for coconut strips, jute products and cotton clothing, respectively. Table 1 and Figure 5 show the calculated efficiencies (η) of the cooler for coconut strips, jute products and cotton clothing from April to August. The comparison of the efficiencies of the cooler by using coconut strips, jute products and cotton clothing from April to August is demonstrated in Figure 5. It can be seen from the figure that the efficiency of the cooler become higher for coconut strips in June when compared with the other media such as jute products and cotton clothing. The higher efficiency of the cooler by the using the coconut strips may be attributed due to the fact that in the case of coconut strips, air can easily penetrate through the media which results a higher drop in the dry bulb temperature of conditioned air at outlet of the cooler.

Table 1. Efficiency of an evaporative cooler for coconut strips, jute products and cotton clothing for the month from April to August.

Media	Efficiency (%)				
	April	May	June	July	August
Coconut strips	55	65	70	67	60
Jute products	50	55	58	56	53
Cotton clothing	30	35	40	37	33

6. CONCLUDING REMARKS

The analysis of the evaporative cooler with its design, fabrication and performance study has been performed on the basis of the hot and dehumidified atmospheric air. The easy design procedure of the cooler and its fabrication process have been provided in a detailed manner and a comparative study has been conducted specifying the efficiency of the cooler by using the cotton clothing, jute products and coconut strips as the media. It is noted that the performance of the cooler is higher for the case in which the coconut strips are used as media when compared with those of others and the efficiency of the cooler in the month of June increases as much as 70%, 58% and 40% for the coconut strips, jute products and cotton clothing, respectively. The higher efficiency of the cooler by the using the coconut strips may be attributed due to the fact that in the case of coconut strips air can easily penetrate through the media which results a drop in the dry bulb temperature of conditioned air at outlet of the cooler as specified earlier.

ACKNOWLEDGEMENTS

The authors express their sincere gratitude to Formerly Professor Dr. Showkat Jahan Chowdhury, Department of Mechanical Engineering, Bangladesh University Engineering Technology (BUET), for his valuable suggestions. The authors are also thankful to Mr. S. Ahmad Chowdhury, student of Mechanical Engineering, BUET, for his cooperation.

REFERENCES

- Franklin, Benjamin. 1758, "[Cooling by evaporation](#)", *Letter to John Lining, London*, June, p. 17.
- Jones Jr., Malcolm. 1997, "[History of Air Conditioning](#) Source", *Air Conditioning, Newsweek (winter)*, Vol. 130, No. (24-A), pp. 42-43.
- Luikov, A.V., Vasiliev, L.L., and Rasin, O.G. 1973, "Peculiarities of evaporative cooling in rarefied gas", *International Journal of Heat and Mass Transfer*, Vol. 16, No. 1, pp. 3-12.

Erens, P.J., and Dreyer, A.A. 1973, "Modelling of indirect evaporative air coolers", *International Journal of Heat and Mass Transfer*, Vol. 36, No. 1, pp. 17-26.

Fisenko, S. P., Brin, A. A., and Petrushik, A. I. 2004, "Evaporative cooling of water in a mechanical draft cooling tower", *International Journal of Heat and Mass Transfer*, Vol. 47, No. 1, pp. 165-177.

Kaiser, A.S., Lucas, M., Viedma, A., and Zamora, B. 2005. "Numerical model of evaporative cooling process in a new type of cooling tower", *International Journal of Heat and Mass Transfer*, Vol. 48, No. 5, pp. 986-999.

APPENDIX

We provide the following parameters for sample calculation in the month of June at 3.00 pm to carry out the performance evaluation of the cooler like as: (i) average velocity of air = 1.21 m/s, Cross-sectional area of cooler = 0.2581 m², Air temperatures inside the cooler: $T_{db} = 31.5^{\circ}\text{C}$ (dry bulb temperature), $T_{wb} = 31.5^{\circ}\text{C}$ (wet bulb temperature) and humidity ratio, $W_i = 0.02075$ kg/kg dry air (at inlet condition); $T_{db} = 28.35^{\circ}\text{C}$ (dry bulb temperature), $T_{wb} = 27.0^{\circ}\text{C}$ (wt bulb temperature) and humidity ratio, $W_o = 0.022$ kg/kg dry air (at outlet condition), Latent heat of vaporization of water = 537 cal/gm.

The mass of air (M_{air}) handled by the cooler can be calculated as follows:

$$M_{air} = (1.21 \text{ m/s} \times 0.2581 \text{ m}^2) \times 1.22 \text{ kg/m}^3 = 0.381 \text{ kg/s}$$

The volume of water vapor (Q_w) added to the air can be calculated as follows:

$$Q_w = [0.381 \text{ kg/s} \times (0.022 - 0.02075) \text{ kg/kg dry air}] / 1000.0 \text{ kg/m}^3 = 0.00171 \text{ m}^3/\text{hr}$$

The cooling effect (C.E.) of the cooler can be evaluated as follows:

$$C. E. = 0.000476 \text{ kg/s} \times 537 \text{ cal/gm} \times (4.187 \times 1000) \text{ J/cal} = 1071 \text{ watt} = 0.304 \text{ TR (ton of refrigeration)}.$$

In a similar manner, we have evaluated the cooling effect (C.E.) of the cooler by using jute products and cotton clothing and have been found out as, 0.292 and 0.256 TR, respectively. However, the value of the load calculation of the room where the cooler is installed is comparably justified with the value of the cooling effect of the cooler (sample load calculation is not shown in the report).

The efficiency of the cooler by using coconut strips as a media can be evaluated as follows:

$$\eta = (31.5 - 28.35) / (31.5 - 27.0) = 70\%$$

In a similar manner, we have evaluated the efficiency (η) of the cooler by using jute products and cotton clothing and have been found out as 58% and 40%, respectively.

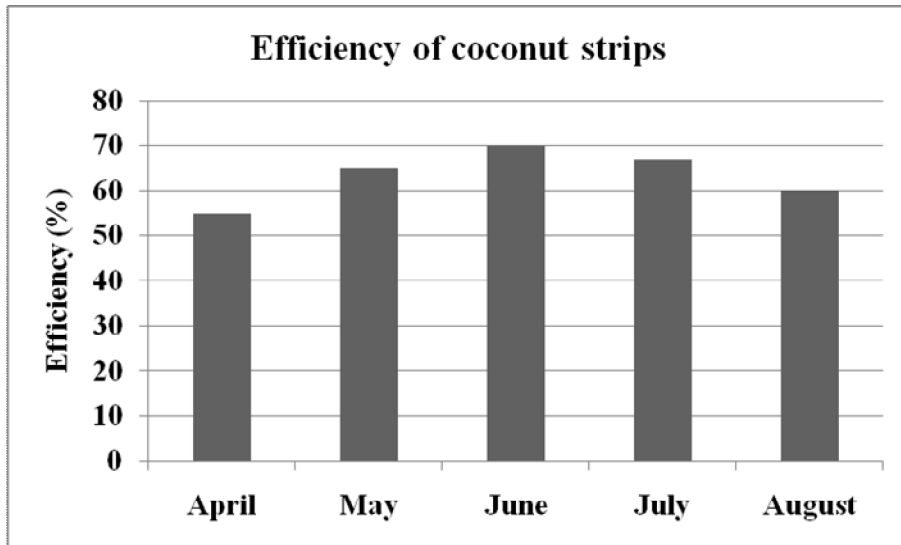
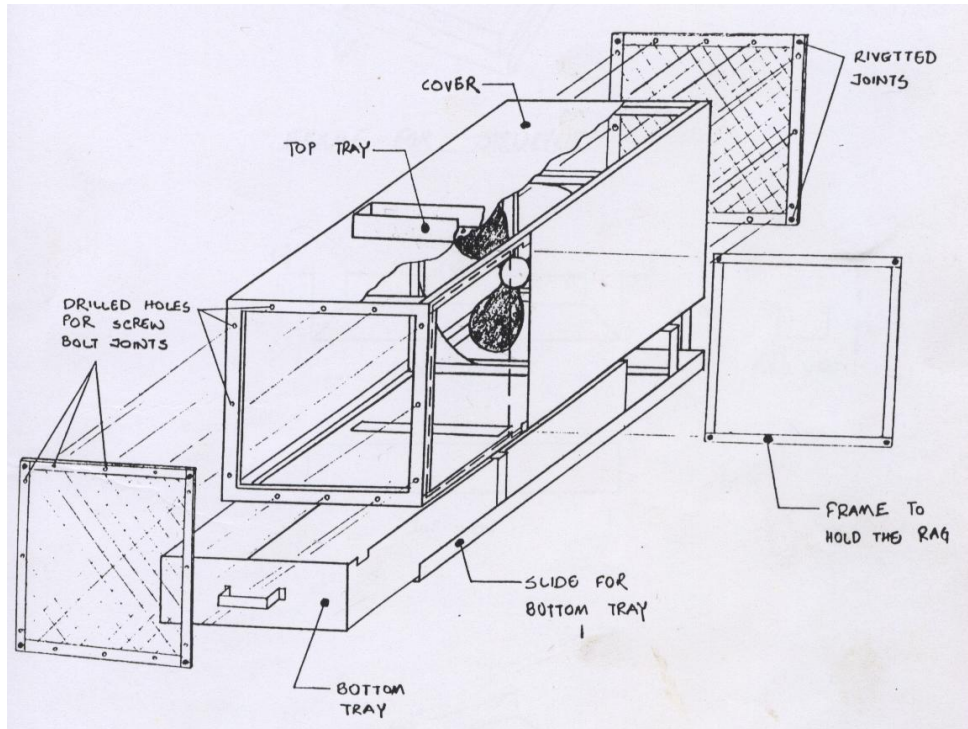


Fig.2: Efficiency of the cooler for coconut strip from April to August

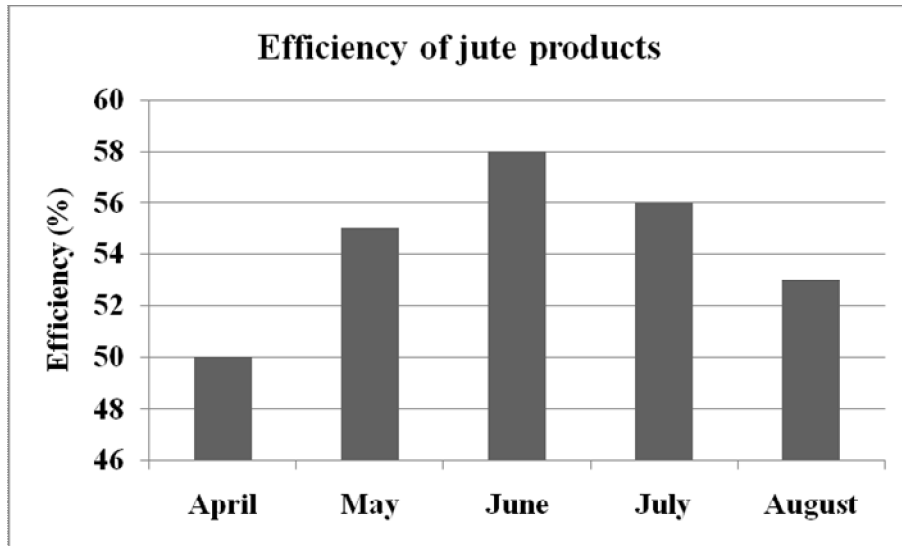


Fig.3: Efficiency of the cooler for jute product from April to August

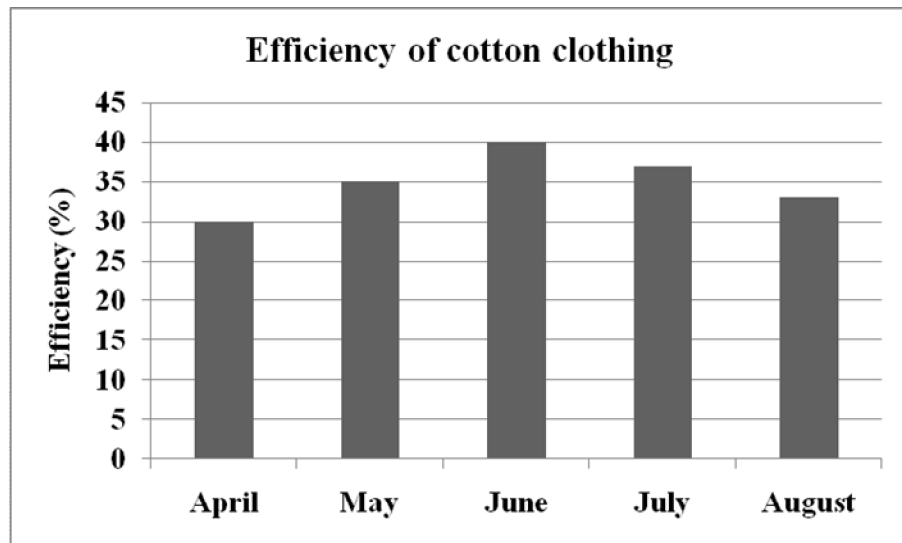


Fig.4: Efficiency of the cooler for cotton clothing from April to August

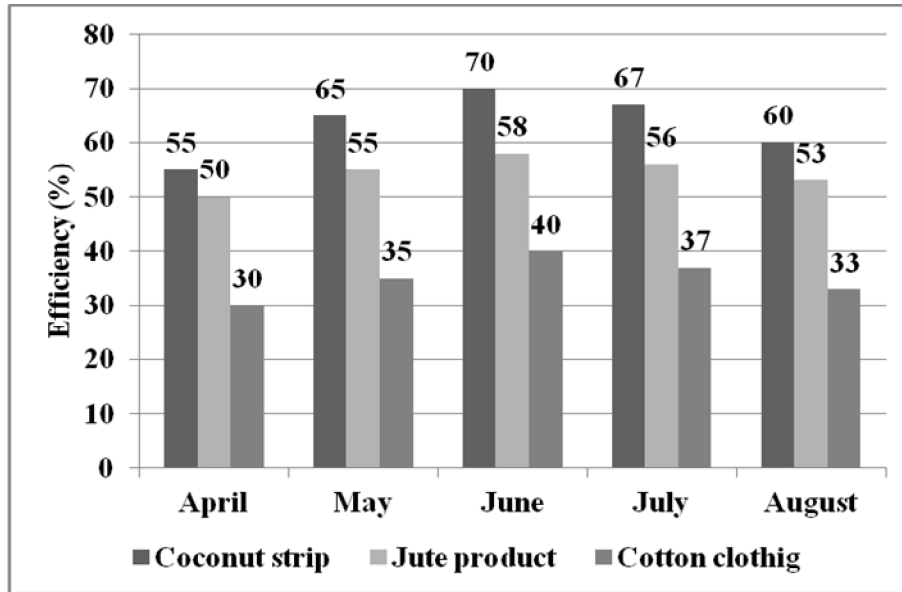


Fig.5: Efficiency of the cooler for coconut strip, jute product and cotton clothing from April to August

MIXED CONVECTION IN A STEP SIZE LID DRIVEN CAVITY

Sourav Saha, Satyajit Mojumder, Sumon Saha, M.A.H. Mamun
Department of Mechanical Engineering,
Bangladesh University of Engineering and Technology, Dhaka-1000.
souravsahame17@gmail.com

ABSTRACT: Lid driven mixed convection has been given prodigious importance due to its wide range of application. A step size cavity has been introduced and geometric effect along with heat transfer effect has been observed. Galerkin weighted residual method of Finite element Method (FEM) has been deployed for the numerical simulation. Numerical solution has been carried out for different Richardson numbers ($Ri=0.1, 1, 10$) and different geometric parameters. It has been found that both Richardson number and geometric parameters have significant effect on heat transfer. Results are presented using streamline, isotherm contour along with related graph and plot.

Keywords: *Mixed convection, Richardson number, step size geometry, heat transfer.*

1. INTRODUCTION

Mixed convection has been given a wide attention through the end of last century due to its application in modern science and technology. It has application in electronics cooling technology, solar collector design, food processing industry, chemical processing technology, space heating and so on [1-3]. Understanding the fundamental pertinent transport process of the heat transfer basically depends on sound insight of the problem. Wide ranges of literature are available for lid driven mixed convection phenomena. They can be broadly classified as two types. In one the side walls of the cavity are lid driven and any of the boundaries contains heat source [4]. In the other type there are oscillating lid driven boundary [5].

Some basic Parameters that control the heat transfer for mixed convection are Reynolds number, Prandtl number, Richardson number, geometric shape, Grashof number and so on. Moallemi and Jang [6] investigated the effect of prandtl number and Reynolds number effect in a laminar mixed convection in a square cavity. Prasad and Koseff [7] experimented the mixed convection for a wide range of Richardson number. Cheng [8] also characterized the effect of Richardson and prandtl number for mixed convection in a square cavity. Amiri et al [9] studied both heat and mass transfer effect in lid driven square cavity concluded that Richardson number plays a vital role. Geometrical shape is very important from the application point of view. Square, trapezoidal, rectangular, triangular shape enclosure are widely studied in last 3 decades [10-12]. Different study of the lid driven phenomena has been studied using nanofluid [13], porous media [14], magneto hydrodynamic [15], double diffusive mixed convection [16] and so on and it has been found in every case geometric shape plays a vital role with the governing parameter. Step size geometry is quite new and it has a wide range of application due to geometrical constraint of space in application area.

The main purpose of this paper is to investigate the heat transfer phenomena in a step size cavity for two different height of the step. It has been found that for different height interesting flow characteristic occurs for different Richardson number. The result are presented by streamline, isotherm contour and with related graph and plot.

2. PROBLEM FORMULATION

2.1. PHYSICAL MODELING

A step size cavity has been introduced which has been presented in the figure 1(a) and 1(b). This type of cavity are very much common in engineering application point of view. A well defined coordinate system has been given along with the boundary condition. This enclosure is lid driven for the upper boundary which has been kept at ambient temperature ($T=T_c$). The bottom wall of the

cavity is heated and kept at constant temperature ($T=Th$). The vertical walls are adiabatic. In the figure the geometric parameter is defined and for the physical modeling of two problems it has been assumed that both the enclosure fig 1(a) and 1(b) has the same dimensionless area thus same volume. The gravity is acting in the negative direction of Y axis. Among the wall only upper wall is moving and other wall are kept stationary. Though radiation has important effect on heat transfer for simplification of the problem it has been neglected. And the heat transfer is in natural convection mode.

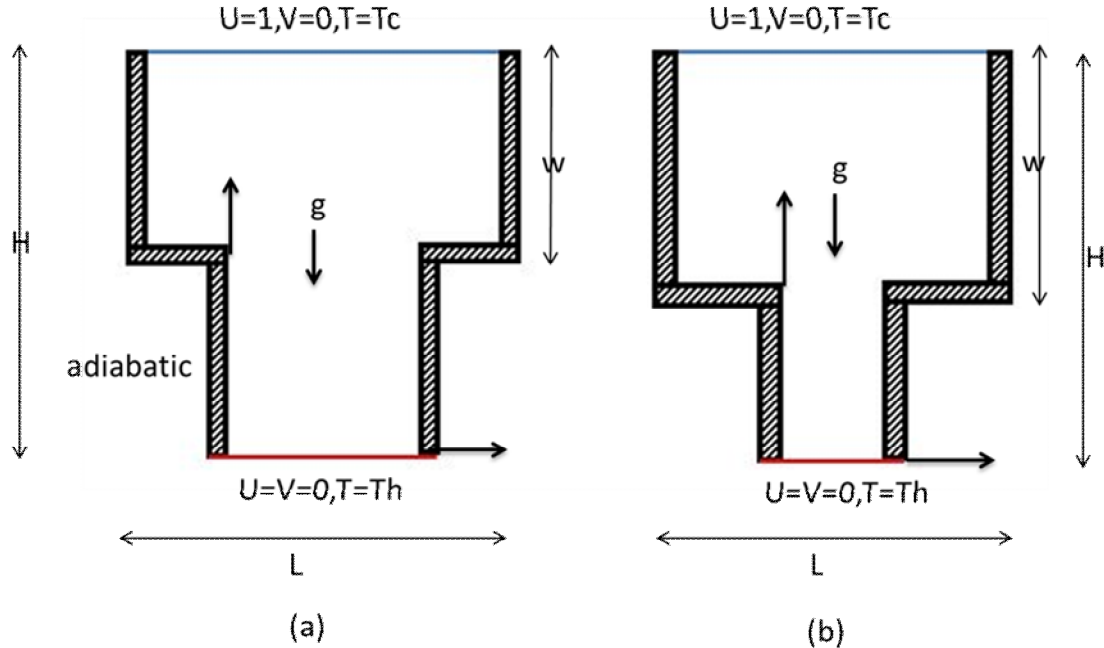


Fig. 1. Schematic of the problem with the domain and boundary conditions (a) $w=0.5$ (b) $w=0.6$

2.2. MATHEMATICAL MODELLING

i) Governing equations

For laminar, incompressible and two-dimensional mixed convection, after invoking the Boussinesq approximation and neglecting the viscous dissipation, can be expressed in the dimensionless form as:

$$\frac{\partial U}{\partial X} + \frac{\partial V}{\partial Y} = 0 \quad (1)$$

$$U \frac{\partial U}{\partial X} + V \frac{\partial U}{\partial Y} = -\frac{\partial P}{\partial X} + \frac{1}{Re} \left(\frac{\partial^2 U}{\partial X^2} + \frac{\partial^2 U}{\partial Y^2} \right) \quad (2)$$

$$U \frac{\partial V}{\partial X} + V \frac{\partial V}{\partial Y} = -\frac{\partial P}{\partial Y} + \frac{1}{Re} \left(\frac{\partial^2 V}{\partial X^2} + \frac{\partial^2 V}{\partial Y^2} \right) + Ri \theta \quad (3)$$

$$U \frac{\partial \theta}{\partial X} + V \frac{\partial \theta}{\partial Y} = \frac{1}{Re Pr} \left(\frac{\partial^2 \theta}{\partial X^2} + \frac{\partial^2 \theta}{\partial Y^2} \right) + \frac{1}{Re Pr} \quad (4)$$

Where, U and V are the velocity components in the X- and Y-directions, respectively, θ is the temperature and P is the pressure. The non-dimensional numbers seen in the above, Gr , Re , Pr and Ri are the Grashof number, Reynolds number, Prandtl number and Richardson number, respectively, and they defined as

$$Gr = \frac{g \beta \Delta T L^3}{\nu^2}, \quad Re = \frac{u_o L}{\nu}, \quad Pr = \frac{\nu}{\alpha} \quad \text{and} \quad Ri = \frac{Gr}{Re^2}. \quad (5)$$

The dimensionless parameters in the equations above are defined as follow:

$$X = \frac{x}{L}, Y = \frac{y}{H}, U = \frac{u}{u_o}, V = \frac{v}{u_o}, P = \frac{p}{\rho u_o^2}, \theta = \frac{T - T_o}{\Delta T}, \Delta t = \frac{q'' L^2}{k}, w = \frac{y}{H}. \quad (6)$$

Where, ρ , β , ν , α and g are the fluid density, coefficient of volumetric expansion, kinematic viscosity, thermal diffusivity, and gravitational acceleration, respectively.

The boundary conditions of this problem are,

- i. The top wall is moving with velocity u in the X direction, while other walls are not moving.
- ii. No slip condition is assumed for all other wall than the upper wall.
- iii. The bottom wall is kept at a higher temperature T_h while the top wall is kept at a lower temperature T_c .
- iv. Other walls are adiabatic.

3. NUMERICAL SCHEME

3.1. NUMERICAL PROCEDURE

Finite element method (FEM) has been used to get the solution of the specific problem. Triangular type of mesh has been employed to the entire cavity. The governing equations are applied to these triangular elements for boundary condition. An iterative method has been used to find out the solution by the (UMPFACK) solver and relative tolerance of 10^{-5} has been set for the error estimation. The entire problem converges for this setting of the numerical procedure. Reynolds number which is governing parameters are fixed at 100 and air is taken as the fluid whose Prandtl number is 0.71 for the entire numerical solution.

3.2. GRID INDEPENDENCY TEST

A grid independency test has been performed to understand the effect of element number taken for the numerical solution procedure and this make the numerical solution more reliable and accurate. The grid independency test result has been presented in figure2. From the figure it is evident that for the lower element number like 761, 1164 the Nusselt number varies in a significant amount. for the element number 2004 the Nusselt number becomes almost constant and for higher number of element it become by or large constant. As the grid becoming independent for element number 2004, it has been taken for the entire numerical simulation of the specified problem.

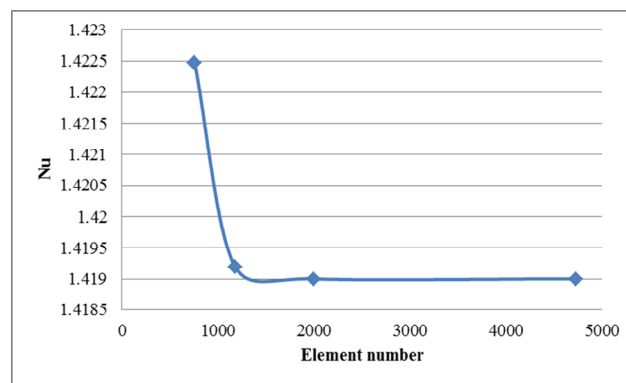


Fig. 2. Grid independency study results for $Ri = 10, w=0.5$ and $Re=100$

4. RESULTS AND DISCUSSIONS

In this paper the results have been generated using finite element method. Each result is followed by a brief albeit sufficient discussion on the physical significance of the result. Firstly isotherm and streamline contours are presented for two different geometries and the effects of varying Richardson number are analyzed. Later, centerline velocity field for the two geometries and comparison of average Nusselt number at the heated bottom wall between the geometries have been presented. This problem contains a relatively newer geometric model and hence this paper aims to study the effect of geometric variation on different physical phenomena.

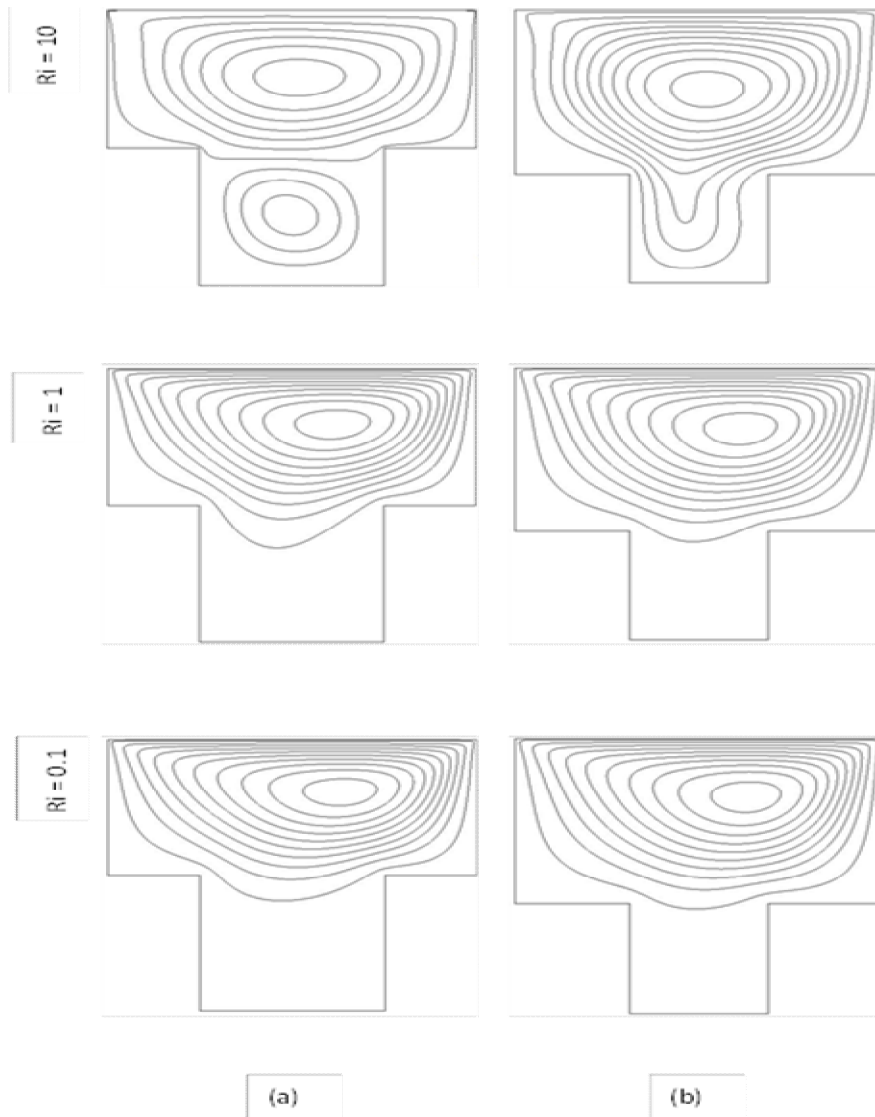


Fig3: Comparison of streamline for (a) $w=0.5$, (b) $w=0.6$

Figure 3 portrays the effect of Richardson number on the streamlines for two different geometries. For $w = 0.5$, as can be seen from the column (a) of the figure, the moving lid has a significant effect on the streamline formation. The eye of the principal vortex is always near the top moving lid, independent of the value of Richardson number. However the Richardson number has particular effect on the strength of the vortex and vortex formation. For $Ri = 0.1$, the buoyant

effect is very negligible and hence strength of the vortex is very low ($\psi_{min} = -3.175e-3$). As the Ri goes to 1, buoyancy starts to have a significant effect on the vortex. However the strength of the vortex does not show much increment ($\psi_{min} = -4.4e-3$).

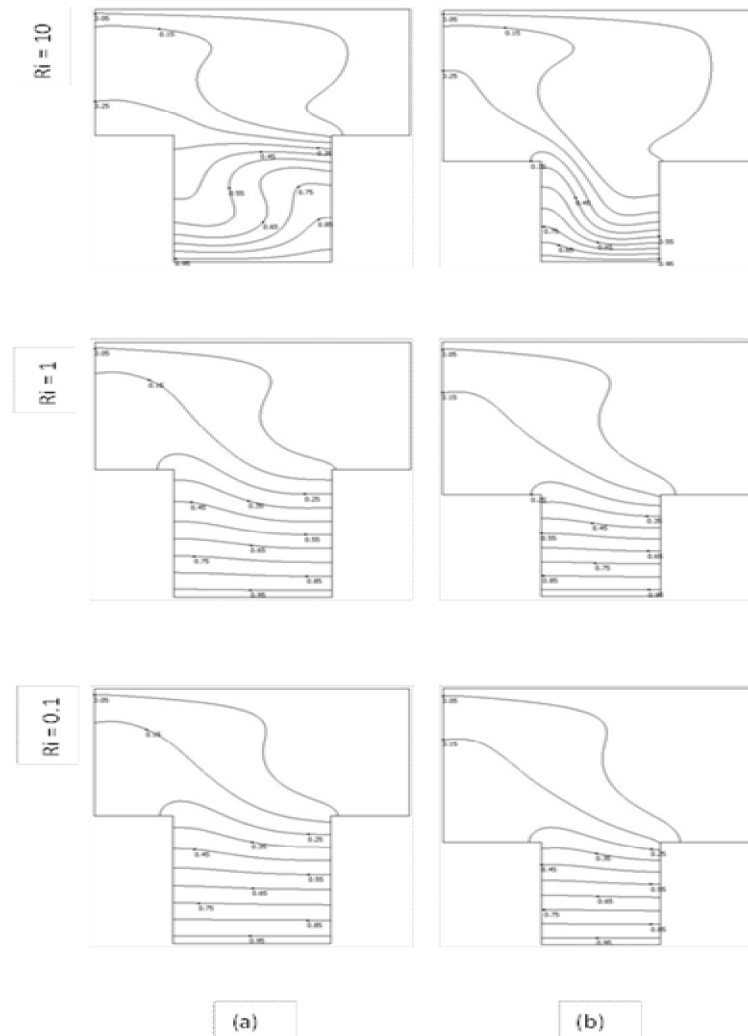


Fig4: Comparison of isotherm for (a)w=0.5,(b)w=0.6

For $Ri = 10$ there is a strong buoyancy induced flow in the cavity. Due to this strong buoyant flow (which originates due to heated bottom wall), there is the presence of another smaller vortex near the heated wall. This indicates local convection heat transfer in that region. In the column (b) similar effects are shown for $w = 0.6$. The overall effect for low Ri value is almost the same except for the fact that the strength of the vortices increase for both $Ri = 0.1$ and $Ri = 1$. Besides this effect, the eye seems to shift towards the middle of the upper chamber. Actually as the upper chamber's area is increased, the vortex gets a larger area to circulate and since the moving lid is adjacent to this chamber, the eye of the vortex shifts towards the middle. The most interesting difference is probably for the case of $Ri = 1$ where instead of two only one larger and extended vortex is formed which is relatively stronger than it was for $Ri = 0.1$ and $Ri = 1$. This result indicates that, as the area of the lower chamber is increased, there is a tendency towards the formation of a small vortex in that chamber. On the contrary if the upper chamber dimension is increased, the chance of creation of another vortex at the lower chamber decreases.

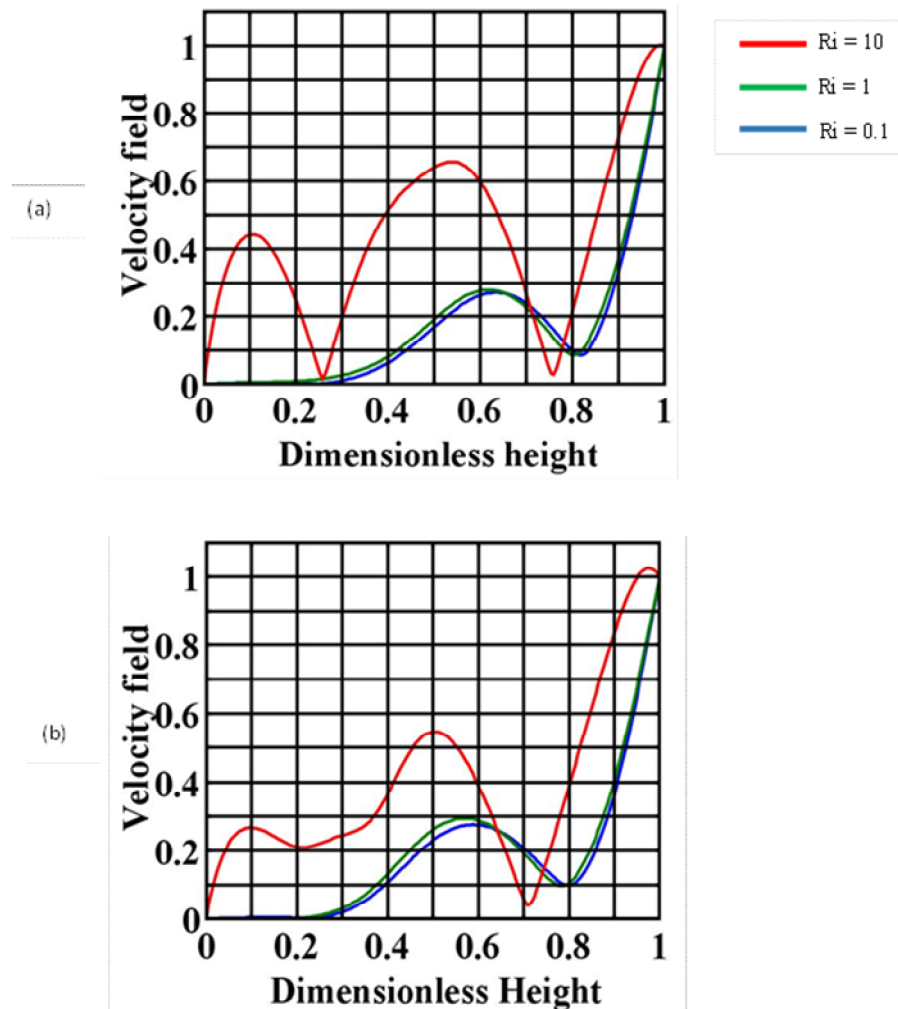


Fig 5: Centerline velocity for the dimensionless height for (a) $w=0.5$, (b) $w=0.6$

Figure 4 shows the isotherm contours for varying Ri and compares the cases between two geometries. In both cases for low Ri value ($Ri = 0.1$ and $Ri = 1$) the isotherm distribution is more dense near the heated wall as expected. For this condition, heat is diffused into the fluid inside the cavity mainly by conduction as the isotherms are nearly parallel to each other. On the other hand for strong buoyancy induced flow i.e. for $Ri = 10$, there is a significant distortion of isotherms near the bottom wall indicating high convective heat transfer rate. The isotherm density in the upper chamber also increases for high Ri value. These plots suggest that, for high value of Ri convection is dominant and heat diffusion is better.

Figure 5 depicts condition of the velocity field at the mid-plane for two different geometries. As can be seen from the figure, the mid-plane velocity is the highest for the case of $Ri = 10$ for both geometries. The velocity is highest near the moving wall due to no-slip condition. Velocity is very low near the .7-.75 dimensionless height region, indicating the center of the vortex there. For $w = 0.5$ there is another extremely low velocity region near 0.35 of the dimensionless height value. This indicates two separate vortices are there for this condition which is true. The general trend is, as the Ri goes up, the mid-plane velocity also goes up.

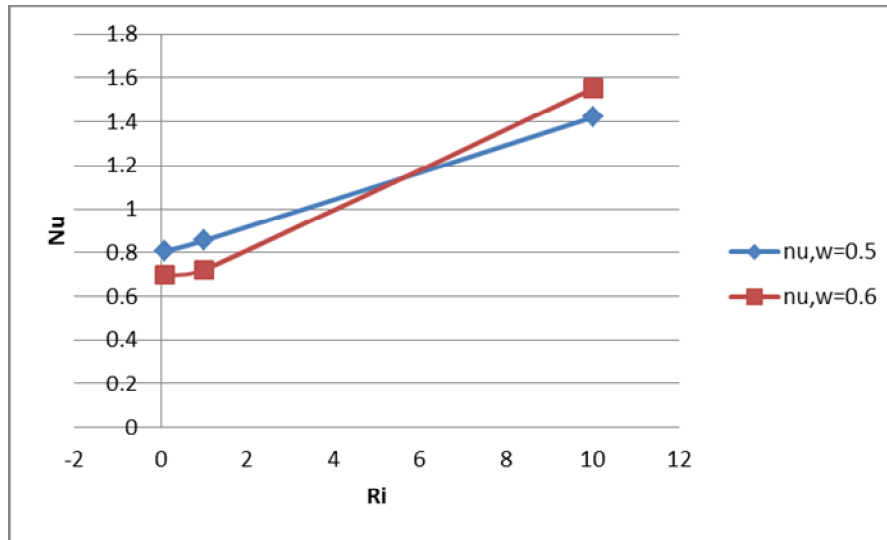


Fig.6: Average nusselt number at the heated bottom surface for different Ri

Figure 6 shows the average value of Nusselt number at the heated bottom wall versus Richardson number plot for two geometries. As can be seen from the figure, for low value of Richardson number the heat transfer characteristics are better for $w = 0.5$. At about $Ri = 5.9$, their performances become comparable. And for higher Ri values than this, $w = 0.6$ shows better heat transfer characteristics.

5. CONCLUSIONS

In this paper a thorough discussion has been made on the problem specification, its background literature and numerical solution procedures. From the result analysis the following conclusions can be drawn

- For high value of Richardson number the geometries show good heat transfer performance.
- As the area of the lower chamber is increased for high Richardson number, the possibility of strong local convection increases near the bottom wall.
- Moving lid dictates the convection.
- For low Richardson number, $w = 0.5$ performs better but for high Richardson number $w = 0.6$ geometry is better from heat transfer point of view.

This paper is concerned with the geometric and buoyant parameters mainly. Since the geometry shows a lot of promise and has got attention lately, the authors hope that the present paper will help the researcher around the world to have a better insight on the problem.

REFERENCES

- [1] Tapas Ray Mahapatra, Dulal Pal, Sabyasachi Mondal, “Effects of buoyancy ratio on double-diffusive natural convection in a lid-driven cavity” International Journal of Heat and Mass Transfer, Volume 57, Issue 2, February 2013, Pages 771-785
- [2] Simon Haque, Iman Lashgari, Flavio Giannetti, Luca Brandt, “Stability of fluids with shear-dependent viscosity in the lid-driven cavity” Journal of Non-Newtonian Fluid Mechanics, Volumes 173–174, April 2012, Pages 49-61
- [3] M. Morzynski, C.O. Popiel, Laminar heat transfer in a two-dimensional cavity covered by a moving wall, Numer. Heat Transfer 12 (1988)265–273
- [4] Khaled Al-Salem, Hakan F. Öztop, Ioan Pop, Yasin Varol, “Effects of moving lid direction on MHD mixed convection in a linearly heated cavity” International Journal of Heat and Mass Transfer, Volume 55, Issue 4, 31 January 2012, Pages 1103-1112

- [5] Siva Subrahmanyam Mendu, P.K. Das, "Fluid flow in a cavity driven by an oscillating lid—A simulation by lattice Boltzmann method" *European Journal of Mechanics - B/Fluids*, Volume 39, May–June 2013, Pages 59-70
- [6] M.K. Moallemi, K.S. Jang, Prandtl number effects on laminar mixed convection heat transfer in a lid-driven cavity, *Int. J. Heat Mass Transfer* 35 (1992) 1881–1892.
- [7] A.K. Prasad, J.R. Koseff, Combined forced and natural convection heat transfer in a deep lid-driven cavity flow, *Int. J. Heat Fluid Flow* 17(1996) 460–467.
- [8] T.S. Cheng, "Characteristics of mixed convection heat transfer in a lid-driven square cavity with various Richardson and Prandtl numbers" *International Journal of Thermal Sciences*, Volume 50, Issue 2, February 2011, Pages 197-205
- [9] Abdalla M. Al-Amiri, Khalil M. Khanafer, Ioan Pop, "Numerical simulation of combined thermal and mass transport in a square lid-driven cavity" *International Journal of Thermal Sciences*, Volume 46, Issue 7, July 2007, Pages 662-671
- [10] Alexandros Syrakos, Georgios C. Georgiou, Andreas N. Alexandrou, "Solution of the square lid-driven cavity flow of a Bingham plastic using the finite volume method" *Journal of Non-Newtonian Fluid Mechanics*, Volume 195, May 2013, Pages 19-31
- [11] Madhuchanda Bhattacharya, Tanmay Basak, Hakan F. Oztop, Yasin Varol, "Mixed convection and role of multiple solutions in lid-driven trapezoidal enclosures" , *International Journal of Heat and Mass Transfer*, Volume 63, August 2013, Pages 366-388
- [12] M.M. Billah, M.M. Rahman, U.M. Sharif, "Heat Transfer Enhancement of Nanofluids in a Lid-Driven Triangular Enclosure having a Discrete Heater" *Procedia Engineering*, Volume 56, 2013, Pages 330-336
- [13] Farhad Talebi, Amir Houshang Mahmoudi, Mina Shahi, "Numerical study of mixed convection flows in a square lid-driven cavity utilizing nanofluid" , *International Communications in Heat and Mass Transfer*, Volume 37, Issue 1, January 2010, Pages 79-90
- [14] Tanmay Basak, S. Roy, Sandeep Kumar Singh, I. Pop, "Analysis of mixed convection in a lid-driven porous square cavity with linearly heated side wall(s)" *International Journal of Heat and Mass Transfer*, Volume 53, Issues 9–10, April 2010, Pages 1819-1840
- [15] S.K. Farid, M.M. Billah, M.M. Rahman, Uddin Md. Sharif, "Numerical Study of Fluid Flow on Magneto-Hydrodynamic Mixed Convection in a Lid Driven Cavity having a Heated Circular Hollow Cylinder" *Procedia Engineering*, Volume 56, 2013, Pages 474-479
- [16] Tapas Ray Mahapatra, Dulal Pal, Sabyasachi Mondal, "Effects of buoyancy ratio on double-diffusive natural convection in a lid-driven cavity" *International Journal of Heat and Mass Transfer*, Volume 57, Issue 2, February 2013, Pages 771-785

A REVIEW OF HEAT TRANSFER ENHANCEMENT USING WINGLETS

M Arshad Zahangir Chowdhury , Md Rizwanur Rahman , Dr. M.A. Rashid Sarkar

ABSTRACT: Application of heat exchangers are very common in thermal power plants ,air-conditioning systems, refrigerators, radiators , cooling of electronics and in process industries. Enhancement of heat transfer through active, passive and compound techniques is an intense area of research. More efficient and less expensive heat exchangers have been developed as a consequence. The present paper is a review of passive heat transfer enhancement using winglets in the recent past.

Keywords: Heat Transfer; Enhancement; Augmentation; Winglets;

1. INTRODUCTION

Now-a-days a significant number of thermal researchers are seeking for new heat transfer enhancing methods between surfaces and surrounding fluids. The technique or method implemented to improve heat transfer performance is referred to as heat transfer enhancement (or augmentation or intensification). Generally , heat transfer enhancement methods are classified into three broad categories :

(a) Active method : This method involves external power input for enhancement of heat transfer. Examples of active methods include induced pulsations by cams and reciprocating plungers , the use of a magnetic field to disturb seeded light particles in a flowing stream , stirring the fluid , vibrating the surface etc.

(b) Passive method : This method involves the use of surface or geometrical modifications to the flow channel by incorporating inserts or additional devices such as inserts , rough surfaces, treated surfaces, extended surfaces, swirl flow device, displacement enhancement device, coiled tube etc. Passive methods do not require external power to maintain enhancement of heat transfer characteristics.

(c) Compound methods : It is a combination of the above two methods.

2. PASSIVE HEAT TRANSFER AUGMENTATION METHODS

The biggest advantage of passive heat transfer enhancement methods is it does not require any external power input. Hence it is most popular. This method is based on the principle of convective heat transfer. In convective heat transfer , one technique of enhancement of heat transfer is to increase the effective surface area and residence time of heat transfer fluids. Use of this technique causes the swirl in the bulk of the fluids and disturbs the actual boundary layer so as to increase effective surface area, residence time and consequently heat transfer coefficient in the existing system.

Implementing winglets are one way of passive heat transfer enhancement. The reasons for this are -

- (1) Introducing a secondary heat transfer surface
- (2) Disruption of unenhanced fluid velocity
- (3) Disruption of laminar sub-layer in the turbulent boundary layer
- (4) Introducing secondary flows

Some of the recent advances in passive heat transfer enhancement using winglets are the subject of this review.

3. REVIEW OF WORK

Allison and Dally [1] studied the effect of delta winglet vortex pair on the performance of a tube fin heat exchanger. They arranged the winglets in flow-up configuration, and placed directly upstream of the tube. In addition to vortex generation the flow is guided onto the tube surface increasing the localized velocity gradients and Nusselt Numbers in this region. The study includes dye visualization and full scale heat transfer performance measurements.

Mechanical Engineering Division

The Institution of Engineers, Bangladesh

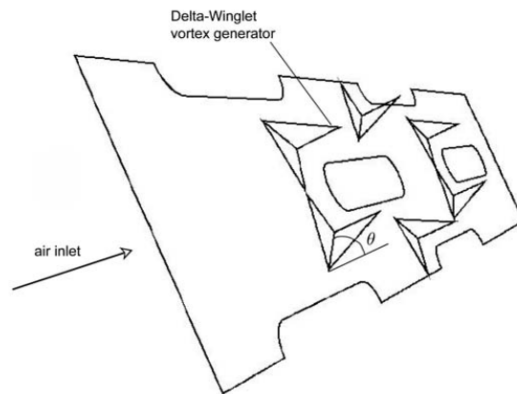
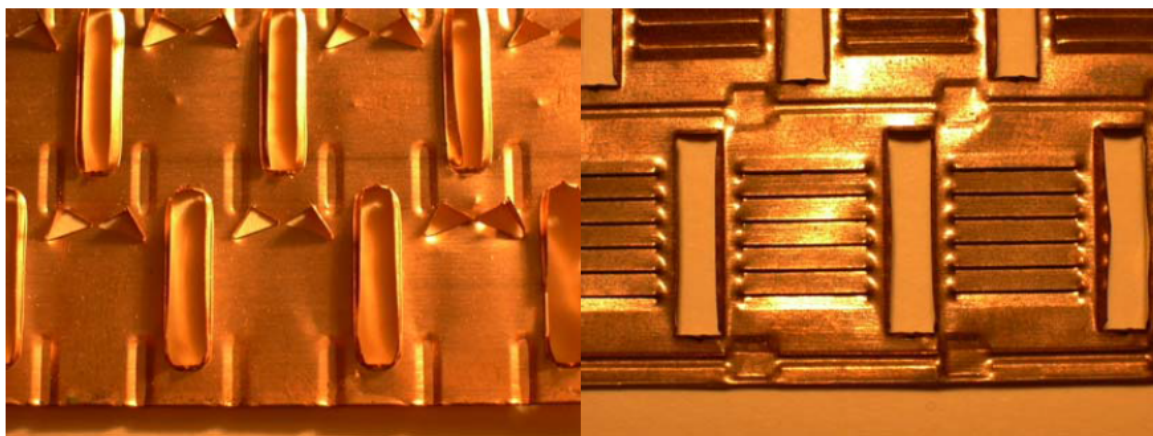


Fig.1: Schematic representation of the delta winglet pair arranged in flow up configuration



a) Flow-Up Delta-Winglet

b) Louvre fin surface

Fig.2: Comparison of test coil fin surface

The results are compared to a standard louvre fin surface. It was found that the winglet surface had 87% of the heat transfer capacity but only 53% of the pressure drop of the louvre fin surface. Various delta configurations were trialed using flow visualization. Finally a flow-up delta winglet pair positioned immediately in front of each tube was chosen. A prototype coil was fabricated and experimentally assessed on a purpose built coil test rig.

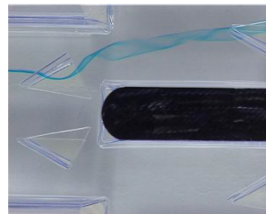


Fig.3: Longitudinal vortex street generated by delta wing vortex generator.

Sanders and Thole [2] studied the effects of winglets to augment tube wall heat transfer in in louvered fin heat exchangers. The majority of most research, aimed towards improving louvered fin exchanger efficiency, has focused on optimizing various parameters of the louvered fin. This experimental study presented in this paper concentrates instead on augmenting the heat transfer along the tube wall of the compact heat exchanger through the use of winglets placed on the louvers. Their experiments were

completed on a 20 times scaled model of an idealized louvered fin exchanger with a fin pitch to louver pitch ratio of 0.76 and a louver angle of 27 degree.

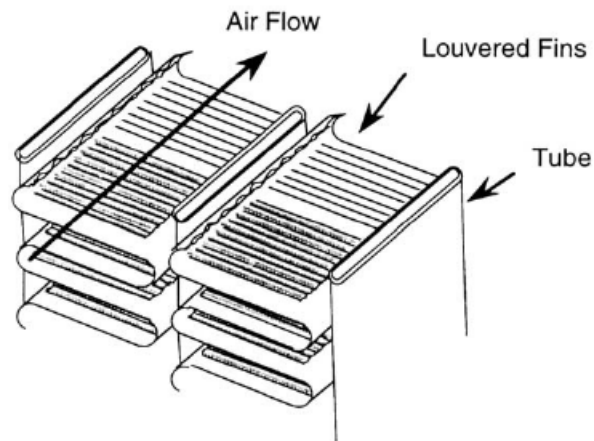


Fig.4: Design of realistic louvered fin heat exchanger

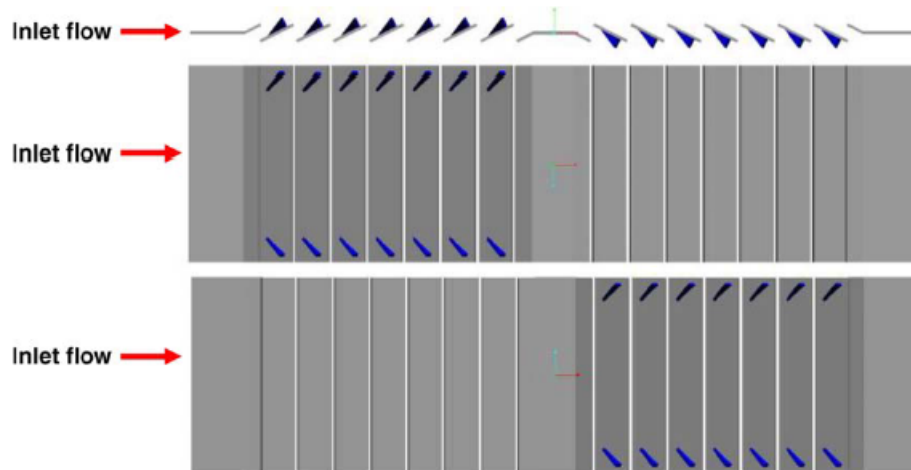


Fig.5: Side, top and bottom view of VG-F winglets all aimed towards the wall

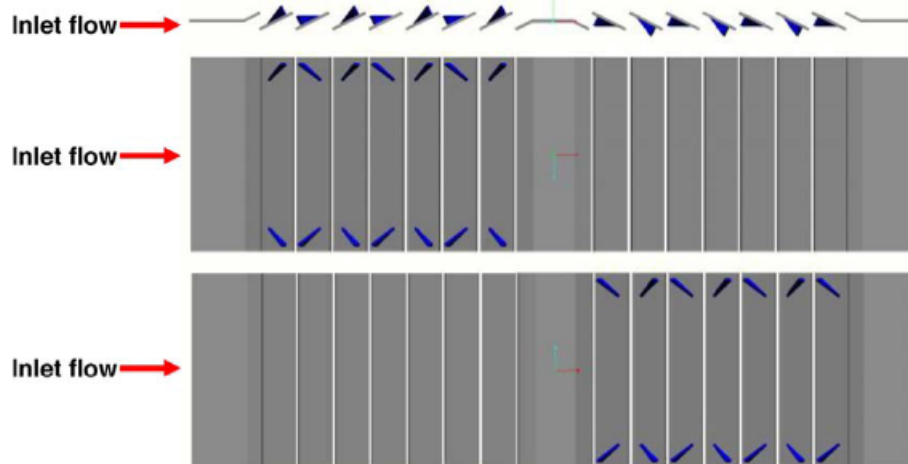


Fig.6: Side, top and bottom view of VG-F/B alternating winglets

This study experimentally explores the use of delta winglets placed on the louvers near the tube wall to augment tube wall heat transfer. Tube wall heat transfer and pressure drop measurements are reported for an idealized louvered fin geometry. Several parameters for the delta winglets were studied to give a wide range of results for determining important trends

The Reynolds numbers tested, based on louver pitch, were between 230 and 1016. A number of geometrical winglet parameters, including angle of attack, aspect ratio, direction, and shape, were all evaluated based on heat transfer augmentation, friction factor augmentation, and efficiency index (combination of both augmentations). In an attempt to optimize these winglet parameters, tube wall heat transfer augmentations as high as 39% were achieved with associated friction factor augmentations as high as 23%.

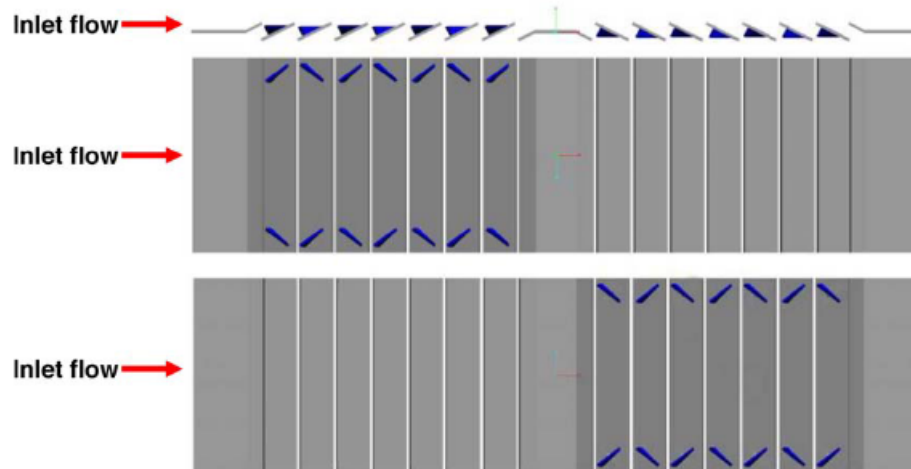


Fig.7: Side , top and bottom view of VG-B winglets with alternating direction.

There were three primary winglet orientations and directions tested: winglets all aimed towards the wall, alternating winglet direction and orientation, and alternating winglet direction with backward winglets throughout. In the configuration where all of the winglets were aimed towards the wall in the VG-F configuration, the average heat transfer augmentations were typically very low. When the winglet direction and orientation were alternated on every other louver, results were significantly improved with a maximum augmentation of 25%. When all winglets were placed in the VG-B orientation with alternating direction, results improved yielding augmentations of up to 33%.

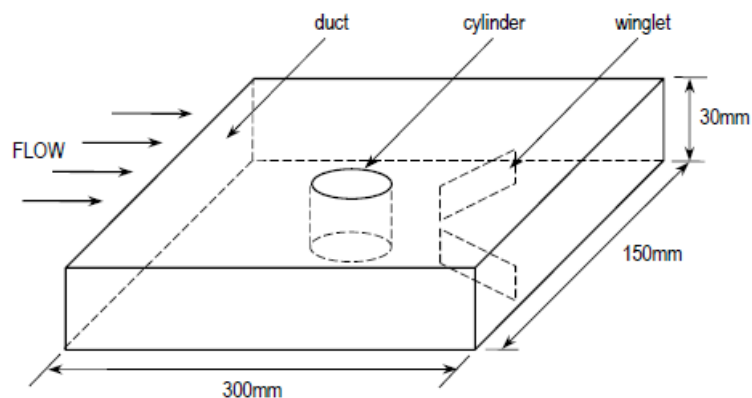


Fig.8: Schematic diagram of test section of flow around a circular cylinder using winglets.

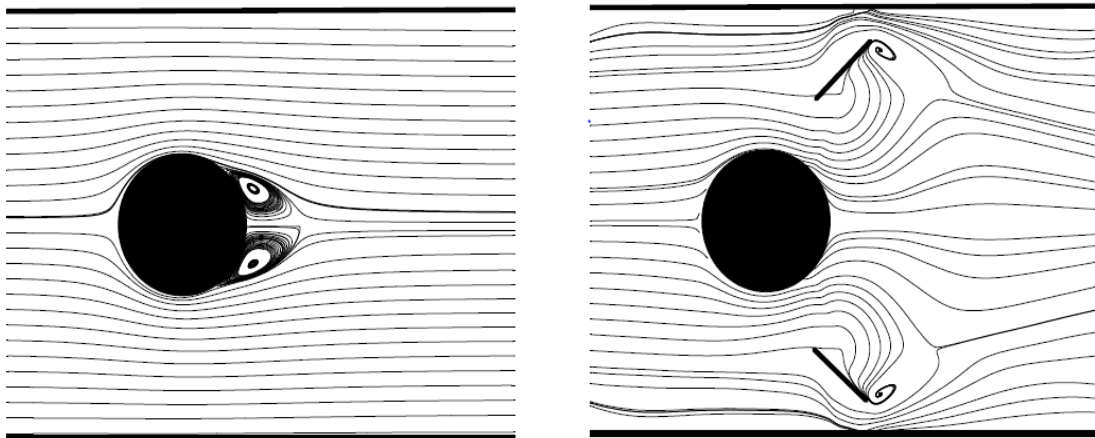


Fig.9: Streamline on cylinder with and without winglets.

Jalil , Abdullah and Yousif [3] studied heat transfer and flow structure around circular cylinder with using rectangular winglets. They conducted an experimental and numerical study to investigate heat transfer and flow characteristics over cylinder (for constant heat flux) with turbulent fully-developed flow by using rectangular winglet with Reynolds number (1.08×10^4), different angle of attack of winglet (20, 26 and 32) and different positions ($X_m/D=0, 0.17, 0.3, 0.5$) and $Y_m/D=0.57, 0.65, 0.72, 0.8$). The effects of turbulence are simulated by $(k-\epsilon)$ turbulence model.

The investigation are needed to enhancement heat transfer from cylinder in gas side through controlling the flow on cylinder surface and prevent growth of boundary layer, (FVM) in general coordinate was use with collocated grid, to solving the governing differential conservation equations. The results were compared with the case of flow without winglet. Good agreement between numerical and experimental results. The results shows that heat transfer from cylinder enhanced as high as (14%) when used winglet and the heat transfer increase with increasing the angle of attack also, pressure drop increasing with using winglet and with increasing the angle of attack.

Mirazel and Sohankar [4] analyzed heat transfer augmentation in plate finned tube heat exchangers with vortex generators (winglets) . They compared the performances of round and flat tubes. Heat transfer augmentation and pressure loss penalty caused by vortex generators (VGs) are numerically studied by them for finned flat/round tube heat exchangers and compared with available experimental results.

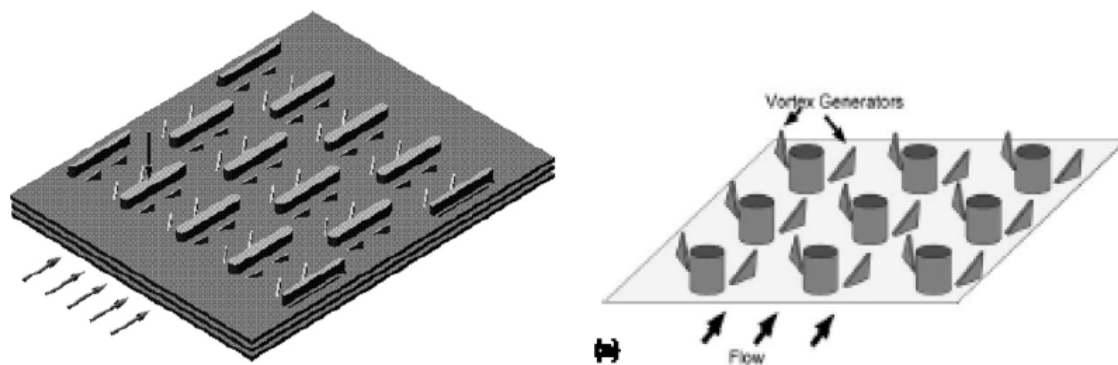


Fig.10: Schematic view of tube fin heat exchangers with vortex generators. Right - flat tube , Left - round tube.

The simulations are performed with the steady three-dimensional incompressible conditions and a *RNG K-ε* turbulence model is used. The Reynolds numbers based on the bulk velocity and the height of channel are selected from 600 to 4050. To compare the effectiveness of VGs on the round and flat tubes for tube-fin heat exchangers, two different configurations are investigated with two and four delta winglet vortex generators for each tube. The streamlines, vorticity, the averaged Nusselt number, the friction factor and the performance factor (*JF*) are provided to evaluate the effectiveness of VGs for the heat exchangers employed. It is found that the flat tube with VGs provides better thermal performance than the round one, especially at the lower Reynolds numbers.

Maniar [5] studied heat transfer enhancement in a rectangular channel using vortex generator in a laminar flow. This research involves the numerical analysis of heat exchange enhancement in a rectangular channel using different types of longitudinal vortex generators (LVG) for a laminar flow.

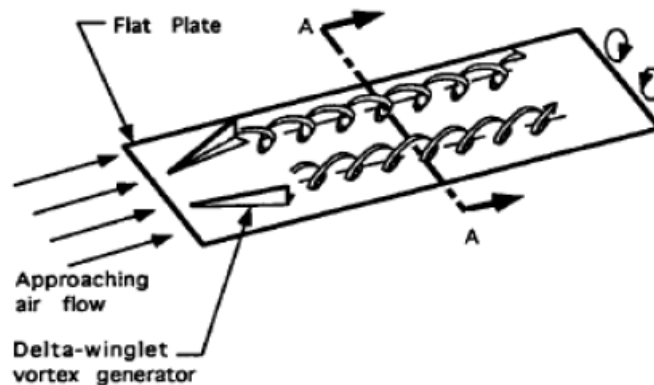


Fig.11: Direction of generated vortices in flow down configuration.

A computational fluid dynamics software package was used to compute the 3-D steady viscous flows with heat transfer. The effects of Reynolds number ranging from 500 to 1000 (laminar flow) are shown from different attack angles of the vortex generators (30° and 45°). Three different types of vortex generators are studied: a delta wing with finite thickness, a trapezoidal delta wing, and a delta winglet pair (also called half delta wing) for a common flow down configuration.

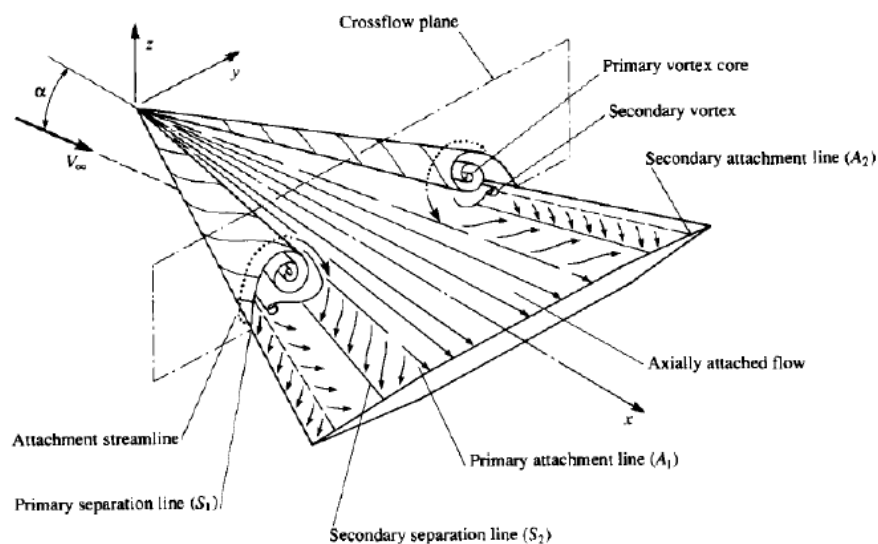


Fig.12: Flow over a trapezoidal delta winglet.

The results show that the average surface Nusselt number ratio for a delta wing at attack angles of 30° and 45° shows that the heat transfer enhancement takes place to some extent and a higher attack angle produces higher heat augmentation but at the cost of pressure loss. The average surface Nusselt number ratio for a trapezoidal delta wing is much higher than that of delta wing at the same attack angles and same chord length of the wing. The only advantage is that the trapezoidal wing has a sharp leading edge which helps in the early generation of primary vortices and, thus, has higher average surface Nusselt number than the delta wing. The important outcomes of these works are tabulated below.

Table 1: Summary of important investigations of heat transfer using wings and winglets

Authors	Fluid	Configuration of Winglet	Type of Investigation	Observation
1. Allison and Dally [1]	Air ($2500 \leq Re \leq 7500$)	Delta	Experiment in tube fin heat exchanger	Winglet surface had 87% of the heat transfer capacity but only 53% of the pressure drop compared to the louvered fin surface.
2. Sanders and Thole [2]	Air ($230 \leq Re \leq 1016$)	Delta	Experiment in louvered fin heat exchanger	<ol style="list-style-type: none"> When all of the winglets were aimed towards the wall in the VG-F configuration, the average heat transfer enhancements were typically very low. When the winglet direction and orientation were alternated on every other louver, maximum augmentation of 25% was recorded. When all winglets were placed in the VG-B orientation with alternating direction, results improved yielding augmentations of up to 33%.
3. Jalil, Abdullah and Yousif [3]	Air ($Re = 1.08 \times 10^4$)	Rectangular	Experiment over cylindrical body	<ol style="list-style-type: none"> Heat transfer increased as much as 14% when using winglets. Heat transfer increased with increasing angle of attack. Pressure drop increased with increasing angle of attack.
4. Mirazel and Sohankar [4]	Air ($600 \leq Re \leq 4050$)	Delta	Experiment in plate finned tube heat exchanger	The flat tube with vortex generators shows better thermal performance than the round one, especially at lower Reynolds numbers.
5. Maniar [5]	Air ($500 \leq Re \leq 1000$)	Delta and trapezoidal	Experiment in rectangular channel	<ol style="list-style-type: none"> Higher attack angles result in enhanced heat transfer but at the cost of higher pressure loss for delta winglet. Trapezoidal wings produce primary vortices and thus have higher surface Nusselt number than delta wing.

REFERENCES

- [1] Alisson CB and Dally BB, "Effect of a delta winglet vortex pair on the performance of a tube-fin heat exchanger." *Heat and Mass Transfer Journal*, Volume 50, Issues 25-26, December 2007, Pages 5065-5072
- [2] PA Sanders and KA Thole , "Effects of winglets to augment tube wall heat transfer in louvered fin heat exchanger" *International Journal of Heat and Mass Transfer* 49 (2006) 4058–4069
- [3] JM Jalil , HK Abdulla and AH Yousif , "Heat Transfer and flow structure around circular cylinder with using rectangular winglet." *Emirates Journal for Engineering Research*, 12 (2), 41-46 (2007)
- [4] M Mirazael and A Sohankar , "Heat transfer augmentation in plate finned tube heat exchangers with vortex generators: a comparison of round and flat tubes." *IJST, Transactions of Mechanical Engineering*, Vol. 37,(2013) No. M1, pp 39-51
- [5] NC Maniar, "Heat transfer enhancement in a rectangular channel using vortex generator in a laminar flow ." M.Sc Thesis submitted to *the University of Texas at Arlington* December 2012

REVIEW OF HEAT TRANSFER AUGMENTATION USING DELTA WINGLET VORTEX GENERATORS

M.A.M.S. Shoshe, R. Ahmed, M.A. Rahman¹, M.A.R. Sarkar²

Department of Mechanical Engineering, Bangladesh University of Engineering & Technology
Dhaka, Bangladesh

¹ ashiqu78@yahoo.com

² rashid@me.buet.ac.bd

ABSTRACT: Heat transfer augmentation techniques are used in heat exchanger, air conditioning, chemical reactors and refrigeration systems. Many techniques have been investigated to enhance heat transfer rate and decrease the size and cost of involving equipment. Among different techniques delta winglet vortex generators become popular in recent days. It generates stream wise vortices which creates high turbulence in fluid flow over the heat transfer surface and shows a very good heat transfer performance. This study presents recent works taken by researchers on delta winglet vortex generators to enhance thermal efficiency in heat exchange with different types and arrangements of delta winglet vortex generators.

Keywords: Heat transfer augmentation Vortex generator Delta-winglet Heat exchanger

1. INTRODUCTION

Heat transfer between fluids at different temperature is common in engineering applications such as heat exchanger, refrigeration system, chemical reactors and air conditioning. By enhancing heat transfer the performance of the device can be improved along with size reduction. The augmentation methods used can generally be divided into two categories, active and passive methods. The active methods require external forces, e.g., electric field, acoustics, and surface vibrations. The passive methods require special surface geometry or fluid additives. Swirl generators, vortex generators, surface treatment and extended surfaces are popular passive methods.

One of the most important passive techniques to augment heat transfer is the use of vortex generators. Transverse vortex generators produce vortices, whose axis is transverse to the main flow direction, whereas, the longitudinal vortex generators generate vortices whose axis is parallel to the main flow direction. Also as described by Fiebig *et al.* [6], when angle of attack of VGs is small, generates vortices are mainly longitudinal, and when VGs are perpendicular to the flow direction, generates vortices are mainly transverse. It has been found that longitudinal vortex generators are more suitable than the transverse vortex generators when the heat transfer augmentation with pressure drop is an important consideration also longitudinal vortices are found to persist for more than 100 protrusion heights downstream.

Longitudinal vortex generators may have any of the four basic shapes i.e. delta wing, rectangular wing, delta winglet and rectangular winglet. The aspect ratio ' Λ ' of a longitudinal vortex generator is the ratio of the square of the span ' b ' and the area of the vortex generator ' s ' i.e. $\Lambda = \frac{b^2}{s}$. The aspect ratio of vortex generator is an important criterion to compare the performance of the different shapes. Among these vortex generators Delta winglet vortex generators (DWVG) is a fine choice because it increases convective heat transfer by developing a boundary layer, swirl, or vortices, as well as through flow destabilization or turbulence intensification [6]. The delta winglet enhances heat transfer more than a rectangular winglet and having the wing pulled backwards it creates very small amount of drag as documented by NASA [7]. Gentry and Jacobi [12] used naphthalene sublimation to measure the performance of vortex generators. They reported average enhancements of 20–50% with accompanying pressure drop penalty of 50–110%, for Reynolds numbers ranging from 400–2000.

In case of winglet, single vortex is generated by the fluid which passes over the winglet; however, for the wing vortex generator, two vortices are produced as the obstructed fluid passes over the wing from both the side edges. Differences between various DWVG are presented in table 1. Figure 1 shows a sketch of longitudinal vortices behind a delta winglet vortex generator placed in a laminar boundary layer on a flat plate (Torii *et al.* [4]). The flow separation at the leading edge of the winglet generates a main vortex and the corner vortex is formed by the deformation of near-wall vortex lines at the pressure side of the winglet. Sometimes an induced vortex is also observed rotating opposite to the main and corner vortex. It should be noted that generation of vortex is preferable as it enhances the heat transfer. In the following section a brief review of the past works done by researchers to enhance the heat transfer performance using DWVG is given.

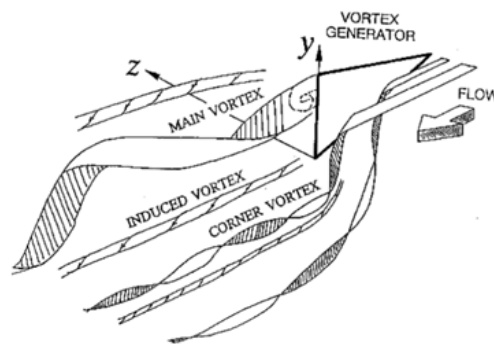
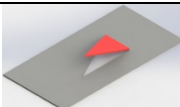
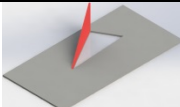
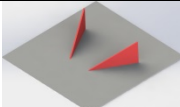
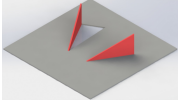

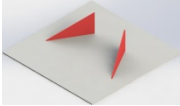
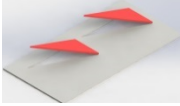

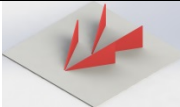




Fig.1: Vortex systems behind a delta winglet (Torii *et al.* [4])

Table 1. Different geometry and arrangements of DWVG

Configuration	Name	Description	Reference
	Delta wing	Its span is attached to the surface. It generates double helical flow.	[41]
	Delta winglet	Its chord is attached to the surface. It generates larger single helical flow	[41]
	Built in DWVG	A premade delta-winglet is attached to the surface of heat transfer.	[23]
	Stamped DWVG	This delta-winglet is a cut off which left a piercing downstream.	[28]

	Common flow up	The secondary flow between two counter rotating vortices is away from the wall.	[46]
	Common flow down	The secondary flow between two counter rotating vortices is towards the wall.	[46]
	In-line DWVG	The winglets were arranged in flow-up configuration, placed directly upstream.	[23]
	Single pair V array DWVG	A single pair of winglet is arranged in V formation.	[8]
	Two row pairs V array DWVG	.Two single pair in two rows in V formation.	[8]
	Two pair V array DWVG	Two pairs of DWVG is arranged one after another in V formation.	[8]
	Three pair V array DWVG	Three pairs of DWVG is arranged one after another in V formation.	[8]

2. EXPERIMENTAL WORKS

Research works on heat transfer augmentation using delta winglet vortex generators has been going on over past few decades. Plenty of works on heat exchangers, pipe flow, refrigeration system, flat surface and many other topics had been carried out. Among them heat exchangers is of top priority due to their large use in industrial work. Research works on fin tube, plate fin and louvered fin heat exchangers are described below.

Fiebig *et al.* [6] considered heat exchanger elements with 3 tube rows and a delta-winglet pair downstream of each tube. For an inline tube arrangement they measured a 55–65% increase in heat transfer, with a pressure drop increase of 20–45%. The staggered arrangement resulted in less enhancement and pressure loss. Numerical studies have also addressed vortex generators in channel flows with tubes. In 1994 Biswas *et al.* [29] reported that a delta winglet pair downstream of tube results in up to 240% local enhancement of the heat transfer in the recirculation zone. For punched delta-winglets in such a flow configuration, the numerical predictions of Fiebig *et al.* [30] showed a 31% enhancement at $Re = 300$.

In 1999, Jahromi *et al.* [31] reported 20–50% enhancements with similar configuration for a Re range of 400–1200. The ratio of increase in Nusselt number to the increase in friction factor ranged between 0.65 and 0.78. Torii, *et al* [13], in their paper showed that in case of staggered tube banks, the heat transfer was augmented by 30 % to 10 %, and yet the pressure loss was reduced by 55 % to 34 % for the Reynolds number ranging from 350 to 2100 deploying DWVG. Kwak *et al.* [14] measured the heat transfer coefficient and pressure drop in 2, 3, 4, and 5-row fin-tube heat exchangers with a common flow up configuration DWVG in a range of $280 < Re < 2400$. Compared with heat exchangers with plain fins, those with DWVG fins showed a 10% increase in heat transfer performance of the j-factor for all heat exchangers, and a 0%–10% increase of the f-factor for the 2, 4, and 5-row heat exchangers. For the 3-row heat exchanger, however, the f-factor dramatically decreased by 30%–50%.

Kwak *et al.* [16] investigated the effect of the number of DWVG rows, the heat exchanger with a single DWVG row experienced 10%–30% larger heat transfer capacity and 34%–55% less pressure drop than the heat exchanger without the DWVG. For the heat exchanger with two DWVG rows, however, heat transfer capacity and the pressure drop increased by 6%–15% and by 61%–117%, respectively, compared with the heat exchanger with a single DWVG row.

Joardar and Jacobi [19] investigated the effect of the number of DWVG rows in the inline array fin-tube heat exchangers. The DWVG was placed in a common flow up configuration. For the single DWVG, the heat transfer coefficient was enhanced by 16.5%–44% as pressure drop increased by less than 12%. For the case of three DWVG rows, the heat transfer coefficient was augmented by 29.9%–68.8% as the pressure drop penalty increased 26% at Re = 960 and 87.5% at Re = 220.

Sohal *et al.* [11], [32] performed an experimental study on local heat transfer in a narrow rectangular duct fitted with a circular tube, and/or winglet vortex generators. The duct was designed to simulate a single passage in a fin-tube heat exchanger at Reynolds number range of 670–6300, the enhancement level is close to 50%. In [37] they also found an average Nusselt number enhancement ratio of 35%. Figure 2 shows the location and geometry used by them.

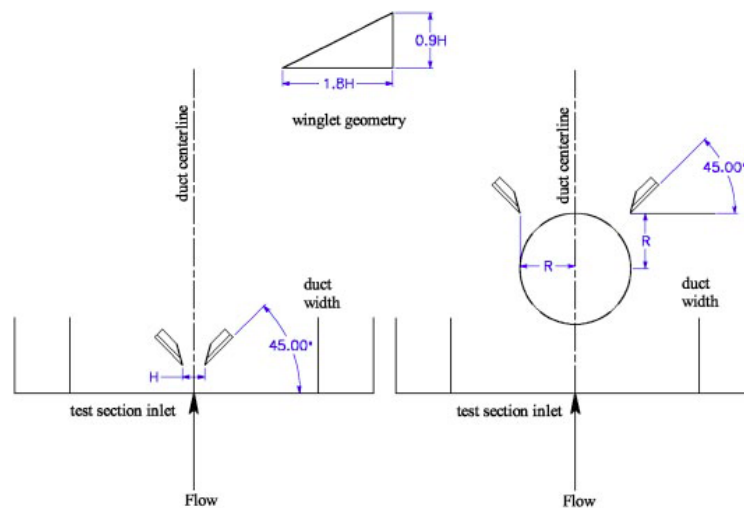


Fig.2: Winglet locations and geometry for finned tube heat exchangers. [Sohal *et al.* [11]]

Allison and Dally [18] similarly examined the performance of the DWVG in flat fin tube heat exchangers, and compared the performance of two fin types. The first is a plain fin with a DWVG and the second is a louvered fin. The DWVG were installed in a common flow up configuration. The j- and f factors of the heat exchanger with the DWVG were 87% and 53%, respectively, of the heat exchangers with a louver

fin. Researchers also investigated the performance of DWVG fins through numerical analysis. Wang *et al.* [36] present airside performance of the delta winglet vortex generator (VG) vs. a wavy fin surface in both dry and wet conditions. For the airside performance tested in dry condition, the heat transfer coefficient for the wavy fin surface is only 6% higher than that of the winglet VG, but the pressure drop is about 15% higher. For the airside performance tested in wet condition, the heat transfer performance of the winglet VG is superior to that of the wavy fin surface. Furthermore, the pressure drop for winglet VG is considerably lower (15 ~ 40%).

Tian *et al.*[33] performed three-dimensional numerical simulations for wavy fin-and-tube heat exchanger with DWVG at Re 500 to 5000. The results show that each delta winglet generates a downstream main vortex and a corner vortex. Nusselt number and friction factor both increase with the increase in the attack angle, and the case of $\alpha=30^\circ$ has the maximum value of j / f . Hwang *et al.* [3] also performs numerical analysis with DWVG in common flow up configuration in fin tube type heat exchangers which suggests that using the DWVG causes a high volume goodness factor. Consequently, a smaller volume is required for the same pumping power. Joardar *et al.* [34] numerically showed that at Re=850 with a constant tube-wall temperature, the 3VG-inline-array configuration achieves enhancement up to 32% in total heat flux and 74% in j factor over the baseline case, with an associated pressure-drop increase of about 41%.

Huisseune *et al.*[35] numerically studied the performance of a compound heat exchanger of louvered and delta winglet and found that the Colburn j -factors of the compound design are higher than when the individual enhancement techniques are applied separately (up to 16% higher compared to the louvered fin heat exchanger and up to 87% higher compared

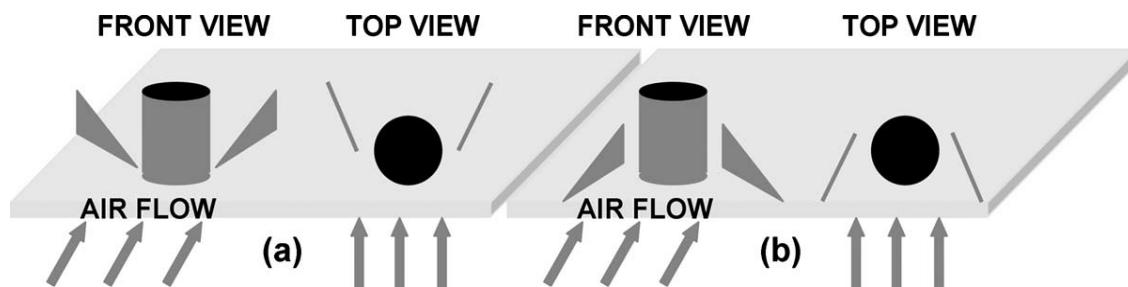


Fig.3: Configuration of winglet-type VG on a fin surface :(a) common-flow down and (b)common-flow-up [Jacobi *et al.*[8]]

to the delta winglet heat exchanger). Also the associated friction factors are up to 37% higher compared to the louvered fin heat exchanger and up to 156% higher compared to the delta winglet heat exchanger. For a fixed pumping power per unit volume, the heat transfer per unit volume of the compound design is up to 14% higher compared to the louvered fin heat exchanger and up to 72% higher compared to the delta winglet heat exchanger. For the same thermal hydraulic performance, the compound heat exchanger can thus be made smaller in size. As a result, the material cost is lower.

El Sherbini and Jacobi [38] tested delta vortex generators on plain-fin-and-tube heat exchangers. The ratio of wing to heat transfer area was 0.23% and $a = 55$, $K = 1$. They achieved a 31% heat transfer enhancement over the baseline, with modest pressure drop penalty of 10% under dry-conditions. Bull and Jacobi [39] reported 10% enhancement in volume goodness factor under dry-conditions for compact plain-fin-and-tube heat exchanger. In this study, $a = 45$, $K = 2$ and wing-to-fin area ratio was 0.89%. For wet-conditions the overall enthalpy transfer coefficient was reduced; however, on the basis

of the London area-goodness factor (j/f) the vortex-enhanced surface was found to be comparable to other enhanced surfaces.

Jacobi *et al.* [8] proposed a new vortex generator (VG) array deployed in a "V", inspired by group movement of animals in nature, aiming to create constructive interference between vortices and improve VG performance with Reynolds numbers of 340, 570, and 940. A single winglet pair is firstly examined at various attacks at 15, 30 and 45 degree angles, followed by multi pair VGs placed at the optimal angle. They conducted the experiment with single winglet pair, two-pair V-array, conventional two-row pairs, and three-pair V-array vortex generators. They concluded that longitudinal vortices are at their strongest immediately after the generators and very persistent throughout the channel. Local enhancement of over 100% is observed at relatively high Reynolds numbers and for a single winglet pair, an appropriate angle of attack is found to be 30°. The design yields 12-36% augmentation in the total heat transfer as compared to 8-26% obtained by the conventional two-row configuration. Figure 3 showed the configuration used.

As for plate fin heat exchangers, Gulshan *et al.* [23], figure 4, conducted experiments with different DWVG at Re 100 and at an angle of attack of 26° yielding an increase in Nusselt number of 74.3% for built in geometry, 130% for stamped one and 75-82% for in line formation. Tiggelbeck *et al.*, [9], investigated the effect of four types of vortex generators (delta wing, delta winglet rectangular wing and rectangular winglet) on local heat transfer and drag of plate fins and compared the results between these types of vortex generators and in the Reynolds number range (2000-9000) with angle of attack range of (30°-90°). The results show there exist an optimum angle of attack between (50° and 70°) for maximum heat transfer and the winglet gives better performance than wings and pair of delta winglet performs slightly better than the pair of rectangular winglets.

Amin *et al.* [24] numerically studied the performance of DW pair which showed an increase of 3.3-25.7% in Nusselt number with 20.1% friction factor increase. Kumar *et al.* [25] numerically showed that at Re 200 and 45°AOA VG should be placed at inlet for maximum performance. Sinha *et al.* working with a wide Reynolds number range (Re 250-1580) and five different combination of series VG pairs showed that, performance of CFU-CFU (common flow up) configuration is best in terms of heat transfer as well as quality factor which also confirmed by Wu *et al.* [26]. And in [27] they confirmed that DWVG is the best choice over different VGs.

In case of louvered fin heat exchangers, figure 5, Jacobi *et al.* [15] experimentally evaluated full-scale wind-tunnel testing of a compact heat exchanger typical to those used in automotive systems for both dry- and wet-surface conditions for a louvered- fin baseline and for a vortex-enhanced louvered-fin heat exchanger. An average heat transfer increase over the baseline case of 21% for dry conditions and 23.4% for wet conditions was achieved with a pressure drop penalty smaller than 7%.

Lawson *et al.* [20] and Sanders and Thole used simplified louvered fin geometry where the louver surface spanned the entire heat exchanger core. Winglets with a thickness of the louvers were shown to have only a small positive effect on heat transfer. Incorporating piercings into the louvered fins was shown to slightly increase heat transfer compared to tests without piercings; however, the maximum winglet augmentation of tube wall heat transfer observed was only 8%. Sanders [21] tested the effects of winglets incorporated into a more realistic louvered fin geometry and measured heat transfer augmentation as high as 53% along the tube wall with only a 21% increase in pressure losses.

Min *et al.* [28] numerically predicted the performances of the plain fin, the fins with punched delta winglets, and the louver fin used in a flat-tube heat at Reynolds numbers of 210 and 840. As compared to the plain fin, the louver fin enhances heat transfer by 114.1-139.1% while the fin with three winglet rows enhances heat transfer by 46.5-76.1%, indicating that the enhancement level of the louver fin is considerably higher than that of the fin with winglets.

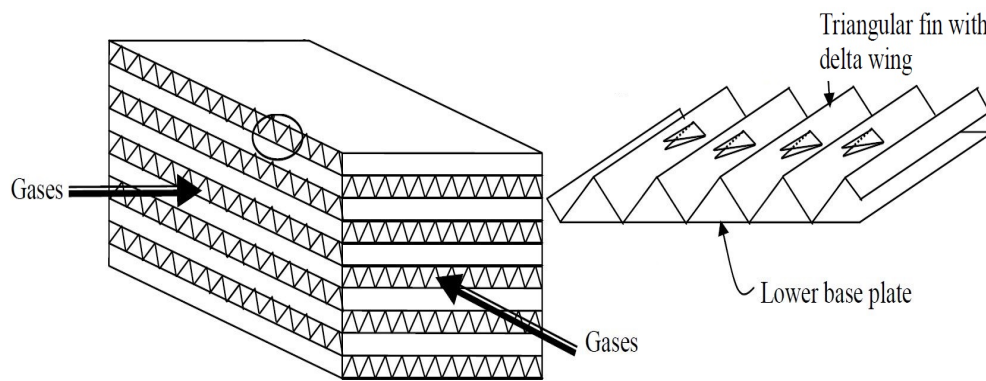


Fig.4: Plate-fin heat exchanger [Gulshan *et al.* [23]]

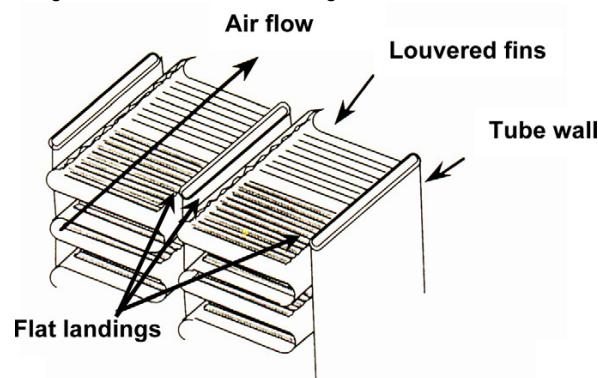


Fig.5: Louvered fin heat exchanger [Lawson *et al.* [20]]

The works done regarding the flow over flat plates can be presented as follows. Gentry and Jacobi [5] studied interactions between longitudinal vortices from delta wing and the laminar boundary layer on a flat plate. For a Reynolds number range of 600–1000 based on plate length, they reported average heat transfer enhancements of 50–60%.

Biswas *et al.* [10] studied the effect of delta winglets on heat transfer over a flat plate. Augmentation is as high as 65% were measured on the plate surface. They concluded that delta winglets show significant promise for improving the heat transfer performance of heat exchangers.

Experiments have been carried out by Aris *et al.* [44] in a rectangular duct supplied with laminar-transition air flow. In the test section, a single, and a pair of active delta wing VGs were placed near the leading edge of a heated plate and tested separately. Promising shape memory response was obtained from the active VG samples when their surface temperatures were varied from 20°C to 65°C. The vortex generators responded by increasing their angles of attack from 10° to 38° and as the designs were two-way trained, they regained their initial position and shape at a lower temperature. At their activated positions, maximum heat transfer improvements of up to 90% and 80% were achieved by the single and double wings respectively along the downstream direction. The flow pressure losses across the test section, when the wings were activated, increased between 7% and 63% of the losses at their deactivated positions, for the single and double VG respectively.

Research works on other heat transfer phenomena conducted are as follows. Li *et al.* [40] investigated the heat transfer performance of compound enhancement with helical fins and DWVG at RE 680 to 16000

on shell of different curvatures. Results showed the increase of performance about 18% to 32%. Eiamsaard *et al.* [22] investigated the heat transfer, flow friction and thermal performance factor characteristics in a tube fitted with delta winglet twisted tape, using water as working fluid at Reynolds number range of 3000–27000 with oblique delta-winglet twisted tape (O-DWT) and straight delta-winglet twisted tape (S-DWT) arrangements. Nusselt numbers from using the O-DWT and S-DWT with twist ratio (y/w) of 3 are around 7–29% and 15.8–45.6% greater than those from the tapes with twist ratios (y/w) of 4 and 5, respectively.

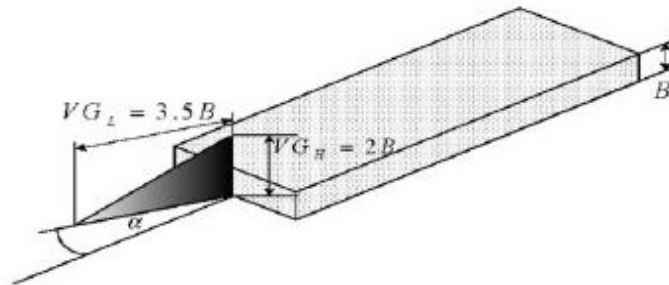


Fig.6: A vortex generator installed in front of an electronic module.[Chomdee *et al.* [17]]

In addition, friction factors for O-DWT and S-DWT with twist ratio (y/w) of 3 are approximately 3.5–22.8% and 17.9–37.8%. The data calculated by them showed that the mean Nusselt number and friction factor for the ODWT are respectively, 4.2% and 7.8% higher than those for the SDWT. Mohammed Ghanem Jehad [42] investigated Friction factors for fully developed flow in an equilateral triangular duct for Reynolds numbers ranging from (24 500) to (75750). He concluded that the flow loss in a triangular duct (corresponding to the friction factor) due to the winglet-pair is less than that due to the wing.

Gentry and Jacobi [12] used naphthalene sublimation to measure vortex strength and local convective coefficients in a developing channel flow with a delta wing placed at the leading edge. They revealed that the tip vortices had a significant impact on heat transfer behavior of both walls and local enhancement by a factor of 3 was acquired in regions where a vortex induced a normal inflow. The average enhancement of 20-55%, along with an additional pressure loss of 50-110%, was reported for Reynolds numbers ranging from 400 to 2000. Sommers *et al.* [43] In this study, an array of delta-wing vortex generators is applied to a plain fin-and-tube heat exchanger with a fin spacing of 8.5 mm. Heat transfer and pressure drop performance are measured to determine the effectiveness of the vortex generator under frosting conditions. For Reynolds numbers between 500 and 1200, a reduction of 35.0% to 42.1% is observed in the air-side thermal resistance. Correspondingly, the heat transfer coefficient is observed to be between 33-53 W/m²-K for the enhanced heat exchanger and between 18-26 W/m²-K for the baseline heat exchanger. A modified volume goodness parameter is also calculated and shows that the enhanced exchanger outperforms the baseline specimen for the range of Reynolds numbers examined.

Yakut *et al.* [45] carried out an experimental study for tapes with double-sided delta-winglets under different geometrical and flow parameters. The optimum results were obtained at a Reynolds number of 16906, 25 mm pitch, 8 mm height of winglet and 30° angle of attack for lower frequencies, optimum conditions occurred at a Reynolds number of 16906 for 75 mm pitch, 8 mm height of winglet and 60° angle of attack. Li *et al.* [46] perform both experiments and simulations to investigate the thermal-fluid characteristics of a flat-fin heat sink with a pair of vortex generators installed in a cross flow channel. The best performance is achieved when the distance between the vortex generator trailing edges equals the length of the heat sink and the distance between the trailing edge of each vortex generator and the front end of the heat sink is zero. An attack angle of the vortex generators of 30° is preferred to optimize the thermal resistance and pressure difference. Regarding the effect of the configuration of

the vortex generators on the performance of the heat sink, a common-flow-up configuration outperforms a common-flow-down configuration.

Phadtare *et al.* [47] suggested that the W.V.G's could be used to enhance blade tip heat transfer cooling as they found that the heat transfer coefficient of the 2D W.V.G. might be a factor of 1.8 higher than that of the smooth tip. This arrangement achieved at the expenses of a penalty of pressure drop around 30% experimentally. They suggested that the W.V.G's could be used to enhance blade tip heat transfer cooling. Chomdee *et al.* [17] experimentally investigate the heat transfer enhancement by delta winglet vortex generators in air cooling of a staggered array of rectangular electronic modules, figure 6. The winglet vortex generators are placed in front of 3×5 modules with 20° attack angle. Each module has dimensions of 1.8×5.4×0.6mm and each one generates heat at 2.5W. The adiabatic heat transfer coefficients, the thermal wake functions including their correlations for the modules with and without the vortex generators are considered at different values of Reynolds number and the module density. It could be seen that the vortex generators could enhance the adiabatic heat transfer coefficients, reduce the thermal wake functions and the module temperatures significantly.

Apart from these very impressive reviews on passive augmentation methods are provided by Sakr *et al.* [1] and Gupta *et al.*[2]. Kattea [48] provides experimental study on the effect of shape and location of various types of vortex generators ahead of a heat exchanger.

3. SUMMARY

This paper presents a detailed review of heat transfer augmentation works done by researchers with the use of delta wing or winglet type vortex generators in the past few decades. Heat transfer enhanced by 20%- 68% in fin tube heat exchanger with the use of delta winglet vortex generators, varying due to the arrangements of DWVG with respect to the flow upstream. As for plate fin heat exchangers the Nusselt number enhancement was as high as 82% for in-line formation of DWVGs. At high Reynolds number the optimum angle of attack is found below 30° where at low Reynolds number the AOA should be 45°. In louvered fin heat exchanger the use of DWVG yields a performance increase of 53% with only 7% increase in pressure loss. The use of DWVG for heat transfer enhancement in flow over flat plates also produce 50%-60% performance improvement. Experiment shows that DWVGs are also effective under frosting conditions. Recently a new formation of DWVG named "V array" formation is adopted by researchers inspired by group movement of animals in nature. Researchers used DWVG in air cooling of electronic modules and suggested that the DWVGs could be used to enhance blade tip heat transfer cooling of the turbine blade.

RECOMMENDATIONS

Analyzing the findings of the experimental works done by the researchers the authors recommends delta winglet vortex generators over rectangular winglet as around same pressure drop DWVG gives better performance. Delta winglet is preferable over delta wings and built in geometry over stumped one. They also recommend the use of a proper angle of attack for better performance. Generally with increasing Reynolds number heat transfer increases, an optimum velocity of flow is also preferable which balances the pressure drop and performance.

REFERENCES

- [1] S. Liu, M. Sakr. A comprehensive review on passive heat transfer enhancements in pipe exchangers. *Renewable and Sustainable Energy Reviews* 19 (2013) 64–81.
- [2] Anirudh Gupta, Mayank Uniyal. Review of Heat Transfer Augmentation Through Different Passive Intensifier Methods, *IOSR Journal of Mechanical and Civil Engineering (IOSRJMCE)* ISSN : 2278-1684 Volume 1, Issue 4 (July-Aug 2012).
- [3] Seong Won Hwang, Dong Hwan Kim, June Kee Min and Ji Hwan Jeong. CFD analysis of fin tube heat exchanger with a pair of delta winglet vortex generators. *Journal of Mechanical Science and Technology* 26 (9) (2012) 2949~2958.
- [4] Torii, K., Nishino, K. and Nakayama, K., 1994, "Heat Transfer Augmentation by Longitudinal Vortices in a Flat Plate Boundary Layer," *Proceedings of the Tenth International Heat Transfer Conference*, Brighton, Vol. 6, pp. 123-128
- [5] Gentry, M. C., and Jacobi, A. M., 1997, "Heat Transfer Enhancement by Delta-Wing Vortex Generators on a Flat Plate: Vortex Interactions with the Boundary Layer," *Experimental Thermal and Fluid Science*, Vol. 14, pp. 231–242.
- [6] M. Fiebig, A. Valencia and N. K. Mitra, Wing-type vortex generators for fin-and-tube heat exchangers, *Experimental Thermal and Fluid Science*, 7 (1993) 287-295.
- [7] National Aeronautics and Space Administration GRADES K-12 Wing Design Aeronautics Research Mission Directorate Museum in a BOX Series.
- [8] Jing He, Anthony M. Jacobi, Air-Side Heat-Transfer Enhancement by a New Winglet-Type Vortex Generator Array in a Plain-Fin Round-Tube Heat Exchanger *Journal of Heat Transfer* Copyright © 2010 by ASME JULY 2010, Vol. 132 / 071801-1.
- [9] Tiggelbeck, St., Mitra, N.K., & Feibig, M., November 1994, "Comparison of Wing Type Vortex Generators for Heat Transfer Enhancement in Channel Flows", *ASME Journal of Heat Transfer*, Vol. 116, pp. (880 – 885).
- [10] G. Biswas, K. Torii, D. Fujii, K. Nishino, Numerical and experimental determination of flow structure and heat transfer effects of longitudinal vortices in a channel flow, *Int. J. Heat Mass Transfer* 39 (16) (1996) 3441–3451.
- [11] Manohar S. Sohal. Improving Vortex Generators to Enhance the Performance of Air Cooled Condensers in a Geothermal Power Plant. The INL is a U.S. Department of Energy National Laboratory September 2005.
- [12] M.C. Gentry, A.M. Jacobi, Heat transfer enhancement by delta-winggenerated tip vortices in flat plate and developing channel flows, *J. Heat Transfer Trans. ASME* 124 (6) (2002) 1158–1168.
- [13] K. Torii, K. M. Kwak and K. Nishino, Heat transfer enhancement accompanying pressure-loss reduction with winglet-type vortex generators for fin-tube heat exchanger, *International Journal of Heat and Mass Transfer*, 45 (2002) 3795-3801.
- [14] K. M. Kwak, K. Torii and K. Nishino, Heat transfer and pressure loss penalty for the number of tube rows of staggered finned-tube bundles with a single transverse row of winglets, *International Journal of Heat and Mass Transfer*, 46 (2003) 175-180.
- [15] AJoardar, A.M. Jacobi, "Impact of leading edge delta-wing vortex generators on the thermal performance of a flat tube, louvered-fin compact heat exchanger", *International Journal of Heat and Mass Transfer*, Vol.48, pp.1480–1493, (2005).
- [16] K. M. Kwak, K. Torii and K. Nishino, Simultaneous heat transfer enhancement and pressure loss reduction for finnedtube bundles with the first or two transverse rows of built-in winglets, *Experimental Thermal and Fluid Science*, 29 (2005) 625-632.
- [17] Suriyon Chomdee and Tanongkiat Kiatsiriroat. Air Cooling Enhancement in Entrance Region with Delta Winglet Vortex Generators Set at the First Row of In-Line Array of Electronic Module. Department of Mechanical Engineering, Faculty of Engineering, Chiang Mai University, Chiang Mai 50200, Thailand
- [18] C. B. Allison and B. B. Dally, Effect of a delta-winglet vortex pair on the performance of a tube-fin heat exchanger, *International Journal of Heat and Mass Transfer*, 50 (2007) 5065-5072.
- [19] A. Joardar and A. M. Jacobi, Heat transfer enhancement by winglet-type vortex generator arrays in compact plain-finand- tube heat exchanger, *International Journal of refrigeration*, 31 (2008) 87-97.

- [20] Michael J. Lawson, Karen A. Thole, Heat transfer augmentation along the tube wall of a louvered fin heat exchanger using practical delta winglets. *International Journal of Heat and Mass Transfer* 51 (2008) 2346–2360.
- [21] P. Sanders, K.A. Thole, Effects of winglets to augment tube wall heat transfer in louvered fin heat exchangers, *Int. J. Heat Mass Transfer* 49 (21–22) (2006) 4058–4069.
- [22] S. Eiamsa-ard, K. Wongcharee, P. Eiamsa-ard, C. Thianpong. Heat transfer enhancement in a tube using delta-winglet twisted tape inserts. *Applied Thermal Engineering* 30 (2010) 310–318.
- [23] Gulshan Sachdeva. Department of mechanical engineering National institute of technology (Institution of National Importance) KURUKSHETRA-136119, INDIA March, 2010.
- [24] Amin Ebrahimi, Saeid Kheradmand. Numerical Simulation of Performance Augmentation in a Plate Fin Heat Exchanger Using Winglet Type Vortex Generators. *International Journal of Mechanical Engineering and Mechatronics* Volume 1, Issue 1, Year 2012
- [25] Anupam Sinhaa, K. Ashoke Ramanb, Himadri Chattopadhyayc, Gautam Biswasas. Effects of different orientations of winglet arrays on the performance of plate-fin heat exchangers. *International Journal of Heat and Mass Transfer*. Volume 57, Issue 1, 15 January 2013, Pages 202–214.
- [26] J.M. Wua, W.Q. Tao. Impact of delta winglet vortex generators on the performance of a novel fin-tube surfaces with two rows of tubes in different diameters. *Energy Conversion and Management* Volume 52, Issues 8–9, August 2011, Pages 2895–2901.
- [27] J.M. Wu, W.Q. Tao. Numerical study on laminar convection heat transfer in a channel with longitudinal vortex generator. Part B: Parametric study of major influence factors. *International Journal of Heat and Mass Transfer* 51 (2008) 3683–3692.
- [28] Jungchin Min, Wei Xu. Numerical Prediction of the Performances of the Fins with Punched Delta Winglets and the Louver Fins and Their Comparison. *Journal of Enhanced Heat Transfer* > Volume 12, 2005 Issue 4 pages 357-371
- [29] G. Biswas, N.K. Mitra, M. Fiebig, Heat transfer enhancement in fin-tube heat exchangers by winglet type vortex generators, *Int. J. Heat Mass Transfer* 37 (2) (1994) 283–291.
- [30] M. Fiebig, Y. Chen, A. Grosse-Gorgemann, N.K. Mitra, Conjugate heat transfer of a finned tube Part B: heat transfer augmentation and avoidance of heat transfer reversal by longitudinal vortex generators, *Numer. Heat Transfer A: Appl.* 28 (2) (1995) 147–155.
- [31] A. Jahromi, A. Bastani, N.K. Mitra, G. Biswas, Numerical investigations on heat transfer in a compact fin-and-tube heat exchanger using delta winglet type vortex generators, *J. Enhanced Heat Transfer* 6 (1) (1999) 1–11.
- [32] James E. O'Brien, Manohar S. Sohal. Heat Transfer Enhancement for Finned-Tube Heat Exchangers With Winglets. Idaho National Engineering and Environmental Laboratory, Idaho Falls, ID 83415.
- [33] Liting Tian, Yaling He, Pan Chu, Wenquan Tao. Numerical Study of Flow and Heat Transfer Enhancement by Using Delta Winglets in a Triangular Wavy Fin-and-Tube Heat Exchanger. State Key Laboratory of Multiphase Flow in Power Engineering, Xi'an Jiaotong University, Xi'an 710049, China.
- [34] A. Joardar, A. M. Jacobi. A Numerical Study of Flow and Heat Transfer Enhancement Using an Array of Delta-Winglet Vortex Generators in a Fin-and-Tube Heat Exchanger. *J. Heat Transfer* 129(9), 1156-1167 (Dec 06, 2006).
- [35] H Huisseune, C T'Joen, P De Jaeger, B Ameel, M De Paepe. Numerical study of a round tube heat exchanger with louvered fins and delta winglets. Ghent University, Department of Flow, Heat and Combustion Mechanics, Sint-Pietersnieuwstraat 41, 9000 Gent, Belgium.
- [36] Wang, C.C.; Chang, Y.J.; Wei, C.S.; Yang, B.C. A Comparative Study of the Airside Performance of Winglet Vortex Generator and Wavy Fin-and-Tube Heat Exchangers. *ASHRAE Transactions*;2004, Vol. 110 Issue 1, p53.
- [37] J. E. O'Brien, M. S. Sohal, T. D. Foust, P. C. Wallstedt. Heat Transfer Enhancement For Finned-Tube Heat Exchangers With Vortex Generators: Experimental And Numerical Results. 12th International Heat Transfer Conference. August 18, 2002.
- [38] A. ElSherbini, A.M. Jacobi, The thermal-hydraulic impact of delta-wing vortex generators on the performance of a plain-fin-and-tube heat exchanger, *J. HVAC&RR es.* 8 (2002) 357–370.

- [39] B.R. Bull, A.M. Jacobi, A study of the application of vortex generators to enhance the air-side performance of heat exchangers, air conditioning and refrigeration center, ACRC Report TR-214, University of Illinois, Urbana, 2003.
- [40] Zhang Li, Xie Caipeng, Li Yaxia, Wu Jianhua. Heat transfer enhancement with helical fins and vortex generators on shells at different curvatures. School of Chemical Engineering, Shenyang University of Chemical Technology, Liaoning, China.
- [41] Chakkapong Supasri, Tanongkiat Kiatsiriroat, Atipoang Nuntaphan. Influence of Vortex Generator on Flow Behavior of Air Stream. International Journal of Mechanical Science and Engineering Vol:7 No:9, 2013.
- [42] Mohammed Ghanem Jehad. Experimental study of the friction factor in equilateral triangular duct with different types of vortex generators (obstacles). Al-Qadisiya Journal For Engineering Sciences Vol. 3 No. 2 Year 2010.
- [43] A. D. Sommers, A. M. Jacobi. Air-side heat transfer enhancement of a refrigerator evaporator using vortex generation. International Journal of Refrigeration 28 (2005) 1006–1017
- [44] M.S. Aris, I. Owen, C.J. Sutcliffe. The development of active vortex generators from shape memory alloys for the convective cooling of heated surfaces. International Journal of Heat and Mass Transfer 54 (2011) 3566–3574.
- [45] Kenan Yakut, Bayram Sahin, Cafer Celik, Nihal Alemdaroglu, Aslihan Kurnuc. Effects of tapes with double-sided delta-winglets on heat and vortex characteristics. Applied Energy 01/2005; DOI:10.1016/j.apenergy.2004.03.003.
- [46] Hung-Yi Li, Ci-Lei Chen, Shung-Ming Chao, Gu-Fan Liang. Enhancing heat transfer in a plate-fin heat sink using delta winglet vortex generators. International Journal of Heat and Mass Transfer Volume 67, December 2013, Pages 666–677.
- [47] G.V.Phadtare, A.A Pawar, S.L.Borse, S.V.Channapattana. Experimental investigations of heat transfer enhancement in tip of 180-degree bend of square duct with vortex generator. International Journal of Engineering Science and Technology (IJEST) Vol. 5 No.07 July 2013.
- Wisam Abed Kattea. An Experimental Study on the Effect of Shape and Location of Vortex Generators Ahead of a Heat Exchanger. Al-Khwarizmi Engineering Journal, Vol. 8, No. 2, PP 12- 29 (2012)

THERMAL TRANSPORT FROM NANOPARTICLES DEPOSITED SURFACE: A MOLECULAR DYNAMICS STUDY

Aashique Alam Rezwan, A K M Monjur Morshed*, M. A. Rashid Sarkar
Department. of Mechanical Engineering, Bangladesh University of Engineering & Technology (BUET), Dhaka-1000, Bangladesh.

ABSTRACT: Surface morphology modifications with nanoparticles play a significant role in thermal transport across the solid surface and adjacent liquid. Thermal transport from nanoparticles deposited solid surfaces has been investigated using Nonequilibrium Molecular Dynamics simulation (NEMD). The molecular system was comprised of the following: solid platinum wall and liquid argon placed over the solid surface. The simulation was started from its initial configuration, and once the equilibrium of the two phase system was established, a temperature gradient is imposed on the simulation domain and total energy flow between the solid wall and liquid molecule was calculated. The results show that the nanoparticles deposited surface decrease surface thermal resistance and thus enhance heat transfer from the solid to the liquid. Although nanoparticles deposited surface always increase thermal transport for the flat surface, however for the rough surface (nanostructured surface) it may increase or decrease depending on the relative size (clearance of the roughness and nanoparticles size).

NOMENCLATURE

m	mass of molecules	Subscript	
r	position vector of molecules	Ar	Argon
F	force vector of molecules	Pt	Platinum
FCC	face-centered cubic	f	coolant
		s	solid
Greek Letters			
ϕ	potential function for molecular interaction potential function	ϵ	energy parameter of the
ϕ	Lenard-Jones potential function particle	Γ	distance between pair
σ	length parameter of the potential function		

1. INTRODUCTION

When heat flows from a solid to the in contact liquid, a thermal resistance is experienced due to phonon scattering at the interface which is called Kapitza resistance [1] or interfacial thermal resistance (ITR). For macro-scale ITR is negligible but when the system size shrinks to nanoscale or heat flux reaches too high, its influence is no longer negligible. Molecular dynamics simulation was employed previously by a number of researchers to investigate the thermal transportation characteristics across the solid–liquid interface[2-7]. Interfacial thermal resistance is reported to be strongly depending on the solid–liquid interaction strength and surface wettability. ITR was estimated for a platinum wall to the liquid argon of about 5–20 nm of the liquid conduction layer thickness [2]. ITR also depends on the interfacial temperature. With the increase of temperature, ITR decreases [8] following a power law relation with the interface temperature.

Surface morphology modifications or alterations with nanostructures or nanoparticles alter inter-surface thermal transport characteristics. Although practically most of the solid surfaces have some molecular level unevenness, in the macroscopic view, the molecular level roughened surface can be considered as a flat surface but that roughness plays a very significant role in heterogeneous boiling and interfacial thermal transport. On a nanostructured surface, the structures are generally integral part of the solid, whereas the nanoparticles are weakly bonded by the van der Waals force to the solid surface. Nanoparticles deposition is relatively simple and have several opportunities to offer, for example it may alter surface wettability, rectify phonon frequency to alter ITR, enhance wetted surface area, alter dynamics of the liquid molecules near the wall surface, etc. Nanoparticles decorated solid surface have been investigated previously for pool boiling of nanofluid [9-11]. Mixed

conclusions have been reported in the literature, heat transfer coefficient (HTC) has been reported by some researcher to be enhanced by 10 to 40%, whereas several researchers have reported HTC to have decreased by 20 to 40% and some researchers have been reported no change in HTC [12-13]. Fundamental understanding about the heat transfer mechanism of the nanoparticles decorated surface is necessary to explain the observed discrepancy and to investigate efficient methods to enhance the surface.

When the nanoparticles are deposited on a solid surface; depending on their relative size (clearance of the surface roughness or size of the cavity and size of the nanoparticles) different types of solid-liquid interface can be developed:(i) nanoparticles can rest on the molecular level flat region; (ii) it can rest on the top of the nanostructures or (iii) it may be trapped between the clearance of the nanostructures. Heat transfer from the solid surface to the adjacent liquid may be different depending on the interface characteristics which may cause contradiction in reported HTC. Classical molecular dynamics (MD) simulation is used in this paper to check this hypothesis.

2. METHODOLOGY OF SIMULATION

Classical MD simulation was employed in this investigation which is fairly a straight forward process. The details of MD systems are as follows:

The molecular system employed for this simulation consists of solid platinum wall, liquid water and iron nanoparticles in a cuboid of dimension $3.45 \times 17.5 \times 4.68$ nm. Three monolayers of platinum molecules, each layer having 216 molecules, are placed at the bottom of the simulation box; arranged in FCC (100) lattice corresponding to its density of 21.45×10^3 kg/m³. To model the nanostructured surface, three nanostructures each having a dimension of $3.45 \times 1.48 \times 0.493$ nm are placed on the solid wall. Spherical nanoparticles corresponding to a density of 8445 kg/m³ are placed over the solid wall and rest of the simulation box is filled with water corresponding to a density of 0.995×10^3 kg/m³. Fig. 1 presents detailed of the simulation domain, wall configuration and nanoparticles size and position used in this study.

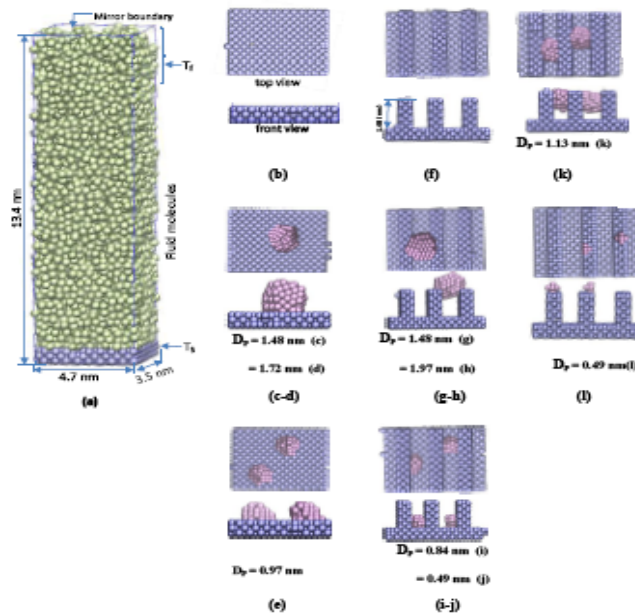


Fig.1: Simulation domain, wall and nanoparticle configuration (a: configuration of the simulation domain; b: configuration of the flat surface; c-e: configuration of the flat surface with different nanoparticles; f: configuration of the nanostructured surface; g-l: configuration of the nanostructured surface with different nanoparticles.

All the interactions between the atoms were mediated by the well-known Lenard-Jones (LJ 12-6) potential [14].

$$\phi(r) = 4\epsilon \left[\left(\frac{\sigma}{r} \right)^{12} - \left(\frac{\sigma}{r} \right)^6 \right] \quad (1)$$

Interaction potential's length and energy parameters were collected from the ref. [5]:

Table 1. Governing Parameters

Parameters	Value	Unit
σ_{Ar-Ar}	0.3405	nm
ϵ_{Ar-Ar}	1.67×10^{-21}	J
σ_{Pt-Pt}	0.2475	nm
ϵ_{Pt-Pt}	8.35×10^{-20}	J
σ_{Ar-Pt}	0.294	nm
ϵ_{Ar-Pt}	1.65321×10^{-21}	J

Although Embedded Atom Method (EAM) potential is more appropriate for Pt-Pt interaction nevertheless LJ potential yields good results for qualitative conclusion. To increase the computational efficiency, all the potentials were truncated at $3.5 \sigma_{Ar-Ar}$.

The equations of motions were integrated using velocity-verlet algorithm with a time step 5 fs. Periodic boundary conditions were imposed laterally (x and z direction). Bottom layer of the wall was kept fixed in order to avoid any migration of the sample [15] and a langevin thermostat was applied to the next three layers, adiabatic imaginary boundary condition was applied to the top of the simulation domain. To maintain shape of the nanostructures, the innermost core of the nanoposts were only allowed to vibrate around their fixed lattice position by applying a spring force with a spring constant of $57 \epsilon/\sigma^2$. All the simulation were performed using LAMMPS [16] and visualization was done using VMD [17].

2. RESULTS AND DISCUSSIONS

2.1. Total Energy Transfer

Fig. 2 presents the total energy transfer between the solid surface and the liquid molecules when T_s and T_f are set to 293K and 453K respectively. Energy transfer rate increases linearly with time. Energy transfer rate is much higher for the nanostructured surface (Fig. 1-f) compared to the flat surface (Fig. 1-b)

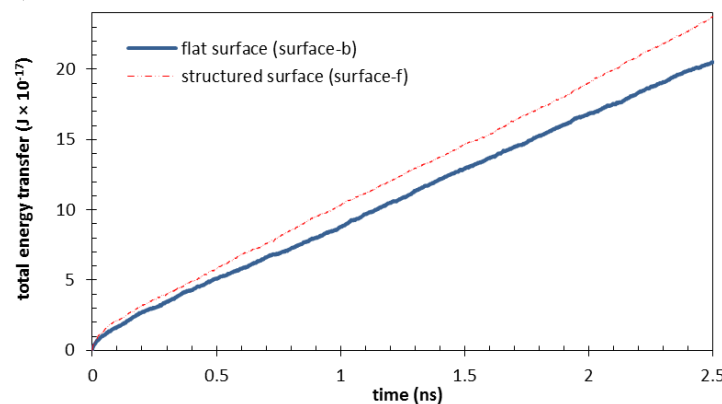


Fig.2: Comparison of the energy flow with time for the nanostructured surface (Fig. 1-f) and flat surface (Fig. 1-b)

2.2. Effect of Coated and Uncoated Surface

Nanostructured surface increases contact surface area, reduces interfacial thermal resistance and alters the dynamics of the liquid molecules at the interfacial region which in turn increases energy transfer from the solid surface to the liquid. A detailed explanation of the mechanism of enhanced

energy transfer for the nanoparticle deposited surface is presented in Fig. 3. From Fig. 3(left) it is obvious that nanoparticle deposition enhances total energy flow for the flat surface regardless of the size and position of the particles, whereas for the nanostructured surface energy flow may increase or decrease depending on the size and position of the particles (Fig. 3(right)).

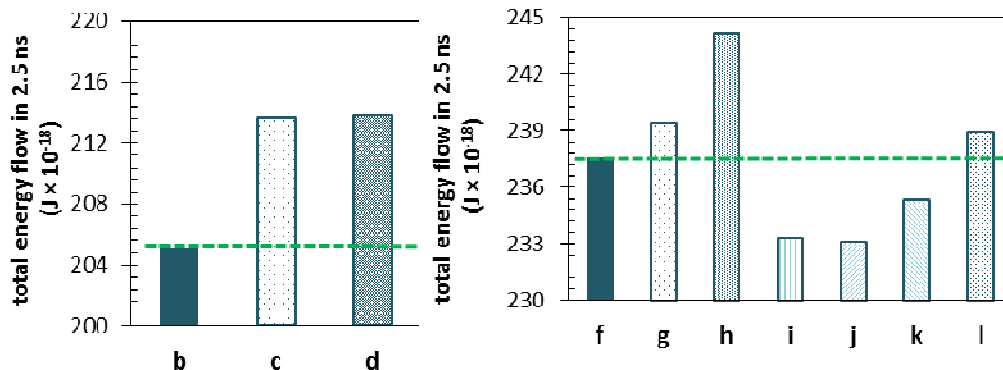


Fig. 1 Comparison of total energy flow between uncoated (left) and coated surface (right)

When the nanoparticles sit over the nanostructures, energy transfer rate increases similar to the flat surface (surface g, h and l). Nanoparticles enhance energy transfer rate by increasing static contact area and by altering the dynamic behavior of the liquid molecules near the solid surface [18]. Energy transfer rate increases with the size and number of the nanoparticles. However, when the nanoparticles are trapped between the nanostructures (which may arise when size of the particles are smaller than the clearance of the nano structures) total energy transfer rate decreases for the solid surface (surface i, j, k). When nanoparticles are trapped inside the nanostructures, it effectively decreases the solid-liquid contact area and due to various interactions inside the nanostructures, the number of heat carrying molecules and the mobility of liquid inside the nanostructures decrease. All these effect causes this reduction in heat transfer.

3. CONCLUSION

Non-equilibrium molecular dynamics simulation was employed to investigate the effect of nanoparticles deposition on heat transfer across flat and nanostructured solid-liquid interface. MD simulation presents a comprehensive view on heat transfer mechanism from the nanoparticles coated surface to the adjacent liquid. Heat transfer rate always increases for the nanoparticles coated flat surface, whereas it may increase or decrease for the rough surface depending on the clearance of the roughness present on the solid surface and size of the nanoparticles. Heat transfer rate decreases when the size of the particles is smaller than the clearance of the roughness and particles are trapped in that clearance. In all other cases heat transfer rate increases for the nanoparticles coated surface compared to the uncoated surface.

REFERENCES

- [1] Swartz, E.T. and R.O. Pohl, Thermal boundary resistance. *Reviews of Modern Physics*, 1989. **61**(3): p. 605.
- [2] Maruyama, S. and T. Kimura, A molecular dynamics simulation of a bubble nucleation on solid surface, in 5th ASME–JSME Thermal Engineering Joint Conference. 1999: San Diego, USA.
- [3] Georgiou, S. and A. Koubenakis, Laser-Induced Material Ejection from Model Molecular Solids and Liquids: Mechanisms, Implications and Applications. *ChemInform*, 2003. **34**(18): p. no-no.
- [4] Maroo, S.C. and J.N. Chung, Molecular dynamic simulation of platinum heater and associated nano-scale liquid argon film evaporation and colloidal adsorption characteristics. *Journal of Colloid and Interface Science*, 2008. **328**(1): p. 134-146.
- [5] Nagayama, G., et al., On the evaporation rate of ultra-thin liquid film at the nanostructured surface: A molecular dynamics study. *International Journal of Thermal Sciences*, 2010. **49**(1): p. 59-66.

- [6] Nagayama, G., M. Kawagoe, and T. Tsuruta, Molecular dynamics simulations of interfacial heat and mass transfer at nanostructured surface, in MNC2007-21410. 2007: Kyoto Japan. p. 1–10.
- [7] Yi, P., et al., Molecular dynamics simulation of vaporization of an ultra-thin liquid argon layer on a surface. *International Journal of Heat and Mass Transfer*, 2002. **45**(10): p. 2087-2100.
- [8] Balasubramanian, G., S. Banerjee, and I.K. Puri, Unsteady nanoscale thermal transport across a solid-fluid interface. *Journal of Applied Physics*, 2008. **104**(6): p. 064306-064306-4.
- [9] Barber, J., D. Brutin, and L. Tadrist, A review on boiling heat transfer enhancement with nanofluids. *nanoscale research letters*, 2011. **6**(280).
- [10] Kim, S.J., et al., Experimental Study of Flow Critical Heat Flux in Alumina-Water, Zinc-Oxide-Water, and Diamond-Water Nanofluids. *Journal of Heat Transfer*, 2009. **131**(4): p. 043204-7.
- [11] White, S.B., A.J. Shih, and K.P. Pipe, Boiling surface enhancement by electrophoretic deposition of particles from a nanofluid. *International Journal of Heat and Mass Transfer*, 2011. **54**(19-20): p. 4370-4375.
- [12] Stutz, B., et al., Influence of nanoparticle surface coating on pool boiling. *Experimental Thermal and Fluid Science*, 2011. **35**(7): p. 1239-1249.
- [13] Taylor, R.A. and P.E. Phelan, Pool boiling of nanofluids: Comprehensive review of existing data and limited new data. *International Journal of Heat and Mass Transfer*, 2009. **52**(23–24): p. 5339-5347.
- [14] Lennard-Jones, J.E. and A.F. Devonshire, Critical Phenomena in Gases. I. Proceedings of the Royal Society of London. Series A - Mathematical and Physical Sciences, 1937. **163**(912): p. 53-70.
- [15] Dou, Y., et al., Explosive Boiling of Water Films Adjacent to Heated Surfaces: A Microscopic Description. *The Journal of Physical Chemistry A*, 2001. **105**(12): p. 2748-2755.
- [16] Plimpton, S.J., Fast Parallel Algorithms for Short-Range Molecular Dynamics *J Comp Phys* 1995 **117**: p. 1-19.
- [17] Humphrey, W., A. Dalke, and K. Schulten, VMD - Visual Molecular Dynamics. *J. Molec. Graphics*, 1996. **vol. 14**: p. pp. 33-38.
- [18] Kunugi, T., K. Muko, and M. Shibahara, Ultrahigh heat transfer enhancement using nanoporous layer. *Superlattices and Microstructures*, 2004. **35**(3–6): p. 531-542.

EFFECTS OF HALL CURRENT ON UNSTEADY MHD COUETTE FLOW

Afroja Parvin , Md. Farid Uddin Mehedi and Md.Mahmud Alam
Mathematics Discipline, Science, Engineering and Technology School
Khulna University, Khulna-9208 , Bangladesh.

Corresponding Email address: Corresponding Author : alam_mahmud2000@yahoo.com

ABSTRACT: An electrically conducting viscous incompressible fluid bounded by two parallel non-conducting plates has been investigated with Hall current. The uniform magnetic field is applied perpendicular to the plate and the fluid motion is uniform at the plate. The lower plate is stationary and the upper plate moves with a constant velocity. Explicit Finite Difference technique has been used to solve the above problem. The Numerical solutions are obtained for momentum and energy equations. The effects of Hall parameter and other parameters describing in the equations are shown graphically. The results of the primary velocity, secondary velocity and temperature distribution are illustrated in the form of the graph. The stability analysis is not shown for brevity.

Keywords : MHD flow, Hall parameter, Joule Heating parameter, Explicit finite difference method and stability analysis.

1. INTRODUCTION

In the past few years, there has been considerable interest in the magnetohydrodynamic effects of Couette flow and channel flows of a Newtonian fluid with heat transfer with or without Hall currents. The flow of an electrically conducting viscous fluid between two parallel plates in the presence of a transversely applied magnetic field has applications in many devices such as magnetohydrodynamic (MHD) power generators, MHD pumps, accelerators, aerodynamics, electrostatic precipitation, polymer technology, petroleum industry, purification of crude oil and fluid droplets spray. The magnetohydrodynamic effects on the formation of Couette flow had been discussed by Tao(1960). Soundalgekar et al.(1979) showed the Hall and ion-slip effects in MHD Couette flow with heat transfer. Soundalgekar and Uplekar(1986) broadly discussed the Hall effects in MHD Couette flow with heat transfer. Attia(2004) discussed the hall effect on unsteady MHD Couette flow and heat transfer of a Bingham fluid with suction and injection. Chen et al.(2012) studied the Unsteady unidirectional MHD flow of Voigt Fluids moving between two parallel surfaces for variable volume flow rates. Hence, the main aim is to study the effects of hall current on Unsteady MHD Couette flow. The system is considered as such that the upper plate is moving with a uniform velocity while the lower plate is fixed. A constant pressure gradient acts on the flow and a uniform magnetic field perpendicular to the plates. Very small value of Magnetic Reynolds Number is assumed to neglect the strong effect of induced magnetic field. The two plates are kept at two different but constant temperatures. The governing momentum and energy equations are solved numerically using the explicit finite difference method. Hence the effect of heat and magnetic field, influence the newtonian flow and eventually interesting effects on both velocity and temperature profile has been observed.

2. MATHEMATICAL MODEL OF THE FLOW

Consider the unsteady, viscous, laminar and incompressible fluid flows between two infinite horizontal plates located at the $y = \pm h$ planes and extend from $x = 0$ to ∞ and from $z = 0$ to ∞ . The upper plate moves with a uniform velocity U_0 while the lower plate is stationary. The upper and lower plates are kept at two constant temperatures T_2 and T_1 respectively, with $T_2 > T_1$. The fluid is acted upon by a constant pressure gradient $\frac{dp}{dx}$ in the x-direction, and a uniform suction from above and injection from below which are applied $\dot{v} = 0$. A uniform magnetic field B_0 is applied in the positive y-direction and is assumed undisturbed as the induced magnetic field is neglected by assuming a very small magnetic Reynolds number. The Hall effect is taken into consideration and consequently a z component for the velocity is expected to arise. Within the framework of the above stated assumption the generalized equations relevant to the unsteady problem are governed by the following system of coupled partial differential equation as;

$$\frac{\partial u}{\partial x} + \frac{\partial v}{\partial y} = 0 \quad (1)$$

$$\frac{\partial u}{\partial t} + u \frac{\partial u}{\partial x} + v \frac{\partial u}{\partial y} = -\frac{1}{\rho} \frac{\partial p}{\partial x} + \frac{\mu}{\rho} \frac{\partial^2 u}{\partial y^2} - \frac{1}{\rho} \left[\frac{\sigma B_0^2}{1+m^2} (u+mw) \right] \quad (2)$$

$$\frac{\partial w}{\partial t} + u \frac{\partial w}{\partial x} + v \frac{\partial w}{\partial y} = \frac{\mu}{\rho} \frac{\partial^2 w}{\partial y^2} - \frac{1}{\rho} \left[\frac{\sigma B_0^2}{1+m^2} (w-mu) \right] \quad (3)$$

$$\frac{\partial T}{\partial t} + u \frac{\partial T}{\partial x} + v \frac{\partial T}{\partial y} = \frac{k}{\rho c_p} \frac{\partial^2 T}{\partial y^2} + \frac{\mu}{c_p \rho} \left[\left(\frac{\partial u}{\partial y} \right)^2 + \left(\frac{\partial w}{\partial y} \right)^2 \right] + \frac{1}{\rho c_p} \frac{\sigma B_0^2}{1+m^2} (u^2 + w^2) \quad (4)$$

The corresponding boundary conditions for the problem

$$t > 0, \quad u = 0, \quad w = 0, \quad T = T_1, \quad \text{at } y = -h$$

$$u = U_0, \quad w = 0, \quad T = T_2, \quad \text{at } y = h$$

Where, B_0 is the uniform magnetic field, ρ is the density of the fluid, σ is the electric conductivity, m is the hall parameter, c_p is the specific heat capacity, μ is the viscosity, k is the thermal conductivity of the fluid, T is the mean fluid temperature at the wall.

Using the non-dimensional variables into the equations (1) to (4) the basic equations relevant to the problem are in dimensionless form

$$\frac{\partial U}{\partial X} + \frac{\partial V}{\partial Y} = 0 \quad (5)$$

$$\frac{\partial U}{\partial \tau} + U \frac{\partial U}{\partial X} + V \frac{\partial U}{\partial Y} = -\frac{dP}{dX} + \frac{1}{R_e} \left[\frac{\partial^2 U}{\partial Y^2} - \frac{H_a^2}{(1+m^2)} (U+mW) \right] \quad (6)$$

$$\frac{\partial W}{\partial \tau} + U \frac{\partial W}{\partial X} + V \frac{\partial W}{\partial Y} = \frac{1}{R_e} \left[\frac{\partial^2 W}{\partial Y^2} - \frac{H_a^2}{(1+m^2)} (W-mU) \right] \quad (7)$$

$$\frac{\partial \theta}{\partial \tau} + U \frac{\partial \theta}{\partial X} + V \frac{\partial \theta}{\partial Y} = \frac{1}{F_r} \frac{\partial^2 \theta}{\partial Y^2} + E_c \left[\left(\frac{\partial U}{\partial Y} \right)^2 + \left(\frac{\partial W}{\partial Y} \right)^2 \right] + \frac{H_a^2 E_c}{1+m^2} (U^2 + W^2) \quad (8)$$

The corresponding boundary conditions are

$$\tau > 0, \quad U = 0, \quad W = 0, \quad T = 0, \quad \text{at } y = -1$$

$$U = 1, \quad W = 0, \quad T = 1, \quad \text{at } y = 1$$

3. NUMERICAL SOLUTION

In this section, the governing second order non-linear coupled dimensionless partial differential equations with the associated initial and boundary conditions have been solved. The explicit finite difference method has been used to solve equations (5)-(8) subject to the boundary conditions. The present problem is required a set of finite difference equation. To obtain the difference equations the region of the flow is divided into a grid or mash of lines parallel to X and Y axis. Where X axis is taken along the plate and Y axis is normal to the plate. Grid spacing in the X and Y directions are shown in Figure1. it is considered that the plate of height $X_{max}(= 100)$ i.e. X varies from 1 to 100 and regard $Y_{max}(= 2)$ i.e. Y varies from -1 to 2. There are $m = 40$ and $n = 40$. Hence the constant mesh size along Y - axis becomes $\Delta Y = 0.05 (-1 \leq Y \leq 1)$ with a smaller time step $\Delta t = 0.0001$.

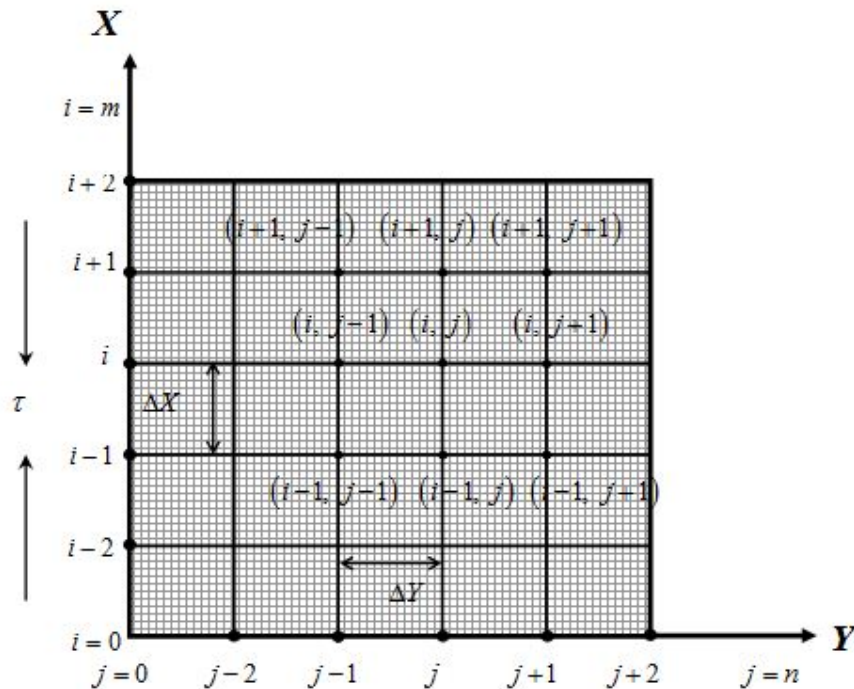


Fig.1: Explicit finite difference system grid

Let U^{n+1}, W^{n+1} and θ^{n+1} denote the values U, W and θ at the end of a time-step respectively. Using the explicit finite difference method the system of partial differential equations (5)-(8) are obtained an appropriate set of finite difference equations;

$$\begin{aligned} & \frac{U_{i,j}^n - U_{i-1,j}^n}{\Delta X} + \frac{V_{i,j}^n - V_{i-1,j}^n}{\Delta Y} = 0 \\ & \frac{U_{i,j}^{n+1} - U_{i,j}^n}{\Delta \tau} + U_{i,j}^n \frac{U_{i,j}^n - U_{i-1,j}^n}{\Delta X} + V_{i,j}^n \frac{U_{i,j+1}^n - U_{i,j}^n}{\Delta Y} \\ & \quad = -\frac{dP}{dX} + \frac{1}{R_e} \left[\frac{U_{i,j+1}^n - 2U_{i,j}^n + U_{i,j-1}^n}{\Delta Y^2} - \frac{H_a^2}{1+m^2} [U_{i,j}^n + mW_{i,j}^n] \right] \\ & \frac{W_{i,j}^{n+1} - W_{i,j}^n}{\Delta \tau} + U_{i,j}^n \frac{W_{i,j}^n - W_{i-1,j}^n}{\Delta X} + V_{i,j}^n \frac{W_{i,j+1}^n - W_{i,j}^n}{\Delta Y} = \frac{1}{R_e} \left[\frac{W_{i,j+1}^n - 2W_{i,j}^n + W_{i,j-1}^n}{\Delta Y^2} - \frac{H_a^2}{1+m^2} [W_{i,j}^n - mU_{i,j}^n] \right] \\ & \frac{\theta_{i,j}^{n+1} - \theta_{i,j}^n}{\Delta \tau} + U_{i,j}^n \frac{\theta_{i,j}^n - \theta_{i-1,j}^n}{\Delta X} + V_{i,j}^n \frac{\theta_{i,j+1}^n - \theta_{i,j}^n}{\Delta Y} \\ & \quad = \frac{1}{R_r} \left[\frac{\theta_{i,j+1}^n - 2\theta_{i,j}^n + \theta_{i,j-1}^n}{\Delta Y^2} \right] + E_c \left[\left(\frac{U_{i,j+1}^n - U_{i,j}^n}{\Delta Y} \right)^2 + \left(\frac{W_{i,j+1}^n - W_{i,j}^n}{\Delta Y} \right)^2 \right] \\ & \quad + \frac{H_a^2 E_c}{1+m^2} [(U_{i,j}^n)^2 + (W_{i,j}^n)^2] \end{aligned}$$

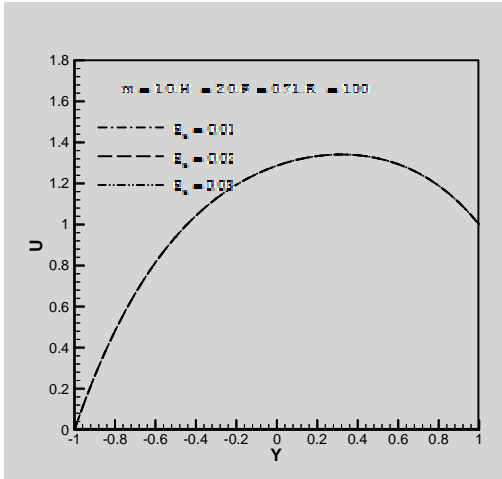


Fig.2: Primary velocity versus Y for different values of Eckert number at $\tau = 5.0$.

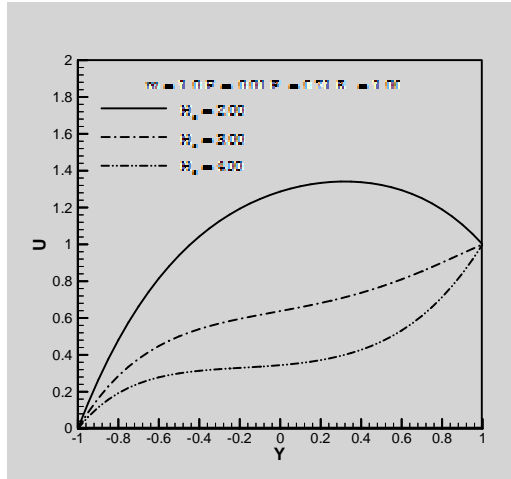


Fig.8: Primary velocity versus Y for different values of Hartmann number at $\tau = 5.0$.

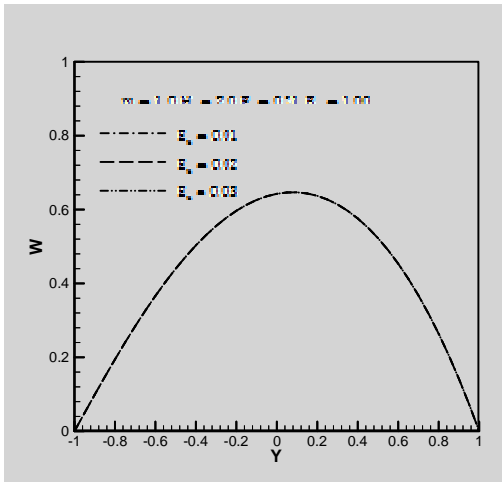


Fig.3: Secondary velocity versus Y for different values of Eckert number at $\tau = 5.0$.

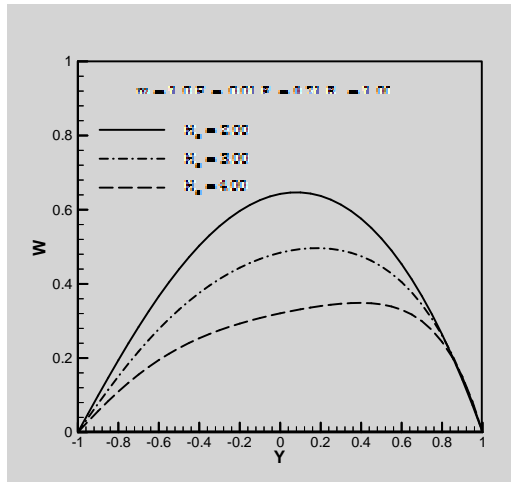


Fig.9: Secondary velocity versus Y for different values of Hartmann number at $\tau = 5.0$.

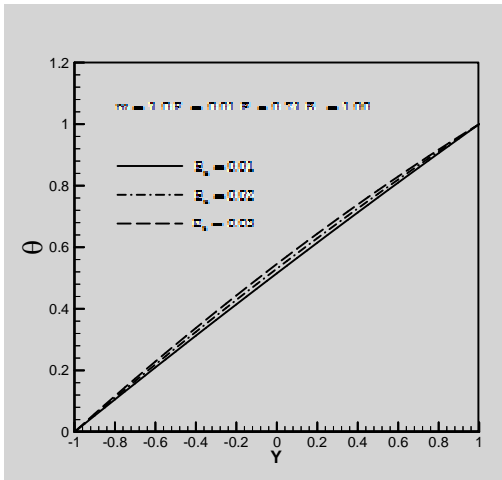


Fig.4: Temperature versus Y for different values of Eckert number at $\tau = 5.0$.

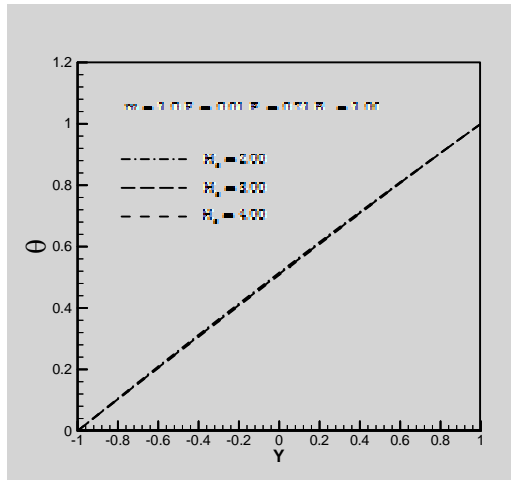


Fig.10: Temperature versus Y for different values of Hartmann number at $\tau = 5.0$.

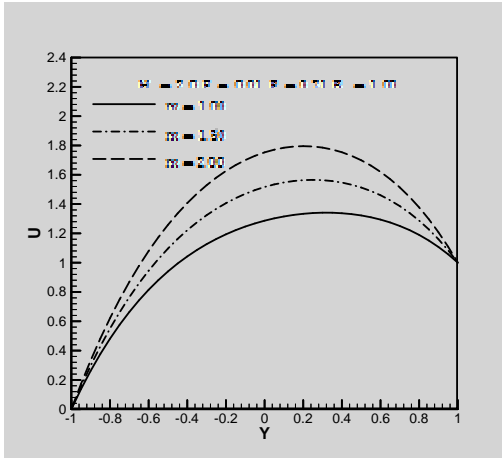


Fig.5: Primary velocity versus Y for different values of Hall parameter at $\tau = 5.0$.

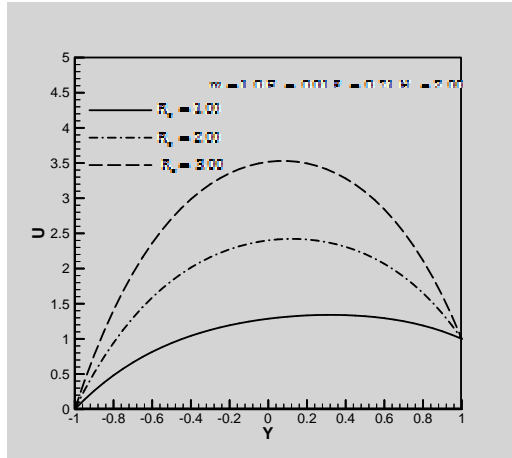


Fig.11: Primary velocity versus Y for different values of Reynolds number at $\tau = 5.0$.

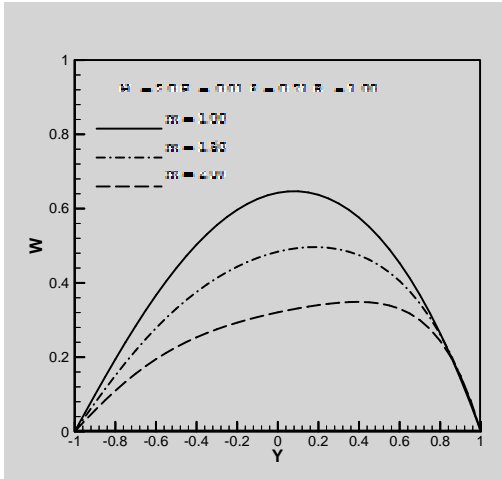


Fig.6: Secondary velocity versus Y for different values of Hall parameter at $\tau = 5.0$.

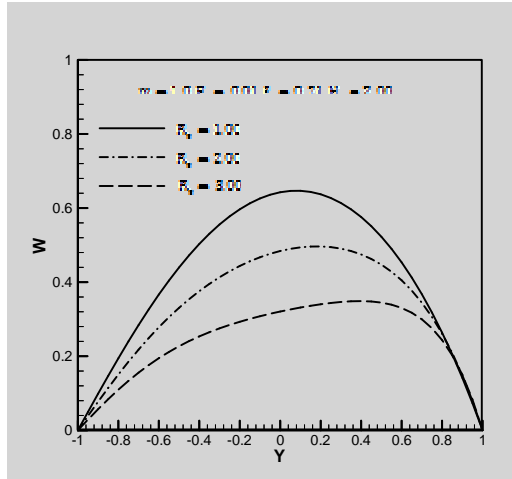


Fig.12: Secondary velocity versus Y for different values of Hartmann number at $\tau = 5.0$.

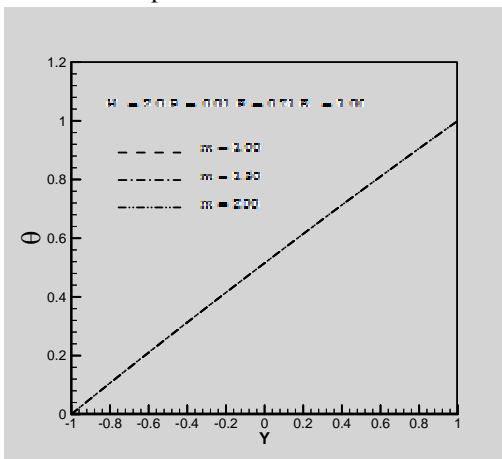


Fig.7: Temperature versus Y for different values of Hall parameter at $\tau = 5.0$.

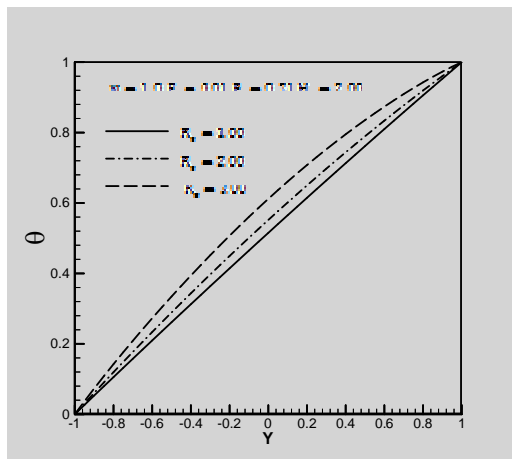


Fig.13: Temperature versus Y for different values of Reynolds number at $\tau = 5.0$.

4. RESULTS AND DISCUSSIONS

Figures (2-4) represents the variation of velocity components U, W and temperature θ for the variation of Eckert number $E_c = 0.01, 0.02, 0.03$. **Figures (2-3)** shows that the velocity distributions has a minor effect for increasing E_c . **Figure 4** shows that θ increases with the increase of E_c .

Figures (5-7) shows the effect of Hall parameter, $m = 1, 1.5, 2$ on velocity components U, W and temperature θ . **Figure 5** represents U increases with the increase of m as the effective conductivity $\left(= \frac{\sigma}{1+m^2} \right)$ decreases with that of m . **Figure 6** shows that the velocity component W increases with the increase of m where W is a result of Hall effect. **Figure 7** shows that the temperature profile has a minor effect for increasing Hall parameter.

Figures (8-10) shows the effect of Hartmann number, $H_a = 2.00, 3.00, 4.00$ on velocities U, W and temperature θ . **Figure 8** represents that U increases with the increase of H_a . **Figure 9** shows that W decreases with the increase of H_a . **Figure 10** shows that the temperature distribution has a minor effect for increasing H_a .

Figures (11-13) illustrates the effect of various Reynolds number $Re = 1.0, 2.0, 3.0$ on the velocity components U, W and temperature θ . **Figure 11** represent the velocity component U increases with the increase of Re . **Figure 12** represents that W increases with the increase of Re . **Figure 13** exhibits that θ increases as Re increases.

REFERENCES

- [1] Attia H.A., Syed M.E. (2004), "Hall effect on unsteady MHD Couette flow and heat transfer of a Bingham fluid with suction and injection", Journal of Applied Mathematical Modeling, vol. **28**, pp. 1027-1045.
- [2] Chen W.F., Lai H Y, Chen C.K.(2012), "Unsteady unidirectional MHD flow of Voigt Fluids moving between two parallel surfaces for variable volume flow rates", Journal of Applied Mathematics, vol. **2012**, pp.12
- [3] Soundalgekar V.M., Uplekar A.G. (1986), "Hall effects in MHD Couette flow with heat transfer", IEEE Transactionson Plasma Science, . PS-**14**, pp. 579–583.
- [4] Soundalgekar V.M., Vighnesam N.V., Takhar H.S. (1979), "Hall and ion-slip effects in MHD Couette flow with heat transfer", IEEE Transactionson Plasma Science. PS-**7**, pp. 178–182.
- [4] Tao I.N. (1960), "Magnetohydrodynamic effects on the formation of Couette flow", Journal of Aerospace Science. vol. **27**, pp. 334.

STUDY AND ANALYSIS OF CONTROL SYSTEM OF A THERMAL POWER PLANT

M. R. Rahman¹, S. K. Alen², Q. M. Z. Hoque³, and M. A. R. Sarkar⁴

^{1,2,4}Department of Mechanical Engineering

Bangladesh University of Engineering and Technology, Dhaka-1000, Bangladesh

¹himel00798@yahoo.com, ²educative.alen@gmail.com, ³210zhoque@dhaka.net,

⁴rashid@me.buet.ac.bd

ABSTRACT: Modern power plants depend heavily on the control system to provide the most reliable means for control, operational efficiency and advanced process optimization. Industrial Control System (ICS) is a term that is used to denote several types of control systems, such as distributed control systems (DCS), supervisory control and data acquisition (SCADA), and some smaller control system configurations, i.e. programmable logic controllers (PLC). Each of these systems has various advantages and disadvantages. The main purpose of this paper is to highlight the salient features of present ICS used in thermal power plants.

Keywords: DCS, SCADA, instrumentation, HMI, data acquisition, server.

1. INTRODUCTION

Today the world depends entirely upon power. The increased generation of power with limited resource has been in the center of attention of the researchers and scientists. Hence the need for sophisticated industrial control systems such as DCS, SCADA, and PLC has risen. Historically, Power Generators depend on the control system to provide the most reliable means for control, operational efficiency and advanced process optimization. The latest ICS designs are now available to improve overall effectiveness in operations as well as optimizing maintenance routines at the plant level and even across an entire corporate fleet. Newer technologies are replacing classical devices constantly with a view to bring more flexibility in handling units and in process optimization. In this text the use of modern control systems in thermal power plants are described along with the general process flow of power generation.

2. WORKING OF THERMAL POWER PLANT

The conversion from coal to electricity takes place in three stages [1]:

Stage 1

The first conversion of energy takes place in the boiler. Coal is burnt in the boiler furnace to produce heat. Carbon in the coal and Oxygen in the air combine to produce Carbon Dioxide (CO₂) and heat.

Stage 2

The second stage is the thermodynamic process:

- (a) The heat from combustion of the coal boils water in the boiler to produce steam. In modern power plant, boilers produce steam at a high pressure and temperature.
- (b) The steam is then piped to a turbine.
- (c) The high pressure steam impinges and expands across a number of sets of blades in the turbine.
- (d) The impulse and the thrust created rotate the turbine.
- (e) The steam is then condensed and pumped back into the boiler to repeat the cycle.

Stage 3

In the third stage, rotation of the turbine rotates the generator rotor to produce electricity based of Faraday's Principle on electromagnetic induction.

The other components like economizer, super heater, air heater and feed waters are used in the primary circuit to increase the overall efficiency of the plant.

3. ELEMENTS OF DCS

A distributed control system [2] (DCS) refers to a control system in which the controller elements are not central in location but are distributed throughout the system with each component subsystem

controlled by one or more controllers. The entire system of controllers is connected by a network for communication and monitoring.

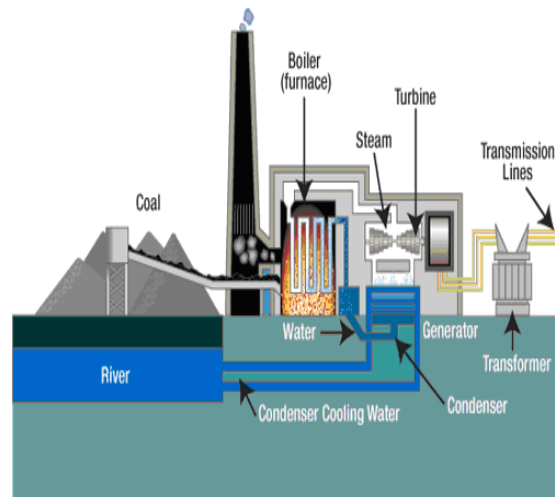


Fig 1: Working of thermal power plant

The elements of a DCS are described below:

A. Domain:

A group of stations connected on the network is called a Domain. Domains are linked by Bus Converters (ABC). Domains can be classified into real domains and virtual domains. Stations that are directly connected on the network are Real or CS domains. Stations that are not directly connected on the network are Virtual Domains, e.g. AC800M, CS1000, Centum-XL stations, Micro-XL Stations etc [3].

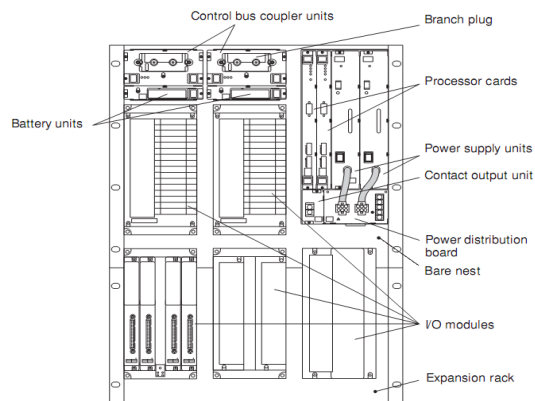


Fig 2: Centum CS 1000

B. Field control unit:

These units are the lowest hierarchical level of a DCS. These function units of the system are distributed and positioned in the field. The units are strong autonomous automation subsystem, whose domain of influence is restricted to a few (1 to 8,16,32) measuring points or control loops. The subsystems are called field stations, as they are autonomous in function and situated in field, [4].

The primary function of field station is to:

- Collect and preprocess analog and digital signals.
- Monitor and log the alarming messages
- Perform open and closed loop control functions

With the above mentioned functions it is apparent that the field stations must be intelligent, CPU based, autonomous system units, provided by a series of process interface modules, as well as with a number of RAM and PROM blocks. They are connected to the bus with the help of a bus interface coupler.

Typical analog inputs and outputs per field station are 4, 8, 16, 48 or 64 and binary inputs and outputs per field station is 2, 4, 8, 16 and 256. In addition to this some fields have special digital inputs such as timers, counters etc. or digital outputs such as pulse and stepper motor output, positioning and motor control etc.

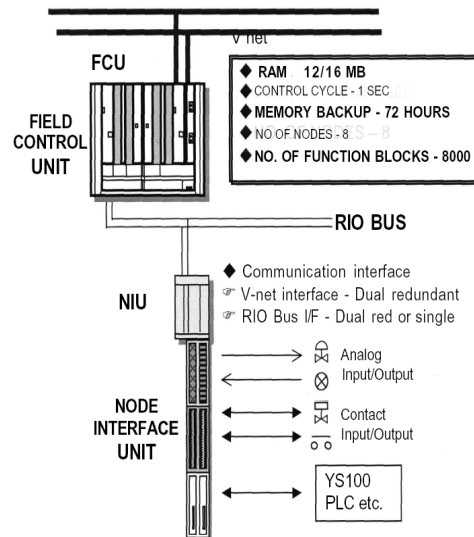


Fig 3: Field control unit

C. Intermediate Stations:

The intermediate functional system units which are placed in between the lowest and the highest hierarchical levels are known as group or supervisory stations. The stations are the autonomous system elements with the restricted domain of influence to a group of field stations, belonging to a closed, well defined, and relatively autonomous part of the plant.

The most common functions of the intermediate stations are

- State observation of the process variables
- Calculation of reference values for control loops at “lowest” level (SV & PV) Tracking if order processing and material and energy balances
- Efficiency analysis
- Reporting
- Data exchange with “higher” level stations (central station)

D. Central Computer Station:

Central computer station enables centralized plant monitoring and direct operation on plant instrumentation. It also offers important program generation and system diagnostics services. The stations are connected to other systems through the system bus which can initiate the necessary data transfers.

Functions of the central computer control are:

- Plant oriented
- General application

E. Monitoring and Command Facilities:

The DCS uses plant monitoring and command facilities which are versatile and intelligent. The use of these facilities enables supervision of the plant state and direct influence of the operator on the processes within the plant. In most of the present process monitoring systems the principle of defining different windows for monitoring different process parameters and messages are being practiced.

F. Data Communication Link:

The present practice is to divide the whole plant controls into a number of distinguishable control loops & allocating stand alone controllers for them. All these controllers, situated in a centrally located control equipment room, are connected together through communication network known as field bus

[5]. The main advantage of a field bus as compared to the conventional point to point data transfer links are:

- Higher information content of the signal to be transferred, including the diagnostic & calibration data
- Lower cabling expenses
- Simplified interface of the process control unit.

4. DCS IN THERMAL POWER PLANT

The process variables are controlled by DCS through valves, pumps or other motors. A motor can be either run locally (form field) or from DCS (remote). In remote mode, the message flashes in the operator screen and further option is available to operate either in auto mode or manual mode. When on manual mode, it can be made to start or stop by pressing the on-off buttons in Digivis. When in auto mode, the command is issued from DCS, based on the logic of the process station.

An example, of process control logic is a set point control loop consisting of a pressure sensor, controller, and valves. Some of the areas of control are:

a) Drum Level Control:

This control loop is used to maintain the drum level at normal operating level of the boiler. Middle value of three transmitters (LT1, LT2 and LT3) is selected for drum level control through Level indicator (L1) block.

If reading of any two transmitters deviates by 10% then the controller should be forced to manual mode. If greater than 10% deviation is observed in all the three transmitters then the boiler should be tripped. In case of failure of one transmitter, average of the other two transmitters should be referred for control and in case of failure of two transmitters, the boiler should be tripped.

The level signal acts as a Process variable (PV) to the controller block LIC. The controller block will vary the percentage opening of the valve LV and hence level control is achieved.

b) Steam Temperature Control:

This control loop is used to maintain the steam temperature at a certain set point. The final steam temperature is measured with the transmitter TT. The output is compared with a fixed set point in the controller TIC. The resultant control signal instructs the spray control valve TV to control flow of water to the attemperator.

c) Furnace Pressure Control:

The furnace pressure is measured with the Pressure transmitter PT. This is used as a Process variable (PV) and is then compared with a fixed set point in the controller PIC. The resultant control varies the speed of the motor that controls the pressure (ID fan).

d) Combustion Control:

The combustion control loop is used to maintain rated steam pressure during fixed and varying conditions achieved by controlling the firing rate and air flow rate to have a proper combustion in the furnace.

The main steam pressure is measured by the pressure transmitter PT and is used as a process variable for the controller PIC. This controller generates an output signal based on the difference between the local set point and the process variable. The output of this controller is then passed on to the boiler lading stations H1C-M1, M2,M3,M4 which act as an auto/manual station for rotary feeder for coal.

The air flow controller is a slave controller with the airflow as the Process variable (FI) and total heat demand as remote set point. This remote set point is total combustion air requirement. The air flow controller generates an output signal comparing the remote set point and the process variable. The output is fed to the FD fan to control the net air flow.



Fig 4: Turbine control module

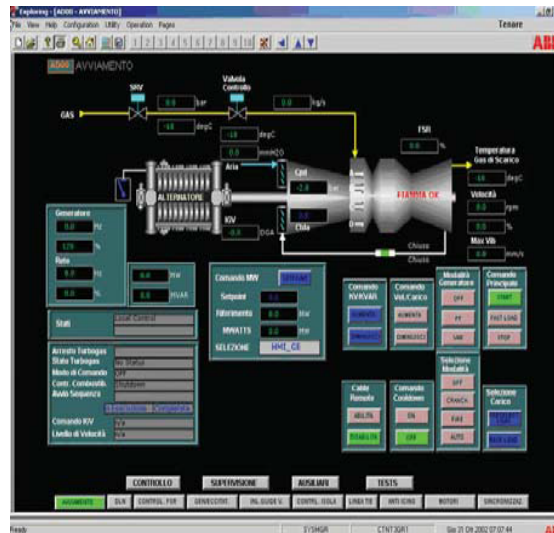


Fig 5: Steam turbine monitoring



Fig 6: Valve positioning module

e) *CBD Tank Level Control:*

This control loop is used to control the CBD tank level. The CBD tank level is measured by the transmitter LT. This level is fed to a level indicating controller LIC as a measured variable. This measured variable is compared with the fixed set point in the Level indicating controller. The controller then operates the CBD level control valve.

Acceptable limit then the corresponding alarm is generated as Low (LAL), Low-Low (LALL), High (LAH) and High-High (LAHH).

f) *Deaerator Level Control:*

This control loop is used to control the deaerator storage tank level. The Deaerator level transmitter (LT) senses deaerator tank level and level is fed to a Level indicating controller (LIC) as a measured variable. The measured signal is compared with the fixed set point in the level indicating controller. The resultant control signal operates the deaerator control valve (LV) which controls the deaerator level.

g) *Deaerator Pressure Control*

This control loop is used to control deaerator pressure. The deaerator Pressure transmitter (PT) senses the deaerator tank pressure and pressure signal is fed to a Pressure indicating controller (PIC) as a measured variable. The measured variable signal is compared with fixed set point in pressure indicating controller. The resultant control signal operates the Deaerator pressure control valve (PV) to control the deaerator pressure.

h) *PRDS Control:*

This loop is used to control the pressure and temperature of the steam going to deaerator and steam header.

For deaerator, the pressure and temperature of the steam going to deaerator is sensed by the Pressure Transmitter (PT) and the Temperature Transmitter (TT) respectively. These signals are given to

Pressure indicating controller (PIC) and Temperature indicating controller (TIC) as process variables respectively.

Pressure indicating controller (PIC) is used to operate the Pressure control valve (PV) to control the pressure of steam. Similarly, Temperature indicating controller (TIC) is used to operate the Temperature control valve (TV) to control the temperature of steam.

For steam header, Pressure transmitter (PT), Temperature transmitter (TT), Pressure indicating controller (PIC) and Temperature indicating controller (TIC) have similar working principle as in the case of the deaerator.

These are provisions to view the valve position through the Position transmitter (ZT) in the DCS.

All connected to plant server and all controllers are connected connectivity server to It has two redundant servers where both the servers are connected to switch 1 and switch 2. Switch 1 and switch 2 helps to communicated between the server, client and controllers. DCSs may employ one or several workstations and can be configured at the workstation or by an off-line personal computer. Local communication is handled by a control network with transmission over twisted pair, coaxial, or fiber optic cable. A server and/or applications processor may be included in the system for extra computational, data collection, and reporting capability.

A typical DCS consists of functionally and/or geographically distributed digital controllers capable of executing from 1 to 256 or more regulatory control loops in one control box. The input/output devices (I/O) can be integral with the controller or located remotely via a field network. Today's controllers have extensive computational capabilities and, in addition to proportional, integral, and derivative (PID) control, can generally perform logic and sequential control [6].

Human Machine Interface:

A DCS typically uses custom designed processors as controllers and uses both proprietary interconnections and communications protocol for communication. The DCS contains input and output modules as component parts. The processor receives information from input modules and sends information to output modules. The input modules receive information from input instruments in the process and transmit instructions to the output instruments in the field. The processor and modules are connected through multiplexer or demultiplexers by computer buses or electrical buses. The distributed controllers are connected with the central controller and finally to the Human Machine Interface [7] (HMI) or control consoles via buses. The figure shows the simulation of the drum level control.

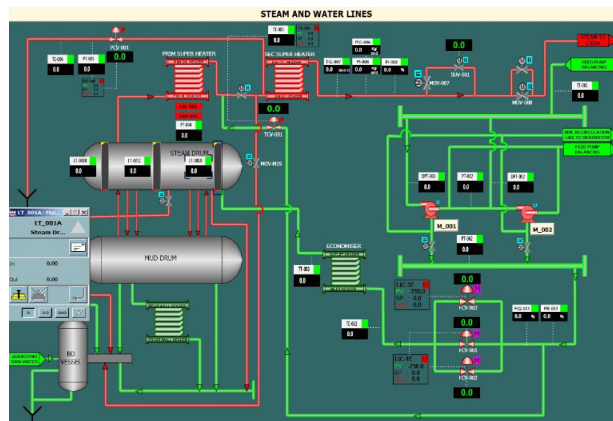


Figure 7: Simulation of the Water and Steam Lines

5. ADVANTAGES OF DCS

- Access a large amount of current information from the data highway.
- Monitoring trends of past process conditions.
- Readily install new on-line measurements together with local computers.
- Alternate quickly among standard control strategies and readjust controller parameters in software.
- A sight full engineer can use the flexibility of the framework to implement his latest controller design ideas on the host computer.

6. ELEMENTS OF SCADA:

SCADA [8] (supervisory control and data acquisition) is a type of industrial control system [9] (ICS). Industrial control systems are computer-controlled systems that monitor and control industrial processes that exist in the physical world. SCADA systems are different from other ICS systems as they are large-scale processes that can include multiple sites, and large distances. These processes include industrial, infrastructure, and facility-based processes.

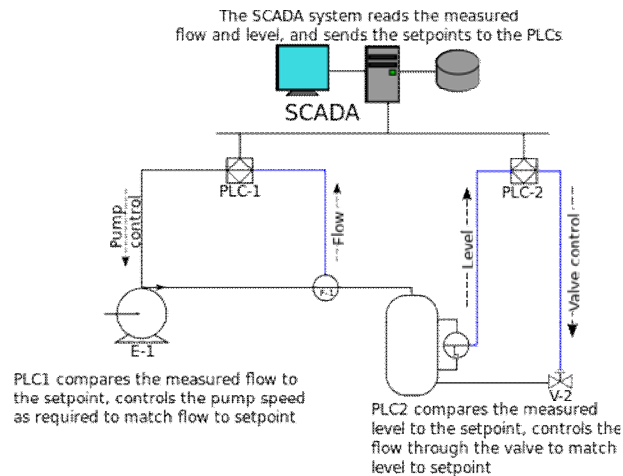


Fig 8: Schematic overview of SCADA

A SCADA system usually consists of the following subsystems:

- Remote terminal units (RTUs) connect to sensors in the process and converting sensor signals to digital data. They have telemetry hardware capable of sending digital data to the supervisory system, as well as receiving digital commands from the supervisory system. RTUs often have embedded control capabilities such as ladder logic in order to accomplish boolean logic operations.
- Programmable logic controller (PLC) [10] connects to sensors in the process and converting sensor signals to digital data. PLCs have more sophisticated embedded control capabilities, typically one or more IEC 61131-3 programming languages, than RTUs. PLCs do not have telemetry hardware, although this functionality is typically installed alongside them. PLCs are sometimes used in place of RTUs as field devices because they are more economical, versatile, flexible, and configurable.
- A Telemetry system is typically used to connect PLCs and RTUs with control centers, data warehouses, and the enterprise. Examples of wired telemetry media used in SCADA systems include leased telephone lines and WAN circuits. Examples of wireless telemetry media used in SCADA systems include satellite (VSAT), licensed and unlicensed radio, cellular and microwave.
- A Data Acquisition Server is a software service which uses industrial protocols to connect software services, via telemetry, with field devices such as RTUs and PLCs. It allows clients to access data from these field devices using standard protocols.
- A human-machine interface or HMI is the apparatus or device which presents processed data to a human operator, and through this, the human operator monitors and interacts with the process. The HMI is a client that requests data from a Data Acquisition Server.
- A Historian is a software service which accumulates time-stamped data, boolean events, and boolean alarms in a database which can be queried or used to populate graphic trends in the HMI. The Historian is a client that requests data from a Data Acquisition Server.
- SCADA is used as a safety tool as in lock-out tag-out
- A supervisory (computer) system, gathering (acquiring) data on the process and sending commands (control) to the process.

- Communication infrastructure connecting the supervisory system to the remote terminal units.
- Various process and analytical instrumentation

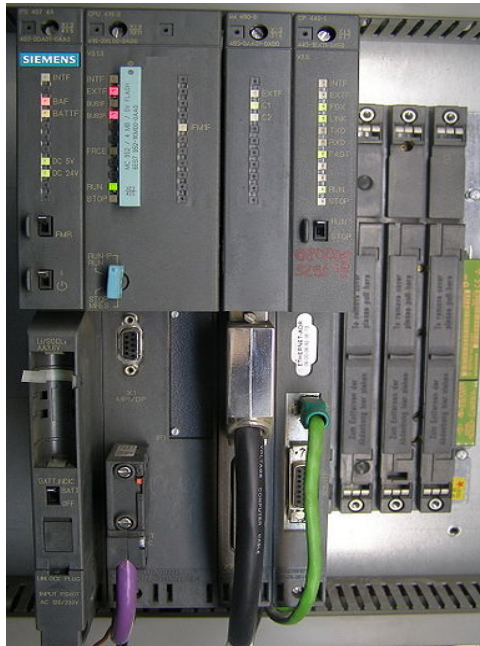


Fig 9: Siemens Simatic S7-400

7. SCADA in thermal power plant

A SCADA system can be used to supervise the operation and data acquisition of a thermal power plant. This system has capacity to supervise the plant as well as necessary facilities to acquire the values of temperature and pressure which are sensed by a temperature sensor and pressure sensor respectively. It can also supervise high and low level position of level sensor available at the thermal power plant. Measurement of previous process data can be supervised in the form of graph plots in the HMI. The SCADA system also facilitates alarms for any bad condition or excess condition of an event. Another available feature of the system is Data acquisition. Data is acquired from the various temperature sensor, pressure sensor and level sensor with the help of data acquisition hardware.

a) Temperature and Pressure measurement:

The thermal power plant consists of temperature sensors (thermocouples) at various places. These temperature sensors are placed near the globe valve to sense the temperature of steam produced in boiler, at condenser inlet and outlet to sense temperature of water. There is a pressure transmitter available near globe valve to sense the steam pressure.

b) Level Measurement:

There are two different level sensors available at water storage tank and diesel storage tank to sense the water level and diesel level respectively.

c) Data logging for temperature and pressure measurement:

SCADA has capability to log values of temperature sensed through temperature sensor and acquired by data acquisition system. Values of steam pressure also logged in the system which is sensed through pressure sensor and acquired through data acquisition hardware.

d) Measurement of historical data:

SCADA has capability to log historical data for the data acquired during Process. This simulation can log the values of Temperature sensor and pressure sensor which was acquired by data acquisition system. Data acquired by data acquisition system can log and these values are displayed in the HMI as a plot of graphs. Historical data provides data logging for the previous activities of the power plant. In historical data logging previous data of particular event is shown in the form of graphs.

e) *Alarm Handling:*

SCADA has provisions for alarm handling. An alarm represents a specific, abnormal condition associated with shared variable or with a user-defined state. Alarms can be set and configured for shared variables. An alarm is the alarm information for the specified shared variables. An event is a type of alarm that occurs instantaneously. An event is virtually any instantaneous activity, whereas an alarm typically denotes an abnormal condition, occurs under certain specific conditions, or must be acknowledged by the user or configured for automatic acknowledgment.

8. ADVANTAGES OF SCADA

- SCADA systems can be distributed over multiple sites and large distances.
- Increase efficiency by minimizing fault response time
- Isolate and precisely locate faults
- Improved operation of the plant resulting in energy savings due to optimization of the system [11]
- Increased productivity of the personnel
- Improved safety of the system due to better information and improved control
- Safeguarding the environment from a failure of the system

9. COMPARISON BETWEEN SCADA AND DCS

DCS	SCADA/PLC
Expensive hardware but engineering is comparatively cheaper	200% cheaper than DCS Hardware is cheaper but engineering is expensive
Control and monitoring over small areas e.g. a process unit	Over large geographical areas
Data transfer via LAN infrastructure	Use leased telephone lines or radios
Large, extensive applications with many control and data transfer Analog control processing	Small medium-sized applications with majority open/close control
Direct control, output directly to field actuators	Send set points to local controllers
DCS was a single vendor solution	With SCADA the connection with the field is done by third party hardware and software
Focused in process industry	Focused in discrete production industry
Inter-related continuous complex processes	Batch processing with low level of process interaction
Robust hardware and software are the part of the equipment on the shop floor and are fixed	Operating system software and the processor used in a SCADA PC undergo quick changes due to heavy competition
Process computer on the shop floor and PCs in the control room	PLC platform for process control and a PC platform (SCADA) for display
Data acquisition is event driven, rely on change. The RTUs can typically operate for extended periods of time w/o communications with the 'Host'	Data acquisition via one database with fixed scan cycle for each data point

Application stored on one database	Application data are divided over several databases
Fast with complex control	Fast when used in logical (on/off) application
Predictable, real time	Not completely predictable
Handle many controls	Limited number of controls

10. SUMMARY

Modern industrial control systems have brought about revolutionary changes in modern power generation systems. ICS has greatly reduced human efforts to monitor and supervise all the systems. New generation ICS has overcome the drawbacks of early ICS and speed up the production process. The errors have been greatly minimized and the response time has also reduced. Although human involvement has reduced, the safety of the plant has not been compromised. The SCADA database architecture is significantly different from the DCS data architecture. DCS involves more complex operation in terms of control, management and processing. But it is fast even with the complex control which can bring flexibility in overall power generation process. Its unique feature of single database make it more advantageous over SCADA which may play a vital role in future days.

REFERENCES

[1] El-Wakil, M. M. (2010). "Powerplant technology". New York, Tata McGraw-Hill.
 [2] "Distributed control system", Retrieved from Wikipedia: http://en.wikipedia.org/wiki/Distributed_control_system
 [3] "Industrial IT for Power Generation"-ABB
 [4] "Distributed Control Systems"- Richard DeVercelly
 [5] Porfilio, R. "Advancing Control System Technology for Your Power Plant", ABB Power Generation.
 Retrieved from: http://www.isa.org/filestore/Division_TechPapers/GlassCeramics/POW08-P059Final.pdf
 [6] Kamei T., T. Tomura, Y. Kato, (2003), "Hitachi's Latest Power Plants Control System", Hitachi Review vol.52, pp. 101-105.
 [7] Orth, J. "Future power plant control - Integrating process & substation automation into one system", ABB AG, Mannheim, Germany.
 [8] "SCADA", Retrieved from Wikipedia: <http://en.wikipedia.org/wiki/SCADA>
 [9] "Industrial control system", Retrieved from Wikipedia: http://en.wikipedia.org/wiki/Industrial_control_system
 [10] Wilson, T. "PLC based substation automation and SCADA systems and selecting a control system integrator"-presented at Western Electric Power Institute.
 [11] "The IDC Engineering Pocket Guide"- IDC technologies. pp. 127-148

ISSUES RELATING TO INSTALLATION AND COMMISSIONING OF COMBINED CYCLE POWER PLANT IN BANGLADESH

P.Chakraborty*, A.Saha*, AtaurRahman**, M.A.RashidSarkar***

*Dept. of Mechanical Engineering, Bangladesh University of Engineering and Technology, Dhaka-1000

**Consultant, Power Plant Projects

***Professor, Dept. of Mechanical Engineering, Bangladesh University of Engineering and Technology, Dhaka-1000

Abstract: Combined Cycle Power Plants (CCPPs) are attractive in power generation due to their higher thermal efficiency than individual steam or gas turbine cycles. The design uses a gas turbine to generate electricity and then captures the resulting exhaust heat to generate steam, which in turn drives a steam turbine significantly increasing the system's power output without any increase in fuel consumption. However, Installation and Commissioning of a combined Cycle Power Plant is a very complicated and troublesome job. In this paper, a brief description of installation and commissioning of a Combined Cycle Power Plant is presented. The paper presents a structured way of installation and commissioning of combined cycle power plants. Some recommendations are also made.

Keywords: Gas Turbine, Steam Turbine, Heat Recovery Steam Generator, Combined Cycle Power Plant

Nomenclature :

GT	Gas Turbine
ST	Steam Turbine
HRSG	Heat Recovery Steam Generator
CCPP	Combined Cycle Power Plant
CCW	Closed Cooling Water
HP	High Pressure
IP	Intermediate Pressure
LP	Low Pressure
CO	Control Oil
LO	Lube Oil
SO	Seal Oil
BFP	Boiler Feed Pump
GTG	Gas Turbine Generator
TCA	Turbine Cooling Air
T/G	Turning Gear
FSNL	Full Speed No Load
GCB	Gear Circuit Breaker
STG	Steam Turbine Generator
AVR	Automatic Voltage Regulator
AGC	Automatic Governor Circuit
COD	Commercial Operation Date
AT	Acceptance Test
RT	Reliability Test
P-test	Performance Test
SOP	Standard Operating Procedures
GRP	Glass-fibre Reinforced Pipe

1. INTRODUCTION

Gas Turbine, Steam Turbine, Gas Booster Compressor and HRSG are the main components in a Combined Cycle Power Plant. The performance of the plant and its life span, depend on the proper installation and commissioning of these components. Timing of commissioning of each equipment in a CCPP may vary from case to case. A CCPP having Brayton based topping cycle and Rankine cycle based bottoming cycle has been considered for discussion to give a brief idea about installation and commissioning process.

Systematic approaches to commissioning is desirable in all kinds of plants. A great deal of effort has been made by Kris Lawry and Dirk John Pons[1], analyzing different perspectives of commissioning. Several workshops have also been conducted by Himadri Banerji [2] about commissioning and start-up a plant. David Horseley [3] explained steps of commissioning in a systematic way.

Different analysis about CCPP (auxiliary power requirement, optimum cycle analysis, thermodynamic analysis, energy analysis etc) have also been made[4-6]. Key elements as well as auxiliary systems (eg. Starting system, ignition system, lub oil system , fuel system and control etc.) of CCPP have been discussed in several books [7-12].

Bangladesh has recently achieved the Milestone of 10,000 MW in our power sector. A wide range of power plants including simple Cycle Power Plant, thermal power plant, Engine based Peaking Power plants are in operation in Bangladesh. Combined Cycle Power Plant is a comparatively new addition in our power sector.

Combined Cycle Power Plant is well known for its new levels of performance and cost savings worldwide. In spite of late addition of CCPP technology in our country, we are proud that, Bangladesh is implementing more new CCPP in Govt., Semi Govt. and Private sectors. One of the oldest CCPP in our Country is owned by Pandekar Energy which is a 360 MW CCPP, situated at the bank of the river Shitalakhya. New Haripur 360 MW CCPP, EGCB Ltd is the latest addition to this family which is a Govt. owned Power plant. Major ongoing CCPP projects in Bangladesh are Meghnaghat 450 MW CCPP, Shidhirganj 335 MW CCPP and Ashuganj 450 MW CCPP and Bheramara 360 MW CCPP. Recently Shirajganj 150 MW Peaking Power Plant has been upgraded to 225 MW CCPP By North West Power Generation Company.

1.1 MAIN COMPONENTS OF A COMBINED CYCLE POWER PLANT :

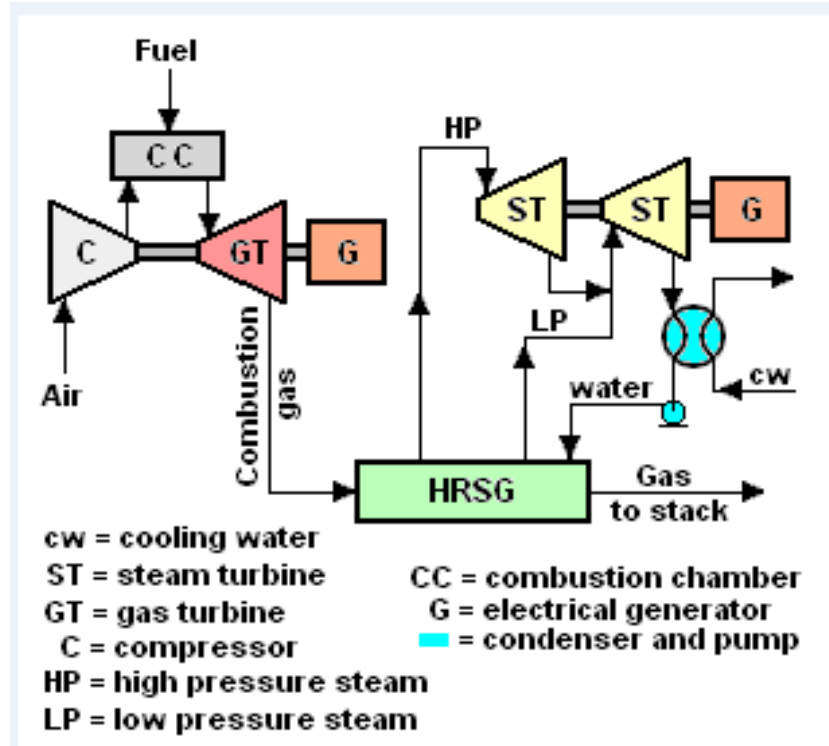


Fig 1 : Key Components of Combined Cycle Power Plant

a) GAS TURBINE :

A gas turbine, also called a combustion turbine, is the most efficient equipment for converting fuel energy to mechanical energy. It sucks air from the atmosphere, compresses it. The fuel is injected and ignited. The combustion gases expand doing work and thereby rotating gas turbine generator.

Compressor: The compressor sucks in air from the atmosphere and compresses it to pressures in the range of 15 to 20 bar. The compressor consists of a number of rows of blades mounted on a shaft. This is something like a series of fans placed one after the other. The pressurized air from the first row is further pressurized in the second row and so on. Stationary vanes between each of the blade rows guide the air flow from one section to the next section. The shaft is connected and rotates along with the main gas turbine.

Combustor: This is an annular chamber where the fuel burns and is similar to the furnace in a boiler. The air from the compressor is the Combustion air. Burners arranged circumferentially on the annular chamber control the fuel entry to the chamber. The hot gases in the range of 1400 to 1500 °C leave the chamber with high energy levels. The chamber and the subsequent sections are made of special alloys and designs that can withstand this high temperature.

Turbine: The turbine does the main work of energy conversion. The turbine portion also consists of rows of blades fixed to the shaft. Stationary guide vanes direct the gases to the next set of blades. The kinetic energy of the hot gases impacting on the blades rotates the blades and the shaft. The blades and vanes are made of special alloys and designs that can withstand the very high temperature gas. The exhaust gases then exit to exhaust system through the diffuser. The gas temperature leaving the Turbine is in the range of 500 to 550 °C.

The gas turbine shaft connects to the generator to produce electric power. This is similar to generators used in conventional thermal power plants.

b) HEAT RECOVERY STEAM GENERATOR(HRSG) :

Heat Recovery Steam Generator is basically a boiler that uses the exhaust from gas turbine to convert water into steam. This steam is used to rotate steam turbine. The exhaust gases then release to atmosphere through stack. The steam leaving steam turbine is condensed in a condenser, this condensed water is sent back to HRSG.

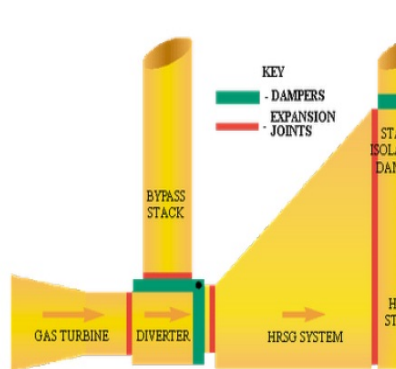


Fig 2 : Exhaust gas flow from GT outlet to atmosphere



Fig 3: Heat Recovery Steam Generator

c) STEAM TURBINE:

Steam turbine is a device that extracts thermal energy from pressurized steam and uses it to do work on a rotating output shaft. Because the turbine generates a rotary motion, it is suited to drive an electrical generator, thus producing additional power, increasing the efficiency of power plant.

2. INSTALLATION AND COMMISSIONING

Installation and Commissioning of CCPP is a very troublesome work. Any flaw which is overlooked can lead to ultimate losses, including the death of attending Personnel. So Proper training regarding Installation, Commissioning and Operation is of utmost importance for smooth running of Plant as well as for the safety of the personnel. The installation team mainly focuses on installing each and every equipment in place, according to the requirement of design and specifications. Then commissioning comes to effect after proper installation of the plant.

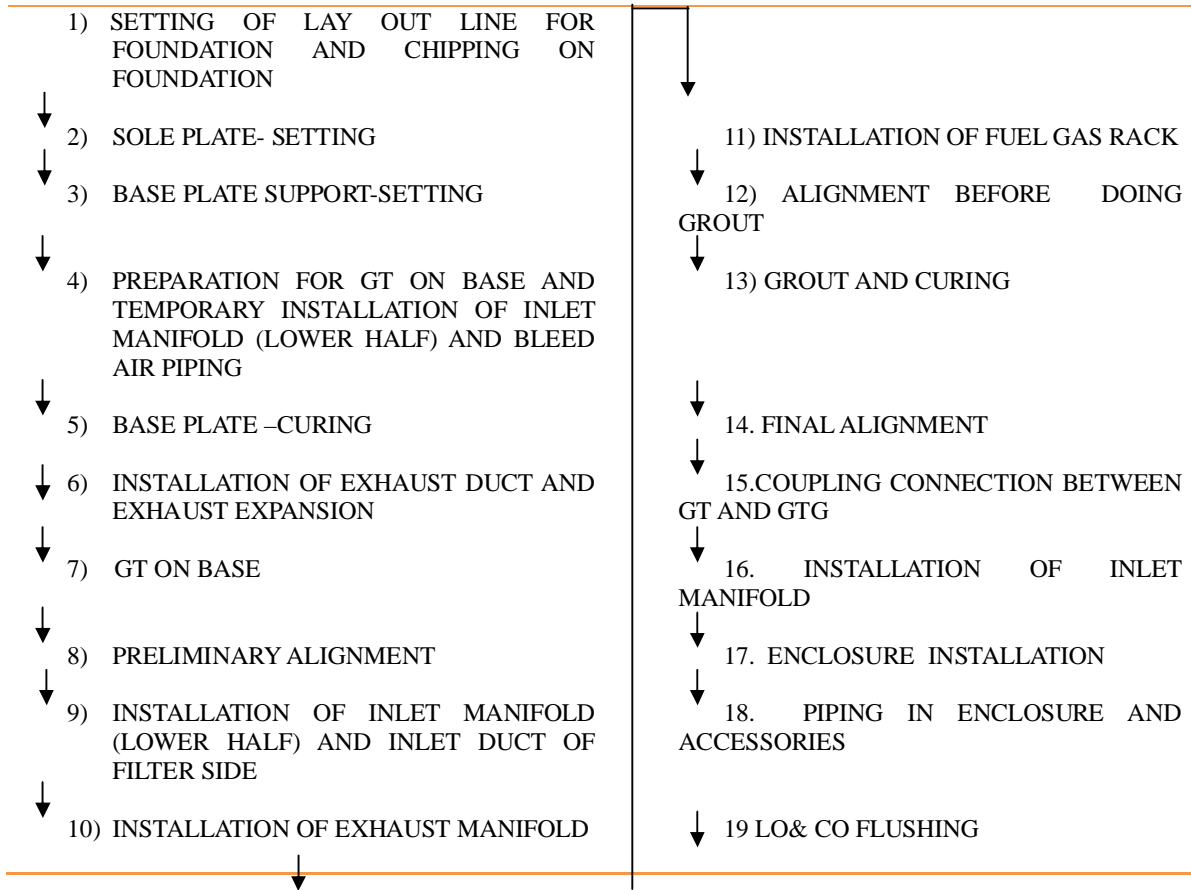
2.1 INSTALLATION OF COMBINED CYCLE POWER PLANT

Installation of CCPP includes a wide and vast range of activities including installation of Water treatment Plant, Gas Booster Compressor, HRSG, Gas Turbine, Steam Turbine, Air Compressor and many more.

2.1.1 INSTALLATION OF GAS TURBINE

For installation of GT, higher level of expertise is required. Special attention must be given to the alignment of GT, quality of grouting material and curing of grouted base of GT. Damp curing is highly recommended to improve the strength of grout and to avoid the cracking of grout due to dryness. Uniform temperature must be maintained to avoid non uniform joint, cracking of grouting.

A probable flow chart of steps of installing Gas turbine is given below-



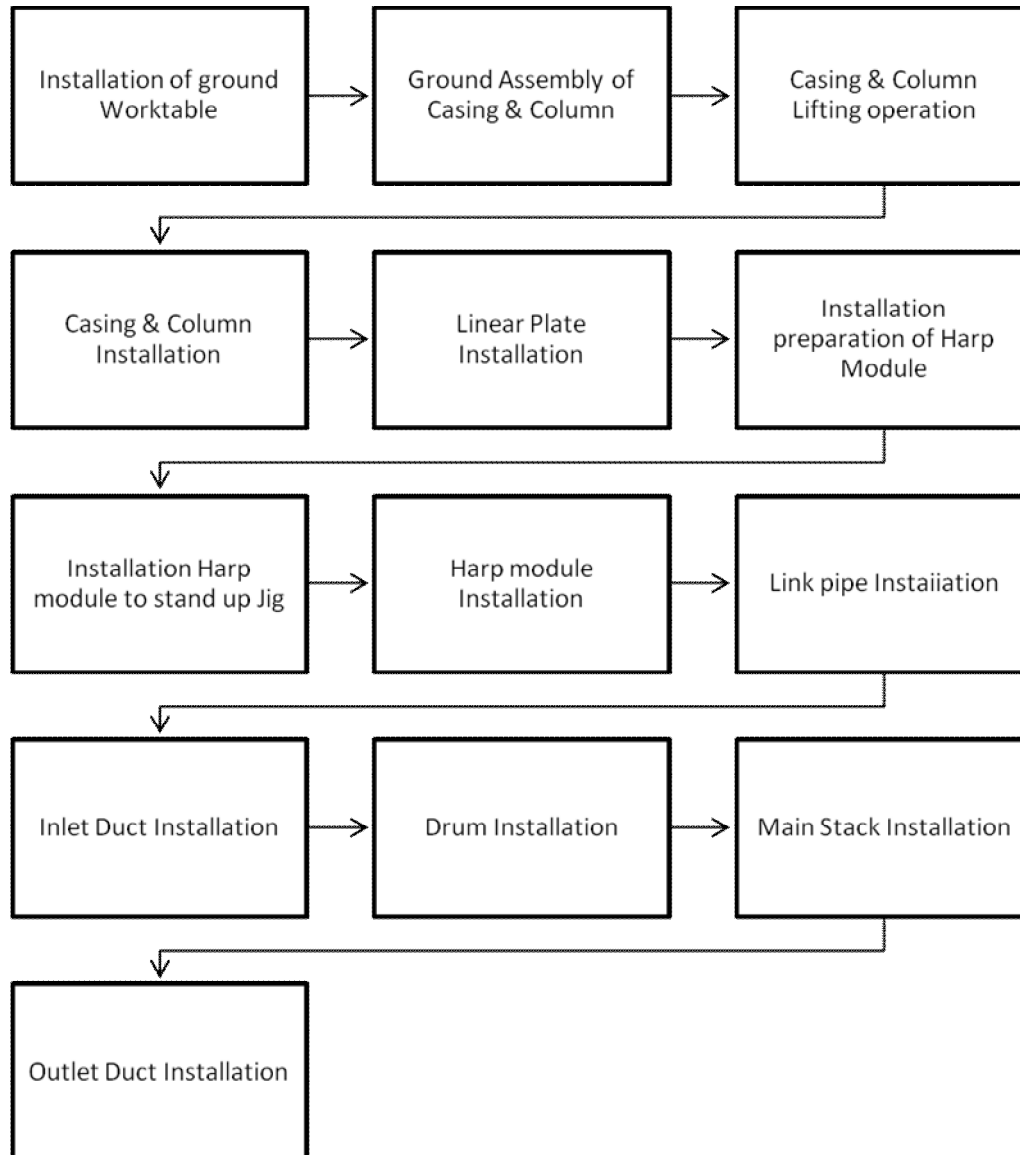
2.2 COMMISSIONING

Power Plant Commissioning is the process of making a live power plant from dead and just expensive structure and equipment through Checking, testing and tuning process.

A series of operation process are done by commissioning personnel in newly constructed power plant until each installed equipment, device and system are combined as a plant and reached to normal operation condition.

Normally Commissioning includes the following items

- Training of commission personnel
- Establishment of Commissioning Process
- Check of Equipment specification, installation and function test
- Pre commissioning Check, test run, tuning and record for each equipment and system
- Cleaning and Leak test for Piping/ Equipment
- Hot Commissioning
- Performance test
- Management of Punch and Pending items



- **COLD COMMISSIONING**

Cold Commissioning means power receiving, for house energizing, flushing and leak check for piping, tank as well as for pre-commissioning check, test run, tuning and record for each equipment/device. Normally, it means the period from erection completion of each equipment to gas turbine initial firing in gas turbine combined Cycle Power Plant.

- **HOT COMMISSIONING**

Hot Commissioning is a chain of operation process to make equipments or systems that are finished with cold commissioning into completed power plant. Normally, it means the period after gas turbine initial firing to commercial operation date in gas turbine Combined Cycle Power Plant.

2.2.1) STEP BY STEP COLD COMMISSIONING:

Step 1: Managing Temporary Power source

Step 2: Switch Gear Test---Transformer Test-Back Feeding

- Step 3: Intake System Checking
- Step 4: Water Treatment and Waste Water Treatment Plant performance checking
- Step 5: Low Pressure, Intermediated Pressure and High Pressure Piping Hydro test
- Step 6: LP, IP, HP and Hot Reheat Line Chemical Cleaning
- Step 7: Closed Cooling Water Line Flushing and CCW Pump Load test
- Step 8: GT Final Alignment
- Step 9: CO, LO, SO Pump test and LO Vapor Extractor test
- Step 10: Control Oil, LubOil, Seal Oil Line Flushing
- Step 11: GT Oil System Interlock Test
- Step 12: Condenser Filling and Leak Test, Condenser Flushing
- Step 13: Boiler Feed Pump LO Flushing, BFP Motor Solo Test, BFP Load Test
- Step 14: Cooling Water Basin Filling, Aux. Cooling Water Pump and Main Cooling Water Pump Test
- Step 15: GTG Air Leak Test
- Step 16: Turbine Cooling Air Cooler (TCA) / Fuel Gas Heater (FGH) Line Flushing
- Step 17: GT Turning Gear Test, T/G Interlock Test, Engage T/G
- Step 18: Diesel Generator Test
- Step 19: ST LO Pump Test, ST LO Flushing, ST LO Vapor Extractor test
- Step 20: ST LO System Interlock test
- Step 21: ST Turning Gear Test, T/G Interlock Test, Engage STT/G
- Step 22: GT Inlet Air Filter System Check
- Step 23: Condense Vacuum Pump Test, Condenser Vacuum Up test
- Step 24: Stack Damper test, GT Spin Test and Blow
- Step 25: Generator Hydrogen Filling
- Step 26: Enclosure Vent Test, Fire Fighting System Test, Nitrogen Purging
- Step 27: Fuel Gas Isolation Valve and Control Valve checking
- Step 28: Igniter test, Fire Detection test and GT Initial Firing

2.2.2) STEP BY STEP HOT COMMISSIONING:

- Step 29: Vibration Checking, GTFSNL Test
- Step 30: GT Dry Low Nox Tuning
- Step 31: GCB Moving Test—Excitation and AVR test, Gen Phase and Protection test, Excitation Online test, GT Initial Synchronization Test
- Step 32: HRSG Steam Blowing, HP and IP Bypass Operation, Hot Reheat Bypass Operation and LP Bypass Operation
- Step 33: STG Air Leak Test
- Step 34: Main Steam Valve Moving and Interlock Test
- Step 35: Steam Control Valve Moving test, Stroke test
- Step 36: ST Interlock Simulation test, Unit General Interlock test
- Step 37: HRSG Safety Valve Test
- Step 38: ST Steam Admission
- Step 39: Gen Hydrogen Filling
- Step 40: ST GCB Moving Test, Excitation and AVR test, Gen Phase and Protection test, Excitation Online test.
- Step 41: ST Vibration Check and Over speed test
- Step 42: GT Tuning and Dump Test
- Step 43: ST Dump Test
- Step 44: Load Swing Test
- Step 45: Load Runback Test
- Step 46: AGC Test
- Step 47: 24 Hours Initial Load Test
- Step 48: Reliability Test
- Step 49: COD
- Step 50: Performance Test and Finally Hot Parts Inspection.

2.2.3) COMMISSIONING MILESTONE:

A milestone is an important event in the commissioning Process. Milestone is a reference point to manage commissioning schedule. Major milestones for each project are dependent on system configuration.

Major milestones in GT Combined Cycle Power Plant are described briefly below:

- **Power Receiving**

Power receiving is to receive electric power initially from grid system in order to establish in house power for commissioning.

- **GT Initial Firing**

GT Initial Firing is to ignite fuel in the GT Combustor initially after completion of Simple cycle BOP cold Commissioning.

- **GT Initial Synchronization**

GT Initial Synchronization is to connect grid system and generate electric power initially after completion of GT and GTG no load test. It's a process to check the interlock and operation for transmission system and related equipment as well as the generator function.

- **Steam Blow Out**

Steam Blow Out is to remove welding slag, rust, mill scale etc. in the HRSG tube and steam piping using high pressure steam, before ST initial Admission. It's a process to prevent damage of Steam Nozzle and Blade by foreign material

- **ST Initial Admission**

ST Initial Admission is to rotate ST initially by steam generated in HRSG after confirmation of good low speed rotation condition.

During this process, ST operation conditions like turbine expansion, bearing vibration and temperature etc. are checked.

- **ST Initial Synchronization**

ST Initial Synchronization is to connect grid system and generate electric power initially after completion of GT and GTG no load test. It's a process to check the interlock and operation for transmission system and related equipment as well as the generator function.

- **Reliability Test**

Reliability Test is to demonstrate and confirm that the Unit is operating and performing reliably, consistently and in accordance with its design intention.

Normally RT duration is consecutive 240 hrs or 480 hrs depending on the each contract.

During this period, the unit should run continuously according to contract's requirements.

- **AT (Acceptance test) & COD (Commercial Operation Date)**

AT means the test in order to demonstrate that the performance guarantees have been satisfied for each Unit or Facility.

AT is started after RT is successfully finished. Detail condition is dependent on the contract. In some plants, AT is not required depending on the related regulation.

COD means Commercial Operation Date, which is the date when the Unit starts operation for commercial purpose after all the required inspection and test including RT and AT are completed.

- **Performance Test**

P-test is to confirm that the actual performance of plant satisfies guaranteed performance in the contract. Normally, P-test is carried out within 3 months after RT unless otherwise stated.

3.4) COMMON TROUBLES GENERALLY ENCOUNTERED:

A wide range of problems, even unknown, arise during commissioning process of a CCPP. Common problems are mentioned below:

A. Design and Manufacturing Trouble:

If valves working at high temperature are not fully made of same material, it may lead to different thermal expansions on different portion of it resulting sticking and damage of it.

B. Installation Trouble:

Sometimes valves are reversely installed unintentionally, as a result, valves may subject to hammering action while operation. Another Common mistake is that, accumulated water inside a equipment sometimes go without noticing and it will lead to corrosion and sometime completed failure can occur due to this corrosion.

If temporary supports under GRP Pipe are not removed, stress concentration can occur at that point during operation and pipes may crack.

C. Management and Operation Trouble:

If HRSG is not operated according to SOP, then tube inside the HRSG may fail due to thermal shock. If foreign materials inside piping are not removed properly, damages of compressor and pump impeller and other equipments can happen.

3.0) SUMMARY & RECOMMENDATIONS :

a) During installing gas turbine in a combined cycle power plant ,some points need to be considered carefully. Sole plate and base plate support should be set accurately . Installation of inlet manifold ,bleed air piping ,exhaust duct and exhaust expansion ,exhaust manifold should be performed according to design . Perfect alignment of gas turbine should be maintained when it is set on base. Coupling connection between GT and GTG should be accurate.

b) Gas turbines are extremely noisy ,so it should be housed in an acoustic enclosure ,which is usually located in a factory-type building to provide weather-proofing and further noise attenuation. Enclosures should be fitted with fire and gas detection systems and have a system of fire suppression. The enclosure must be ventilated with ambient air and the intake ducting is fitted both with filters and with a silencer to minimize noise.

c) Since the heat recovery steam generator of a combined cycle power plant are different in structure and design from those of conventional boilers, a number of erosion caused by water have been reported . Valve erosion troubles have arisen in the steam system, feed water system and condensate water systemsince the start-up of a power plant. Also,leakage troubles from mechanical seals of feed water pump have happened .The troubles seemed to be caused by effects of iron scale accumulation or by feeding water containing iron scale as sealing water . However, since this kind of problem has never seen with conventional boilers , investigations into the cause and protective measures are required.

d) Installation of steam turbine also requires some monitoring . Typical turbine problems include pitting corrosion, corrosion fatigue, stress corrosion cracking ,deposit build up, solid particle erosion , water droplet erosion of wet stages. Turbine component failures and loss of efficiency and generating capacity resulting from deposition are very costly.

e)Commissioning is an integral part of plant modification project on which the success of the project greatly relies .So systematic approaches should be followed for commissioning although it is often carried out in an ad hoc manner. Sometimes it results in unwanted situation and catastrophic failure.The disastrous failure of Chernobyl nuclear power plant(1986), caused by operators attempting an ad hoc test of efficacy of a modified emergency cooling system [1] .

f)The response of equipment during commissioning is sometimes unpredictable and can lead to hazardous consequences. The success of Commissioning team depends on the proper installation of system and Pre-commissioning. As Bangladesh still depends on other developed country for making a power plant, highly skilled personnel should be developed through effective local and foreign trainings.

g) A power learning Institute for Engineers in Bangladesh at IEB with Modern Simulation facilities and model of CCGT, is highly required to keep pace with modern power technology.

REFERENCES

- [1] Kris Lawry and Dirk John Pons , Integrative Approach to the Plant Commissioning Process, Integrative Approach to the Plant Commissioning Process, Volume 2013 (2013), Article ID 572072

- [2] Dr. Himadri Banerji, "World Class Manufacturing: Plant Start-up and Commissioning Procedure",
- [3] David Horsley, "Process Plant Commissioning", 2nd edition, 1998
- [4] Tejay N Raval, Dr R N Patel, "Optimization of Auxiliary Power Consumption of Combined Cycle Power Plant", *Procedia Engineering* 51 (2013) 751 – 757
- [5] A.L.Polyzakis, C.koroneos, G.Xydis, "Optimum gas turbine cycle for combined cycle power plant" *Energy Conversion and Management* 49 (2008) 551–563
- [6] Ivar S. Ertesvag, Hanne M. Kvamsdal, Olav Bolland, "Exergy analysis of a gas turbine combined cycle power plant" final version 21 May 2004) - Accepted for publication in *Energy*
- [7] Rolf Kehlhofer, Frank Hannemann, Franz Stirniman, "Combined Cycle Gas & Steam Turbine Power Plants", 3rd edition, ISBN: 978-1-59370-168-0
- [8] P K Nag, "Power Plant Engineering", third edition, twelfth reprint 2011, ISBN-13: 978-0-07-064815-9
- [9] Larry Drbal, K.Westra, P.Boston "Power Plant Engineering", 1996, ISBN: 0412064014 Book ID: PE-1039
- [10] M.M.Elwakil, "Powerplant Technology", third reprint 2011
- [11] Philip J. Potter, "Power Plant Theory and Design", 2nd edition, 1988, R.E. Krieger edition
- [12] A.K.Raja, Amit Prakash Srivastava, Manish Dwivedi, "Power Plant Engineering", New Age International | 2006 | ISBN: 8122418317, 8122423337